Freie Universität Berlin

# Azobenzene Based Molecular Switches on Noble Metal Surfaces: Structure and Isomerization at the Nanometer Scale

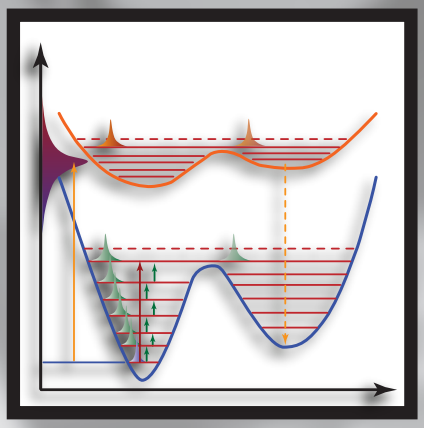

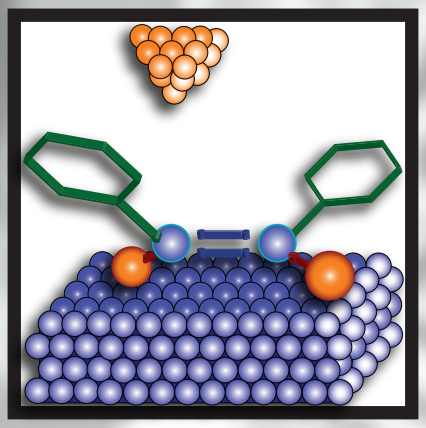

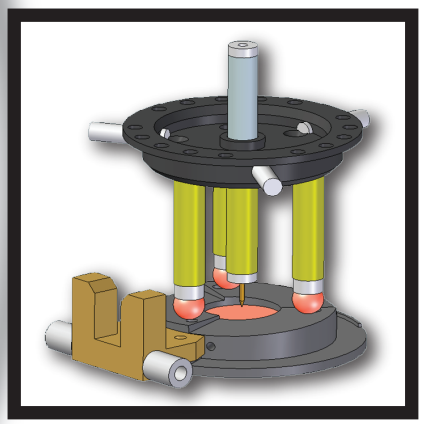

Disputation am 06.07.2009

Nils Henningsen

im Fachbereich Physik
der Freien Universität Berlin
eingereichte Dissertation

Diese Arbeit entstand in der Arbeitsgruppe von Prof. Dr. José Ignacio Pascual am Fachbereich Physik der Freien Universität Berlin.

Disputation am 06. Juli 2009

Promotionskommission:
Vorsitzender: Prof. Dr. Maarten P. Heyn
Stellvertreter: Prof. Dr. Felix v. Oppen

Erstgutachter: Prof. Dr. José Ignacio Pascual
Zweitgutachter: Prof. Dr. Karsten Horn
Weitere Mitglieder:
Dr. Petra Tegeder, Dr. Barbara Sandow,
Prof. Dr. Wolfgang Kuch, Dipl. Phys. Gunnar Schulze

# Azobenzene Based Molecular Switches on Noble Metal Surfaces: Structure and Isomerization at the Nanometer Scale


Nils Henningsen

PhD thesis submitted to the
department of experimental physics
of the Free University Berlin

# Kurzfassung

Im Rahmen dieser Doktorarbeit werden mittels Rastertunnelmikroskopie die Adsorptions- und Schalteigenschaften von Azobenzolderivaten auf verschiedenen Edelmetall-Oberflächen untersucht. Hierbei wird gezeigt, welche Herausforderungen die Suche nach schaltbaren Oberflächenfunktionalitäten birgt. So können die Konfigurationen eines Derivates mit der Abkürzung **DMC** nur dann durch Tunnel-Elektronen reversibel (*trans-cis-trans*) auf einer Metalloberfläche geschaltet werden, wenn die Bedingungen zulassen, dass sowohl der *trans*- als auch der *cis*-Zustand auf der Oberfläche stabil sind.

Anhand einer Vielzahl potentieller molekularer Schalter kann gezeigt werden, wie intermolekulare Wechselwirkungen und Wechselwirkungen zum Substrat konkurrierend die Wachstumseigenschaften der Moleküle beeinflussen. Während die lateral wirkenden Kräfte die Ordnung der Moleküle durch Wasserstoffbrückenbindungen bestimmen, beeinflussen die Wechselwirkungen zum Substrat das *cis-trans*-Schaltverhalten der Moleküle.

In schwach gebundenen Systemen, wie zum Beispiel auf einer Gold-Oberfläche, wird durch den Überlapp von $\pi$-Elektron-Orbitalen mit elektronischen Zuständen in der Oberfläche eine planare Adsorption der Moleküle in ihrem *trans*-Zustand bevorzugt. Durch die sterische Wechselwirkung zur Oberfläche kann so der Rotations-Freiheitsgrad eines Phenylrings eingefroren und durch Spitzen-Manipulation, aber auch durch Probentemperatur oder Dichte der Bedeckung aktiviert und somit geschaltet werden. Für den speziellen Fall von **DMC** kann diese Konformationsänderung in einem elektrischen Feld durch die Anregung eines kurzlebigen ionischen Zustandes und sukzessiver Relaxation beobachtet werden .

Wenn die Kopplung zur Oberfläche durch eine starke kovalente Bindung zwischen Molekül und Oberfläche bestimmt wird, wie beispielsweise auf Kupfer, ist eine dreidimensionale molekulare Geometrie bevorzugt, die dem *cis*-Zustand ähnelt. Die kovalente Bindung ergibt sich aus der Kopplung von freien Elektronenpaaren im Zentrum des Moleküls und prägt dort der dreizähligen Bindungskonfiguration den dreidimensionalen Charakter auf. Auf Grund der stärkeren Substratkopplung in der dreidimensionalen Konfiguration kann ein adsorbiertes *trans*-**DMC** in die *cis*-Konfiguration geschaltet werden, aber nicht wieder zurück. Auf einer Silber-Oberfläche, die mit dem organische Molekül eine nicht ganz so starke Bindung eingeht wie Kupfer, kann schließlich dasselbe Azobenzol-Derivat reversibel geschaltet werden.

Da die kovalenten Bindungen zum Substrat das Schaltverhalten der Moleküle beeinflussen, wird erwartet, dass durch die Kopplung metallischer ad-Atome an die Diazo-Brücke das Schaltverhalten der Moleküle beeinflusst werden kann. Tatsächlich kann nachgewiesen werden, dass ko-adsorbierte Kobalt-Atome mit den erwähnten Elektronenpaar-Orbitalen Koordinationsbindungen eingehen, die durch spektroskopische Untersuchungen klassifiziert werden können.

## Abstract

This work deals with scanning tunneling microscope investigations of switching and adsorption phenomena of several azobenzene derivatives on various noble metal surfaces. The adsorption phenomena of molecules depend on lateral intermolecular interactions and on vertical molecule-substrate interactions. Both interactions compete with each other upon ordering on the surface and they influence not only the adsorption geometry but also their ability to undergo isomeric switching between the two structures, the *cis*- and the *trans*-configuration. A *cis-trans* isomerization is hindered for many of the investigated example systems. Still, in the example of one azobenzene derivative named **DMC** reversible *trans-cis-trans*-isomerization could be observed.

The $\pi$-surface coupling favors planar adsorption of the molecules via the overlap of molecular $\pi$-orbitals and electronic states of the surface. $\pi$-surface interactions are observed for instance on weakly coupling gold substrates. By the planar adsorption the rotational degrees of freedom of phenyl rings are frozen, which are known to be not restricted for the free molecule. This rotation can be activated on the surface by temperature and upon molecular ordering. For **DMC**, the switching between two rotational conformations can be induced by tunneling electrons via the excitation and subsequent de-excitation of an ionic short-lived state under the influence of an electric field.

The central diazo unit, responsible for the switching, reacts sensitively on the coupling strength to the surface. This is one of the reasons for different switching characteristics on the gold, copper and silver surfaces. Furthermore, this coupling can be used to tune the molecular switching.

In strongly adsorbed systems covalent bonds stabilize the molecules, for instance on a copper surface. Two lone-pair electron orbitals in the center of the molecule couple with substrate atoms and favor a three-dimensional adsorption geometry. In this case, tip-induced manipulation of a *trans*- to a three-dimensional structure resembling the *cis*-configuration could be observed. However, the adsorption of the latter configuration is so strong that inverse-switching to the *trans*-state is suppressed. The slightly weaker reactivity of a silver substrate enables a reversible switching, since the covalently bonded *cis*- and the planar *trans*-configuration have a comparable stability on this surface.

As one possible approach we show that anchoring to cobalt atoms revealed promising possibilities for specific and variable functionalization of surfaces by switchable molecules. The individual cobalt sites could be identified by means of their spectroscopic fingerprint, arising from special coordination bonds between the Co atoms and the switchable molecule.

# Contents

**Kurzfassung** iii

**Abstract** iv

**Introduction** 1

**1 STM-Theory, Setup and Introduction to the investigated Molecules** 5
1.1 STM Theory . . . 5
1.1.1 Treating a STM Gap Theoretically . . . 6
1.1.2 Scanning Tunneling Spectroscopy (STS) . . . 8
1.1.3 STM Representation of Molecular Adsorbates . . . 9
1.1.4 Molecular Manipulation . . . 13
1.2 Technical Realization . . . 17
1.2.1 Setup . . . 17
1.2.2 Performance . . . 20
1.3 Adsorption Process . . . 22
1.3.1 Classification of Attractive Interactions . . . 22
1.3.2 Complexity of Adsorption . . . 25
1.3.3 Electronic Effects upon Adsorption . . . 26
1.4 Molecular Switches: Example Systems . . . 27
1.4.1 Ring-Opening/Closing Reactions . . . 28
1.4.2 Switching the Magnetic Moment: Spin State . . . 28
1.4.3 *Cis-Trans* Isomerization . . . 29
1.5 Azobenzene . . . 30
1.5.1 Free Diazo-Group . . . 31
1.5.2 Adsorbed Azobenzene . . . 33
1.5.3 Azobenzene in Surface Science . . . 34

**2 Ordering Processes of Azobenzene Derivatives on Metallic Surfaces** 35
2.1 Molecular Architecture of Azobenzene Derivatives . . . 35
2.2 Self-Ordering Processes Mediated by Molecular End Groups . . . 39
2.2.1 Stabilization in 2D islands . . . 39
2.2.2 Assembly in Clusters . . . 41
2.2.3 Assembly in Networks . . . 42
2.3 Role of the Surface Material, Temperature and Molecular Density in the Self-Assembling Process of Azobenzene Derivatives . . . 43
2.3.1 Surface Reactivity . . . 43

2.3.2 Active Intramolecular Conformational Dynamics . . . . . 44
2.4 Formation of Supra-Molecular Building Blocks . . . . . 48
2.5 A Molecule as one-dimensional Quantum Well . . . . . 52

**3 Conformational Switching of DMC-Azobenzene on Noble-Metal Surfaces 55**
3.1 Ring-Rotation of *trans*-DMC on Au(111) . . . . . 56
3.1.1 Tunneling Spectroscopy . . . . . 59
3.1.2 Intramolecular Dynamics . . . . . 60
3.1.3 Quantum Chemical Calculations . . . . . 61
3.2 Irreversible *Trans-Cis* Isomerization on Cu(100) . . . . . 64
3.2.1 Isomeric Manipulation . . . . . 65
3.2.2 Electronic Structure . . . . . 68
3.2.3 Discussion . . . . . 69
3.3 Lifting and Reversible Isomerization of DMC on Ag(100) . . . . . 71
3.3.1 Lifting a Molecule . . . . . 72
3.3.2 Reversible Isomerization . . . . . 74
3.4 Conclusion . . . . . 76

**4 Chemical Fingerprint of Coordination Bonds 79**
4.1 Planar Metal-Organic Networks . . . . . 80
4.2 Cobalt Clusters on Au(111) . . . . . 81
4.3 Co-Adsorption of Cobalt and DMC . . . . . 81
4.4 Spatially Resolved Tunnelling Spectroscopy . . . . . 83
4.5 Spatial Mapping of Cobalt States . . . . . 84
4.6 Coordination Geometry Mediated by Electron Donation . . . . . 86
4.7 Conclusion . . . . . 87

**Conclusion 89**

**References I**

**Apendix XII**

**Acknowledgements XIII**

**Curriculum Vitae XV**

# Introduction

Around the year 400 B.C. the Greek philosopher Demokrit rationalized that all matter is made of atoms. Nowadays, the strategy in nanotechnology somehow argues that all possible matter can be designed from these atomic building units. In the so-called bottom-up approach it is claimed that matter of certain functionality may be formed. In particular small functional units for data storage and data processing are desired, in order to follow the ongoing trend of miniaturization in electronic devices.

The idea of bottom-up designed nano devices may solve one dilemma of the present development in computer chip fabrication. The number of transistors per square centimeter in a computer processor rises exponentially from one generation of chips to the next one. This was expressed in Moore's law 1965 [Moor 65]. It causes that soon the circuit sizes will enter regimes of size, where quantum mechanical effects have to be considered [Sze 85]. Also the devices' heating, caused by electron currents in smaller circuits, is an important issue, which motivates to search for new strategies for data processing and to investigate for instance efficient molecular electronics as an alternative to classical electronics.

The variety of atoms and even the larger variety of combined atoms in molecules is enormous. Hence, the challenge is to choose molecular structures, which qualify as functional units, prove their characteristics, and illustrate their possible integration in nano devices. We can assume, that in the last three billion years, a permanent testing and discarding process – called evolution – acted as efficient debugger on any kind of matter on earth [New 98]. The development in microbiology and biochemistry opens perspectives in the search of useful molecular functional units amoung the large amount of candidate molecules. For instance, it is well understood that a photo-isomeric unit has developed in the eye's retina, embedded in a protein, which makes human kinds seeing colors. It transmits a photo activated signal into the inner part of the photoreceptor cell, for further neuronal processing in the autonomic nervous system [Grtn 01, Morg 09]. The photo-isomerization transforms photon energy into a geometrical change of the molecular unit from one into another configuration. This isomerization hence fulfils the basic requirements for a molecular switch, an essential functionality in molecular electronics.

Strategies of interfacing such reversible switching units, by means of reading and writing the configurations have to be developed. Furthermore, it is necessary to understand basic phenomena that influence the molecular properties. The aim to

create a switch, robust against its environment, sensitive to the addressing, small in size, and efficient, requires the detailed investigation of the switching mechanisms and it requires to study the interaction processes that a switching unit undergoes with its surrounding. In particular, a supporting material may disturb the ability of a molecule to switch, but will be needed when embedding the switch in a device.

The topographic, spectroscopic and manipulation techniques of a scanning tunneling microscope are possible methods to address properties of adsorbed molecules with a lateral resolution in the pico-meter range. In the scope of this work various derivatives of azobenzene – a small *cis-trans*-isomerizing molecule – are studied adsorbed on noble metal surfaces. The different adsorption processes have a strong influence on the molecular properties due to inter-molecular interactions as well as interactions between molecule and surface. As a result the *cis-trans*-isomerization is prohibited in most of the cases.

The ordered structures of azobenzene molecules are stabilized by a sum of hydrogen bonds or are embedded in coordination bond networks. These inter-molecular interactions compete upon adsorption with two types of coupling towards the surface. There are $\pi$-surface interactions, maximizing the overlap of the delocalized molecular electron systems with surface's electronic states and covalent interactions, bonding the nitrogen atoms of the central diazo unit with surface atoms. While the $\pi$-surface interactions are dominating the adsorption of weakly coupled systems, as we observe on gold surfaces, the covalent bonds establish on more reactive surfaces such as copper.

In the case of azobenzene adsorbed on Au(111), the $\pi$-surface interaction favors a planar adsorption of the molecules. Thus, the *trans*-configuration is the only one observed. The planar confinement of phenyl rings on a gold surface freezes a rotational degree of freedom, which is unrestricted in the free molecule case. This rotational motion can be activated thermally or by a dense packing, but also by STM induced manipulation. The dynamics of this rotational switching is explained by an ionic excitation and subsequent de-excitation process in an electric field.

When adsorbed on a copper surface, a covalent bond formation stabilizes the molecule in its center. This stronger molecule surface coupling occurs by hybridization of molecular states with states of the surface. Here, tip induced manipulation can change a molecule from a planar *trans*-configuration into a three-dimensional one resembling the *cis*-configuration. In fact, the stability of the latter is so strong that back manipulation into the *trans*-state is not possible.

By the variation of substrate materials, the strength of the covalent bond changes and the relative stability of the *trans*- and *cis*-configuration can be tuned. Thus, it will be shown that on a silver surface reversible isomerization is possible.

Besides steric surface hindrance and planar confinement, the bond configuration of the diazo unit determines the isomerization of the molecule. This diazo group

represents the switching "hinge" and supports different adsorption configurations depending on its surface coupling [Henn 07, Henn 08b]. By the formation of metal organic complexes involving individual cobalt atoms bonded to the lone-pair electron orbitals of the diazo unit we expect that a certain coupling can be reached, that enables isomeric switching. However, the resulting complex structures reveal two types of coordination bonds between cobalt atoms and molecules, which can be individually probed by tunneling spectroscopy.

In the first chapter of this thesis scanning tunneling microscopy and spectroscopy will be introduced, adsorption phenomena will be classified and the molecular system of azobenzene with its special characteristics will be presented. The second chapter deals with various adsorption phenomena of the different azobenzene derivatives. The third chapter focusses on the particular molecular example of Di-Meta-Cyano-Azobenzene (**DMC**). This molecule is investigated on three different substrate materials, each of which has special influence on the molecule and on its ability to perform reversible switching. In the fourth chapter it will be shown that **DMC** can form metal-organic nanostructures when mixed with individual cobalt atoms.

The work presented in this thesis was embedded in the collaborative research center (SFB) 658 on molecular switches on surfaces, funded by the German Research Foundation (DFG). The project allowed interdisciplinary interaction to different groups at the Free University Berlin, the Technical University Berlin, the Humboldt University Berlin, the University of Potsdam and at the independent research institutes Fritz-Haber- and Max-Born-Institute. The explored molecules were synthesized in the work group of K. Rück-Braun at the Technical University Berlin by B. Priewisch and C. Gebhardt [Prie 05, Prie 06]. Support from theoretical studies was given by J. Dokić, T. Klamroth, P. Saalfrank and R. Rurali [Fuch 06, Henn 08b].

# Chapter 1

# STM-Theory, Setup and Introduction to the investigated Molecules

The studies of molecular adsorbates on surfaces requires a technique that probes molecular properties locally. Topographic, but also electronic and vibrational features can be resolved by Scanning Tunneling Microscopy (STM) and Scanning Tunneling Spectroscopy (STS), which hence qualify for such purposes of investigation. Before concentrating on the results obtained and measurements presented in this thesis, these techniques will be introduced. Then a STM apparatus, operating at low temperature, will be explained. It was set up during my Diploma (Aug. 2004 - Aug. 2005). This equipment and another equivalent one from our laboratory was utilized in all experimental studies presented.

One aim of this work is to observe one individual molecule switching, when adsorbed on a metal substrate. To underline the complexity and the challenge of this topic, in this chapter it will be focussed on adsorption phenomena. Also, the properties and switching mechanisms of some prototype molecular switches will be summarized and subsequently the characteristics of the switchable azobenzene molecule will be introduced.

## 1.1 STM Theory

During the last decades low temperature STM became a powerful tool in surface science, utilizing the quantum mechanical tunneling effect. The atomic stability at 5 K and the lateral resolution allows to analyze a metal's top layer in real space. Additionally adsorbates, in particular molecules, lately gained interest in this field. However, the interpretation of STM data is non-trivial. Therefore it is important to abbreviate the theoretical understanding of a tunneling gap, which becomes complex, when molecular adsorbates are located in this tunneling gap.

The first STM was build by G. Binning and H. Rohrer in 1981 [Binn 82a, Binn 82b, Binn 83, Binn 87]. Since then it has become a standard tool for surface analysis. The simplified operating mode can be summarized as

following (sketched in figure 1.1 (a)). A metallic tip scans a metallic sample surface in the picometer scale by piezo electrical motion, steered from a computer. When a bias voltage (of $V_B \lesssim |\pm 5|$ V) is applied to the sample, the resulting tunneling current ($I$) between tip and surface is utilized as a feedback parameter, which is used to adjust a constant tip-sample distance ($Z$). By recording the tip position, derived from the voltages controlling the piezo motion, one can reconstruct two dimensional maps of the surface's *electronic topography*. In this way, topographies with atomic resolution of the substrate can be achieved. For understanding the processes of electron transport through the tunneling junction, which is forbidden in classical electrodynamics, a quantum mechanical view needs to be introduced.

### 1.1.1 Treating a STM Gap Theoretically

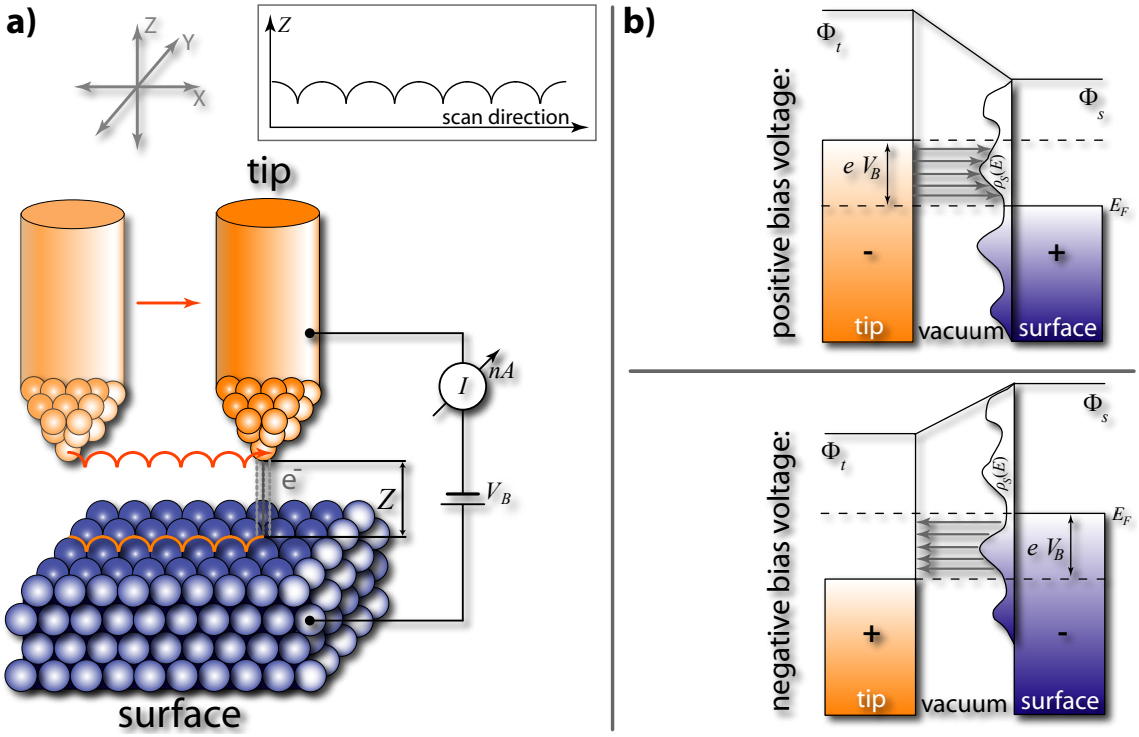


**Figure 1.1:** (a) Schematic view of the operating principle of an STM, with a metallic tip, scanning the surface. Under the use of the tunneling current ($I$) as feedback parameter, the atomic topography of the surface is reconstructed. (b) Shows the theoretical understanding of the tunneling process, where the main contribution of the tunneling current results from the density of states of the surface within a certain energy window $[E_F; E_F + eV_B]$ probing the surface's unoccupied states at the upper scheme and the occupied states in the lower panel.

The standard text book example in quantum mechanics describes a tunneling gap as potential barrier. Herein the transmission probability for electrons can be computed assuming the electrons have wave character [Schw 02]. The quantum mechanically non-zero transmission probability for electrons results in a measurable current, depending on the bias voltage and the tip sample distance. These three parameters

($I$, $V_B$ and $Z$) are the important variables, parameterizing local information of the tunneling gap. Experimentally information can be extracted from the tunneling system by analyzing the functions $I(V_B)|_{Z=const.}$, $I(Z)|_{V_B=const.}$, or $Z(V_B)|_{I=const.}$.

By the simple assumption of treating electrons as plane waves, the tunneling current can be derived, showing the most important dependencies. It emerges as a function with an ohmic term $V_B/Z$, multiplied by an exponential function that depends on $Z$, $V_B$, the metal's work function ($\Phi$) and a normalization constant ($\alpha$):

$$I \propto \frac{V_B}{Z} \cdot \mathrm{e}^{-\alpha \cdot Z \sqrt{\Phi - \frac{e\,V_B}{2}}} \tag{1.1}$$

A more sophisticated approach, elaborated by Bardeen, treats all electrons as sets of quantum mechanical wave functions of the tip ($\Psi_\mu$) and the surface ($\Psi_\nu$) respectively, with the energy eigenvalues $E_\mu$ and $E_\nu$, defined with respect to the Fermi energy ($E_F$) [Bard 61]. The tunneling current then depends on the overlap integral of wave functions of the tip and the sample as following:

$$\begin{aligned} I &= \frac{2\pi}{\hbar} e^2\, V_B \sum_{\mu,\nu} |M_{\mu,\nu}|^2 \delta(E_\mu - E_F)\, \delta(E_\nu - E_F) \\ \text{with } M_{\mu,\nu} &= -\frac{\hbar^2}{2m} \int_S \left(\Psi_\mu^* \nabla \Psi_\nu - \Psi_\mu \nabla \Psi_\nu^*\right) \overrightarrow{dS}, \end{aligned} \tag{1.2}$$

where the exchange integral of the transition matrix elements $M_{\mu,\nu}$ represents the electron density in the surface $S$ between tip and sample and hence quantifies the strength of coupling.

In the work of J. Tersoff and D. R. Hamann, the wave function of the tip is specified to be spherical and of the surface to be a superposition of periodic plane waves [Ters 83, Ters 85]. These assumptions simplify the matrix elements $M_{\mu,\nu}$ and, for bias energies close to $E_F$, the tunneling current becomes proportional to the Local Density of States $\rho_s$ (LDOS) of the surface at corresponding tip position $\vec{r}_0$:

$$I(V_B) \quad \propto \quad \rho_s(\vec{r}_0, E_F + eV_B). \tag{1.3}$$

Generalizing this approach for higher energies and various tip shapes, the current can be described by an integration within an energy window between $E_F$ and $E_F + eV_B$ over the LDOS of the tip $\rho_t$ and the surface $\rho_s$ as well as over the transmission coefficient $T(E, V_B, Z)$, as sketched in figure 1.1 (b) [Lang 86]:

$$I(V_B) \propto \int_{E_F}^{E_F + eV_B} \rho_s(E) \cdot T(E, V_B, Z) \cdot \rho_t(E - eV_B)\, dE. \tag{1.4}$$

The transmission coefficient is a parameter that accounts for a voltage drop-off in the vacuum region. It depends for instance on the the work functions of tip and sample, and describes how individual states contribute to the tunneling current [Sell 85].

### 1.1.2 Scanning Tunneling Spectroscopy (STS)

The $I(V_B)$ spectroscopy reveals information of the density of states in the tunneling junction. In contrast to the topographic mode of an STM, where the tip sample distance is continuously re-adjusted by a computer controlled feedback system, the $I(V)$ measurement requires, the $Z$ to be constant. Consequently, the feedback loop is switched off once the tip is positioned (in $X$, $Y$ and $Z$), for the time of the spectrum. When the bias voltage is ramped through the desired range, the current is recorded. This characteristic curve carries all information about the LDOS, hidden in the energy integral according to equation 1.4. The LDOS of the surface ($\rho_s$) can be extracted by differentiation, thus the differential conductance ($dI/dV_B$) can be expressed as

$$\begin{aligned}\frac{dI}{dV_B} &\propto \rho_t(E_F)\rho_s(E_F+eV_B)T(E_F+eV_B,eV_B,z)+\\ &+ \int_{E_F}^{E_F+eV_B}\rho_t(E-eV_B)\rho_s(E)\frac{dT(E,eV_B,z)}{dV_B}dE+\\ &+ \int_{E_F}^{E_F+eV_B}\rho_s(E)\frac{d\rho_t(E')}{dE'}T(E,eV_B,z)dE.\end{aligned} \tag{1.5}$$

Assuming constant tip density of state ($\rho_T$) (as for an ideal spherical tip) and transmission coefficient $T(E_F+eV,eV,z)$, the second two terms vanish and in good approximation the differential conductance becomes proportional to the density of states of the sample:

$$\frac{dI}{dV_B} \propto \rho_t(E_F)\rho_s(E_F+eV_B)T(E_F+eV_B,eV_B,z). \tag{1.6}$$

The experimental acquisition of $dI/dV_B$ curves is achieved by lock-in technique. For this purpose, a high frequent sinusoidal voltage $V_{mod}$ of small amplitude is added to the bias voltage $V_B$. The slowly and linearly changing bias voltage is approximated to be constant within the lock-in iteration times (time constant usually $\lesssim 10$ ms). A resulting response signal of the tunneling current can be expressed as

$$\begin{aligned}I(V_B+V_{mod}) \approx I(V_B) &+\tfrac{dI(V_B)}{dV_B}V_{mod}\sin(\omega t) &+\frac{d^2I(V_B)}{dV_B^2}V_{mod}^2\sin^2(\omega t)+\cdots\\ &\Downarrow &\Downarrow\\ &\text{AC}\propto\rho_s(E) &\text{AC}^2\propto\text{IETS}\end{aligned} \tag{1.7}$$

The amplitude of the oscillating component (AC) in the responding tunneling current delivers the first derivative and, thus, is proportional to the surface's density of states.

Besides obtaining the differential conductance curve $dI/dV_B \propto \rho_S(eV_B)$, there are several spectroscopic methods utilizing this lock-in technique that will be named briefly in the following:

- Topographic surface scanning at certain bias energies and simultaneous recording of the $dI/dV_B|_{V_B=const.}$ signal allows to construct a second map with locally

resolved information of the sample's conductance. The so-called *conductance maps* show lateral distribution of the density of states at the corresponding energy $eV_B$.

- As seen from equation 1.7 the second harmonic signal delivers the Inelastic Electron Tunneling Spectrosctrum (IETS) and reflects information of the second derivative of the tunneling current $d^2I/dV_B^2$ [Jakl 66, Klei 73, Stip 98]. For small bias voltages, this reveals information of inelastic excitations during the tunneling process, associated for instance to the excitation of molecular vibrations.

- When the feedback circuit continuously adjusts the tip height according to equation 1.1 during spectroscopy, in order to keep the current $I$ constant, the $dI/dV_B$ presents LDOS in a wider energy window (up to $\sim \pm 10$ V) than in standard STS, because the electric field is kept constantly low and does not cause damaging of surface areas or adsorbates.

- Spectroscopy and lateral data can be recorded simultaneously. In the so-called *Current Imaging Tunneling Spectroscopy* (CITS) the topography is scanned while in each pixel the $I(V_B)$ characteristic curve and $dI/dV_B$ are recorded. The resulting data sets are three-dimensional matrices containing the laterally resolved spectroscopic information. The acquisition of such CITS matrices requires extremely good stability of the tunneling junction in terms of temperature, noise, creep and drift, since they usually take several hours to record.

### 1.1.3 STM Representation of Molecular Adsorbates

The analysis of solid metals and their surfaces provides knowledge about their geometrical structure and about electronic characteristics, both of which are not particular local features and hence much better measurable and resolved by area averaging methods. However, the resolution in real space, provided by STM, qualifies it as a good tool to study local structures with certain topographic electronic or vibrational local features.

Adsorbates and in particular molecules adsorbed on a metal perturb the substrate's structure *i.e.* by breaking the solid's periodicity. Furthermore they influence the surface's electron density locally. Vice versa, the adsorbates carry their own electron systems *i.e.* distributed in populated and unpopulated orbitals, which become affected upon adsorption. The molecular orbitals may interact with the electronic system of the surface in various ways (ranging from a weak distortion to hybridization with surface states). Since the LDOS is the important parameter probed by STM (recall figure 1.1 (b)), interaction phenomena of adsorbate and surface will be reflected in the recorded STM data. The interpretation of topographic and spectroscopic data always has to be done in the context of interaction between surface and adsorbate. Three different contributions to the tunneling process through an adsorbate can be distinguished as sketched in figure 1.2 (a).

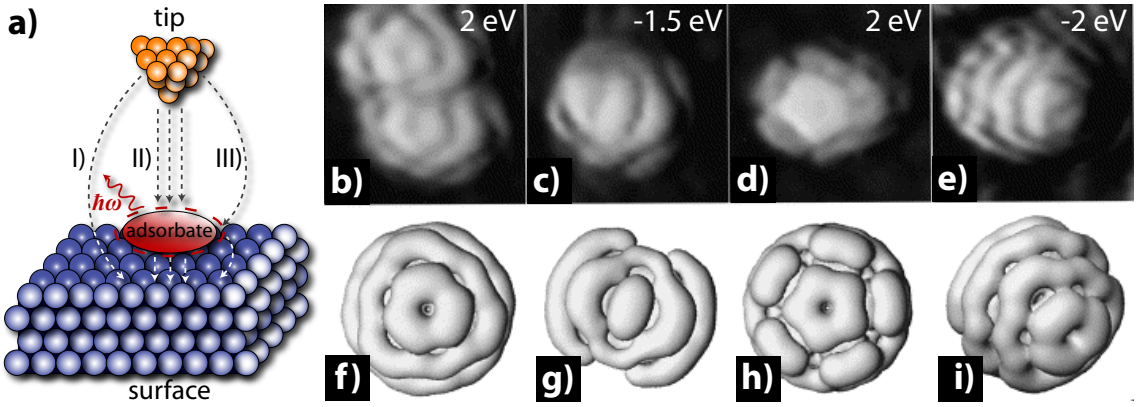


**Figure 1.2:** Schematic view on tunneling processes through molecules: The sketch (a) summarizes all tunneling paths for electrons from the tip to the sample, which add up in the tunneling current: (I) The direct tunneling path through vacuum, (II) resonant tunneling paths through different molecular states, and (III) inelastic scattering of electrons with molecules, exciting vibrations of the adsorbate. (b-e) Comparison of experimental STM images of individual $C_{60}$ molecules on Si(111) obtained at different sample biases, showing resolution of molecular orbitals in different geometries. Calculated shapes of their molecular orbitals (f-i) were performed with the SIESTA programme [Orde 96, Sanc 97], based on DFT. Figure (b-i) from reference [Pasc 00].

I **Direct Tunneling:** The electron tunneling directly from the tip to the surface is determined by the previously seen surface's LDOS, neglecting the adsorbate. When a molecule is present in the tunneling junction, this direct channel has a minor weight to the total current, since the transmission through this channel decreases exponentially with the tip-sample distance. Here, the distance is in general larger than without adsorbate and consequently direct tunneling might only be important, when absolutely no adsorbate resonance contributes to the overall transport. This would be the case, if the sample bias is adjusted to the adsorbate's energy gap.

II **Resonant Tunneling:** When adsorbate resonances, related to electronic states, are involved in the tunneling process an enhanced transmission is observed. This resonant tunneling occurs, when the adsorbate has sufficient LDOS in the probed energy regime. Usually the resonant channel dominates the electron flux between tip and sample, because due to broadening of molecular states, these states are accessible also for tunneling electrons of comparable low energy. If electronic states can be addressed individually by adjusting the bias energy, features in the corresponding STM topography can resemble the related molecular orbitals. Such an example is presented in figure 1.2 (b-i), taken from reference [Pasc 00], where $C_{60}$ molecules are adsorbed on Si(111). They show characteristic topographic shapes for different bias energies. Usually the orbitals closest to $E_F$ determine the molecules' topographic shape. The distribution of adsorbate's resonances in energy are directly seen in spectroscopic $dI/dV_B$ plots.

III **Inelastic Tunneling:** When electrons scatter with molecules, they can excite vibrations of the adsorbate or phonons in the substrate [Temi 08b, Pasc 06,

Fran 09]. Each vibrational mode acts as a channel for the overall electron transport through the STM junction. Depending on the energy regime of the sample bias, differently many modes are activated and contribute to the total tunneling process.

### Topography of Molecules

The interpretation and identification of adsorption geometries of molecules is often a difficult task, in particular when the molecular structures are complex or if the molecules have some internal degrees of freedom. In many cases STM topographies can only be interpreted by comparing them with iso-surfaces of free molecular orbitals, derived from theoretical calculations. They display the points of constant LDOS of certain molecular states and reflect the distribution of the corresponding orbitals in space. In general, this agrees well with the adsorbed molecular structure, when the molecule is weakly coupled to the surface and the free molecular states are not disturbed. Upon complex adsorption processes hybridization, bond formation, surface screening, level alignment (charge transfer), and level broadening can occur. These issues have to be considered theoretically, and usually the whole substrate system needs to be modeled. On surfaces *density functional theory* (DFT) calculation promise to describe such systems better than semi empirical calculations [Repp 05, Lilj 07].

In figure 1.2 (b-i) a study, obtained by J. I. Pascual *et al.* is presented [Pasc 00]. The example shows four topographies (b-e) of $C_{60}$ fullerene molecules adsorbed on a Si(111) surface in different orientations, which display good agreement to DFT calculated iso-surfaces of the free molecules (f-i). The similarities of shapes allows to determine the orientations of the molecules and their ionization states. Comparing the shapes, the authors can deduce the origin of the mapped orbitals responsible for the topographic features. In this example, the special shapes are not only originating from different molecular resonances, but also from the different degeneracies of the highest occupied molecular orbital (HOMO). Depending on the binding site on the surface and the orientation of the fullerene, the symmetry and hence the five-fold degeneracy of this orbital breaks. The resulting orbitals are distributed over a wide energy range around the Fermi level, and hence determine the appearance in the STM topographies.

### Spectroscopy of Molecules

Beside the topographic appearance of a molecular adsorbate, seen in STM data, the alignment of their energy levels can be probed by STS and vibrational excitations can be seen by IETS.

#### Vibrational States

The energy activating a vibrational mode usually lies below $\hbar\omega \approx 200$ mV as depicted in figure 1.3 (a). Such threshold energies for activating vibrational excitations can be obtained in the $d^2I/dV^2$ spectra (IETS), as peaks in the positive range

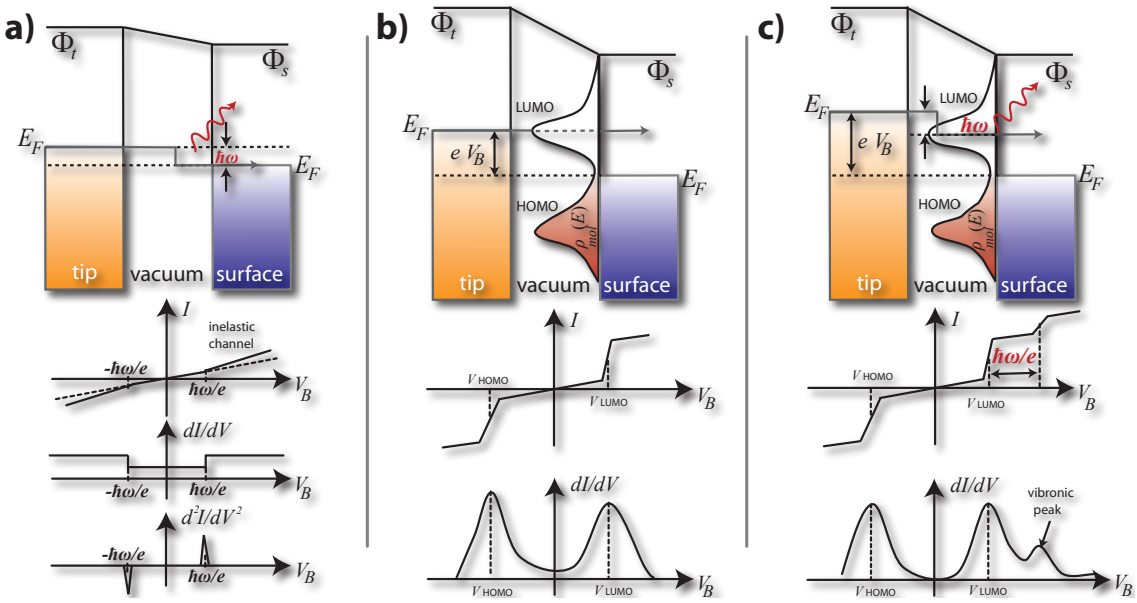


**Figure 1.3:** (a)-(c) Show schematic energy diagrams of the tunneling junction with the work functions of tip $\Phi_t$ and sample $\Phi_s$, the according Fermi energy levels $E_F$, as well as the resulting $I(V_B)$ and derived $dI/dV$ curves below. The applied bias voltage $V_B$ shifts the Fermi levels of electron reservoirs with respect to each other. The size of the energy window between them defines the number of electrons participating in the tunneling process. In scheme (a) inelastic tunneling electrons excite a vibrational mode. The opening of such inelastic channels changes the slope of $I(V_B)$ at energies $\pm\hbar\omega/e$, symmetrically with respect to $E_F$, which are detectable as peak and dip in the $d^2I/dV_B^2$ spectrum. (b) when molecular orbitals enter in the energy window, the tunneling current ideally shows a step in the $I(V_B)$ and a peak evolves in the $dI/dV$. In (c) a vibronic excitation causes a side band of the LUMO resonance in the $dI/dV$ spectrum, separated by $\hbar\omega/e$ above the LUMO.

and symmetrically to $E_F$ as dips in the negative range via lock-in technique. This happens because each vibration opens an additional transport channel contributing to the total conductivity.

Figure 1.4 (a) shows examples of a vibrational spectra of PTCDA molecules on Ag(111). The data have been obtained by R. Temirov *et al.* [Temi 08b]. In the different data sets the STM tip is positioned at different molecular sites. The 47 meV vibration is seen in all the different places, however with different intensities due to different surface coupling strengths. The 33 meV vibration is only observed, when the STM tip is positioned aside of the molecule, where the LUMO has highest intensity. So, these two vibrational modes are the only ones that couple with a large cross section to the LUMO and hence are the only ones observed by STM.

### Electronic States

The probed density of states in the tunneling junction is determined by the electronic system of molecule and substrate according to equation 1.4. Depending on the molecule surface interaction, molecular states align in a specific way with respect to the surface Fermi level. The molecular states closest to the Fermi energy (highest occupied molecular orbital (HOMO) and lowest unoccupied molecular

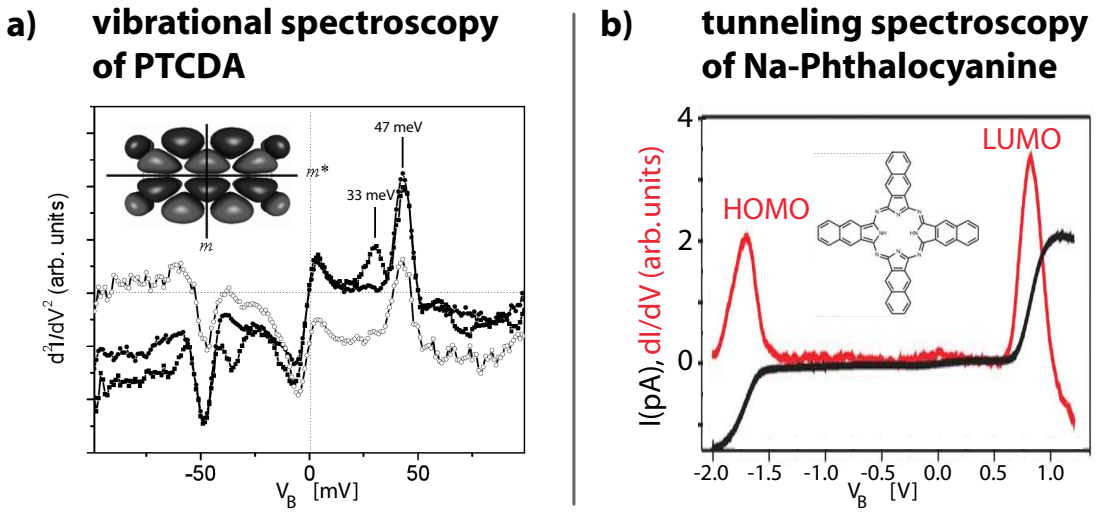


**Figure 1.4:** (a) Vibrational spectroscopy by means of inelastic tunneling through PTCDA molecules at different sites. Examples of (b) resonant elastic spectroscopy (STS) showing the LUMO and HOMO of Phthalocyanine adsorbed on a NaCl bilayer on Cu(111). Figure (a) from reference [Temi 08b]; (b) from reference [Lilj 07].

orbital (LUMO)) can be probed by resonant tunneling. An enhanced tunneling probability is detected, when the energy window $[E_F,\ E_F + eV_B]$ opens for the energy of a given orbital, as seen in figure 1.3 (b). The enhancement can be detected as a peak in the differential conductance $dI/dV$ vs. $V_B$ plot.

One example, where pure molecular density of states are seen, is given in figure 1.4 (b), published by P. Liljeroth *et al.* [Lilj 07]. The HOMO-LUMO gap of $\sim$2.5 eV is clearly seen between the resonances of the HOMO and LUMO, when Na-Phtalocyanine is adsorbed on a NaCl bilayer on a Cu (111) surface. Due to the decoupling of the insulating NaCl bilayer the molecular orbitals stay almost unperturbed.

#### Vibronic States

When molecular states are little broadened, side peaks can be resolved in the $dI/dV$ spectra as seen in figure 1.3 (c). They are associated to a coupling of molecular electronic states and a vibration [Qiu 03, Qiu 04b, Wu 04]. Such side peaks are energetically visible at $\hbar\omega$ above the molecular state, where $\omega$ represents the oscillatory frequency for the inelastic state.

### 1.1.4 Molecular Manipulation

Besides its topographic and spectroscopic capability, the STM has also been developed as a tool for various kinds of manipulations of adsorbates. The STM tip can be used to inject electrons into adsorbates, to apply local electric fields, to push or to pull adsorbates across the surface [Elst 08, Pasc 03, Henz 06, Henz 07, Alem 06, Dri 08, Gros 03, Gril 05, Gril 07, Hla 03, Hla 04, Neel 07, Schu 08, Meye 00].

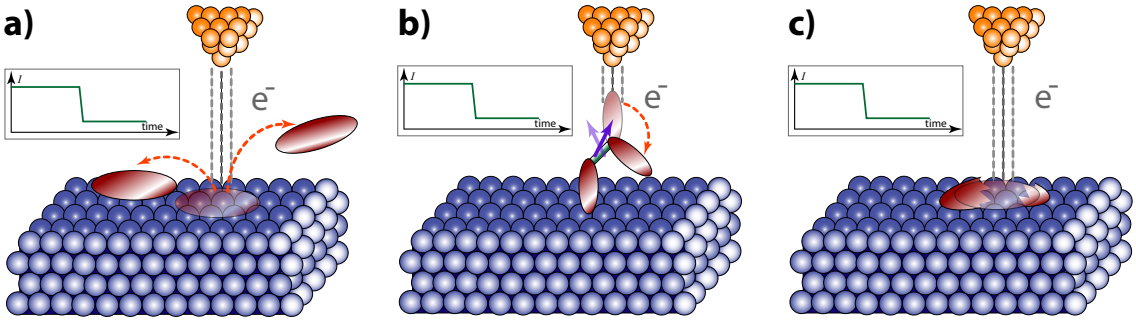


**Figure 1.5:** Scheme of different manipulation experiments. Due to a change of an adsorbate in the tunneling junction, sudden jumps in the current signals are seen. By analyzing how the events depend on the yield, the current or the bias, a picture of the involved processes can be drawn. This is the case for *e.g.* (a) diffusion or desorption, (b) for switching of configuration or spin state or (c) for dissociation or fusion processes of adsorbates.

Hence, isomerization, diffusion, desorption, fusion and dissociation processes can be investigated with the help of this technique. Also contacting of molecules by a single point can be achieved and transport experiments through molecules can be performed [Laff 09, Temi 08a, Temi 08b, Kock 09].

### Electron Induced Manipulation Processes

Tip induced manipulations are interesting methods to induce changes in molecular adsorbates. For instance they can modify molecules that intrinsically display two or more conformational states, configurations or adsorption geometries. The investigation of molecular switches – the main aim of this work – focuses on several processes that trigger switching reactions. Possible mechanisms are vibrational excitation by inelastic processes, excitation of ionic states or the influence of an electric field [Stok 98, Last 05, Sloa 05].

A simplified theoretical description of a molecular switch is given by a double well potential ($V_{pot}$), where two minima represent these two switchable states (*e.g.* geometrical configurations) A and B, as displayed in figure 1.6 (a). The reaction coordinate ($r$) is for simplicity one-dimensional, representing a complex motion in space by the trajectories of many nuclei. In this picture, we can rationalize the switching from A to B by three different electron induced processes: excitation of ionic states upon electron attachment (*yellow arrow*), direct vibrational excitation (*red arrow*), or vibrational ladder climbing (*green arrows*) [Cond 26, Cond 28, Cool 36, Pasc 03].

When molecular switching results from vibrational or electronic excitations (ionization), the transition only occurs above a threshold value in energy, which is related to the type of excitation induced. It identifies the electronic state or the vibrational mode involved as indicated by the yellow and red arrows in figure 1.6 (a), respectively. For electronic excitations, the threshold energy is related to the alignment of molecular resonances and can be compared with corresponding peak

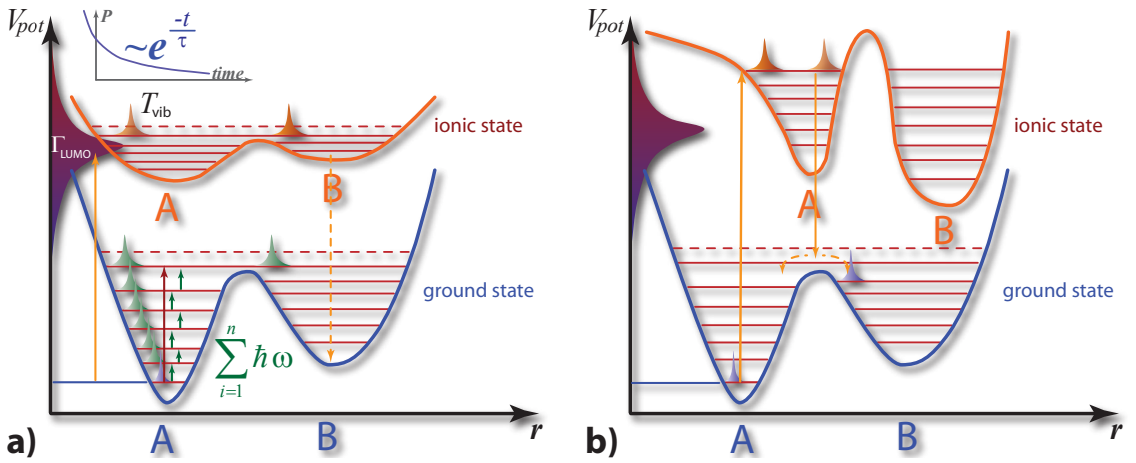


**Figure 1.6:** Neutral and ionic double well potentials representing a switchable system with two states in (a) the minima of both potential are at same coordinates, in (b) they are shifted with respect to each other. (a) Shows various electron induced activation mechanisms, starting from the ground state in A: (**i**) an electronic excitation (*yellow arrow*) into the ionic molecular state can initiate switching, where the ionic potential is somewhat flatter. Hence the transition to B is more likely than in the deep minima of the ground state. (**ii**) Direct vibrational excitation (*red arrow*) directly allows the molecule to overcome the potential barrier or (**iii**) multiple vibrational excitations (*green arrows*) climb a ladder of vibrational modes in a Frank-Condon principle. (b) Shows a configuration of ground and ionic state's potential, where fast excitation- and de-excitation processes can cause a configurational change from A to B, because the molecule's coordinate is found in the proximity of the ground state's local maximum after the de-excitation.

positions in a $dI/dV$ spectrum. In the case of an excitation via multi vibrational modes, the energy sum of all modes involved, allows to overcome the energy barrier from one molecular configuration A to the other B by means of the Frank-Condon principle [Cond 26, Cond 28, Cool 36, Pasc 03]. Since each mode needs one electron to scatter with, such multi electron processes can be identified by analyzing the yield for switching as a function of the current.

In order to inspect the likelihood of the different processes initiating a configurational change to occur, we will roughly estimate the timescales of the possible processes involved and compare them with the duration of a nuclear motion and with the rate of tunneling electrons.

### Electron Attachment

Typical spectroscopic line widths of molecular electronic resonances amount to ∼300 meV, while broadening effects due to the experimental setup can be neglected.[1] From this width a lifetime of $\tau_{LUMO} \approx 10^{-15}$ s can be extracted. The tunneling rate with a typical feedback current of 1 nA is $\Gamma_{tunnel} \approx 10^{10}$ s$^{-1}$, meaning every $1/\Gamma_{tunnel} \approx 10^{-10}$ s an electron scatters with the molecule. This highlights

[1] The spectroscopic lines usually appear broadened due to the lock-in modulation of $E_{mod} = 10$ meV and due to thermal effects of $k_B T \approx 1$ meV.

that a multiple ionized state is not probable due to a good surface coupling.

The minimum duration of the nuclear motion, describing the switching event can be approximated by a quarter of the period ($T_{vib}^{ion}$) of a higher vibrational mode in the ionic potential. Usually such vibrations are seen at energies of $\hbar\omega^{ion} \approx 10$ meV, which results in a timescale of $T_{nuc} = \frac{1}{4}T_{vib}^{ion} \approx 10^{-13}$ s for this kind of motion. Compared to the lifetime of the ionic state, which is exponentially depopulated according to $e^{-t/\tau_{LUMO}}$, the ionic excitation yields a very small final switching probability.

### Vibrational Excitation

Vibrational ground state excitations exist for an estimated time of $\tau_{vib} \approx 10^{-11}$ s. Hence, they last long enough for triggering a configurational motion in the molecule and are very efficient. However, their excitation energy of ∼10 meV does usually not match the heights of configurational barriers of some 100 meV. A coherent excitation of multiple vibrational modes as indicated by the red arrow in figure 1.6 (a) would enable the switching of configuration. The threshold for a configurational change is then directly associated to the barrier height of the ground state potential.

The stepwise Frank-Condon excitation is quite unlikely for triggering the switching mechanism, due to the discrepancy of the vibrational life time ($\tau_{vib} \approx 10^{-11}$ s) and the rate of tunneling electrons ($\tau_{tunnel} \approx 10^{-10}$ s). This discrepancy results in a probability of $10^{-5}$ for one electron to scatter with a single excited vibrational mode. With all $n$ involved modes, this probability shrinks to $(10^{-5})^{n-1}$.

| type of process | duration or life time |
|---|---|
| tunneling process | $1/\Gamma_{tunnel} \approx 10^{-10}$ s |
| vibrational excitation | $\tau_{vib} \approx 10^{-11}$ s |
| nuclear motion | $T_{nuc} \approx 2 \times 10^{-13}$ - $10^{-12}$ s |
| electron attachment | $\tau_{LUMO} \approx 10^{-15}$ s |

**Table 1.1:** List of approximate time scales and related rates for processes and excitations that qualify as electron induced switching mechanisms.

### Influence of the Potential Landscape

The precise nuclear motion of the configurational switch is given by a complex potential landscape. In the simplified one-dimensional description, not only the ground state but also the shape of the ionic potential and its relative orientation with respect to the ground state's potential are important, when excitation or ionization processes are involved.

Figure 1.6 (b) shows an example situation, where the ionic potential surface has a larger barrier between the two configurations A and B than the ground state potential. Hence, the configurational reaction will hardly occur in the ionic state. Still, the ionization initiates a possible configurational change, because of the special alignment of the anionic minima with respect to the ground state's minima.

After an excitation and subsequent de-excitation process at the coordinate A, both processes confined as fast vertical transitions, indicated by yellow arrows, the configurational coordinate is found near the potential's local maximum. Here the relaxation into both ground state configurations A and B is possible. Such a complex process can be observed even if the ionic state is short-lived. The considerable geometrical different alignment of minima of the ground and ionic state can be caused from *e.g.* an external field, interacting with polar parts of the molecule.

## 1.2 Technical Realization

To obtain results of all the previously discussed kinds of phenomena and to investigate the adsorbate's properties and processes in the tunneling junction, an experimental setup is required with adequate stability, working at low temperature. In the time from summer 2004 until summer 2005 a low temperature STM has been built up during my diploma, following the design of J. I. Pascual. In the following, the setup will be introduced briefly and some examples will illustrate its performance.

### 1.2.1 Setup

The ultra high vacuum (UHV) setup, in which the STM apparatus is located, is divided into a preparation chamber and a measuring chamber. The preparation chamber is equipped with common devices for sample cleaning (ion sputtering, annealing, rest gas analysis), with a sample garage, and with a custom-built Knudsen cell for molecule sublimation. The sample can be transferred into the measuring chamber by means of a manipulator with a liquid helium cooled flux cryostat.

#### Sample Preparation

Metallic single crystal samples are cleaned by repeated cycles of sputtering and annealing. The annealing temperatures are at approximately 70% of the melting temperature and listed in table 5.1 in the appendix. The sputtering with $Ne^+$ ions with 1.5 keV is done under normal incidence. Molecules are sublimated onto the cleaned single crystal kept at variable temperature. Sample temperatures in the following of this work refer to the temperature of the sample during sublimation. The sublimation temperatures in the Knudsen Cell for the different molecules are listed in table 5.2 in the appendix. In some cases the sample is subsequently annealed to higher temperatures to allow the adsorbates to rearrange and stabilize. After precooling by the flux cryostat the sample is transferred into the measuring chamber and clamped in the measuring stage.

### STM-Head

The STM measuring stage is permanently kept at low temperatures, attached to commercial liquid Helium (lHe) bath cryostat. Two metallic cylindric shields, at temperatures of 70 K and at 5 K, are surrounding the measuring stage and the cryostat, protecting the measuring stage from outside radiation. On the one hand a base temperature of constantly 4.7 K is reached by this construction, on the other hand it causes a very low lHe consumption of ∼8 ml/h. Three sets of small windows are inserted into the shields for some view to the measuring stage, needed *e.g.* while transferring the sample. Four shutters (three from the sides and one from the bottom) in the shields allow mechanical access:

- to insert the sample,
- to allow manipulators to clamp the sample stage or un-clamp it for mechanical damping while measuring,
- to tune the tip-sample distance,
- to exchange the tip,
- and to dose gas in situ.

Drawings of the STM are shown in figure 1.7 (a, b): The STM is attached to the lHe cryostat by a plate on top. The measuring stage can be clamped onto a plate (violet) (for transferring the sample) or un-clamped (for measuring) with a screwing mechanism from the bottom. In the un-clamped position (as shown) the sample stage is hanging freely from three springs and six metal wings underneath act against permanent magnets for eddy current damping. An elevator controlled from the side can tune the tip sample distance. For measuring, the sample holder is pushed into the sample stage with the manipulator from the preparation chamber, and is fixed by a double spring mechanism.

When the sample stage is un-clamped, the scanner stands on a threefold circular ramp of the sample holder (see figure 1.7 (b)), where the sample is attached from underneath[2]. Sapphire balls at the three outer piezo sticks act as feet for the scanner. By applying voltage signals to the different segments of the outer piezo elements with smooth line shape the tip is moved with high precision. Erratic saw tooth signals cause a slip and stick motion. Hereby the scanner can be moved over the ramp. Rotational motion adjusts the tip-sample distance. The central piezo element is responsible for the tip height controlled by the feed-back loop in a constant current mode. The U-shaped part attached to the sample holder is used as a handle for sample transferring with the manipulator from the preparation chamber. Two ceramic cylinders hold electrodes for contacting to a bi-metal temperature gauge.

In all our experiments we use tungsten tips, that were electrolytically etched in sodium hydroxide solution (NaOH). The tip is placed inside a stainless steel tube located in the central piezo element, connected by electrically shielded cables. All

[2]The fixing of sample in the sample holder has been improved in the last year by constructing a triangular supporting plate (see figure 5.1 in the Appendix).

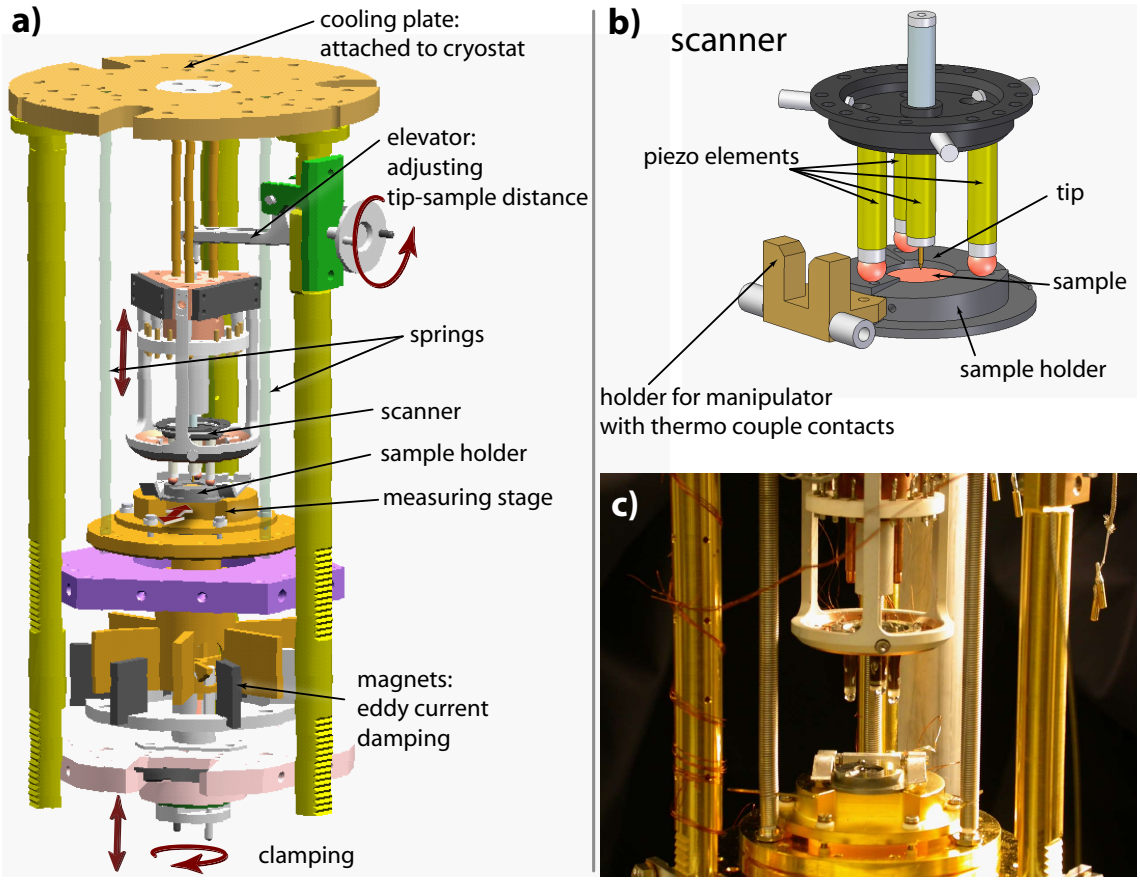


**Figure 1.7:** The setup of the constructed STM head: (a) CAD drawing, showing clamping and damping mechanisms of the measuring stage. It is coupled to the lHe bath cryostat by the upper plate. (b) Photograph of the same view as in (a) clearly seen three of the four piezo sticks with sapphire balls as feet and the tungsten tip. (c) CAD drawing of the scanner on the three fold circular ramp made from molybdenum, which also acts as sample holder with two contact pins for temperature recording while preparation.

cables reaching the STM head (for steering the piezo motion, for applying the bias voltage, for temperature reading and the current cable) are guided through the lHe cryostat and out of the UHV system.

Figure 1.7 (c) shows a photograph of the STM. Here the sample stage is clamped, causing a larg distance between sample and tip. The fixed position of the sample holder allows to grab it with the help of the lHe flux cryostat and transfer it into the preparation chamber or back.

### Data Acquisition and Processing

After amplification (gain of typically $10^8$ V/A or $10^9$ V/A) the tunneling current signal is recorded by a commercial STM electronics, that controls the $X$,$Y$ and $Z$ position of the tip [Meye 96, Meye 98]. The feedback process is implemented in an autonomously working *digital signal processor* (DSP) board. The output

parameters like bias voltage or feedback current are set by the software and also the scanner motion is controlled via the PC. Voltage ramps for spectroscopy can be defined in the software and the resulting topography data, current, and optional spectroscopy data can be recorded and saved. For spectroscopy measurements an external lock-in amplifier is used, outputting the sinusoidal $V_{mod}$, added to the bias voltage. The current is guided into the lock-in amplifier and the response signals from the lock-in amplifier are recorded via extra channels in the STM electronics simultaneously to the current.

The topographic and spectroscopic maps shown in this thesis are subsequently processed and treated digitally with the help of the WSxM software [Horc 07].

### 1.2.2 Performance

The following section shows various measurements proofing that our design is well suited to perform very sensitive topographic and spectroscopic measurements. Due to its compactness the setup has high stiffness resulting in a high stability of the tunneling junction. In particular the symmetry compensates piezo creep and thermal drift very well. The good thermal coupling to the lHe reservoir allows very fast cooling to the equilibrium temperature after transferring ($\lesssim$ 20 min), which results in a very little consumption of cryogenic liquids.

#### Atomic resolution

In a first step of optimization the clean surface of Au(111) was mapped with the STM and atomic resolution has been obtained. By the atomic periodicity the lateral piezo motion can be calibrated with a remaining uncertainty of $\lesssim$10%. The calibration needs to be rechecked once in a while, because the polarization of piezos is weakened slowly.

Figure 1.8 (a) shows one of the first topographies obtained with this equipment (on October, $12^{th}$ 2005) that shows atomic resolution of an Au(111) surface. From the tunneling parameters (comparably low $V_B$ and high $I$), we can deduce a very narrow tunneling gap, proving the comparably good stability of the tunneling junction. Beside the fine corrugation with $\sim$0.04 Å height resulting from the atomic lattice, a wider structure is obtained, seen in four brighter lines. This is the *reconstruction* of the Au(111) surface with a periodicity of 22 lattice sites [Bart 90, Nara 92]. It is caused by the release of surface tension and can be seen as domain walls between areas, where the topmost layer assembles in two different geometries with respect to the lower lying ones. In the top layer the Au atoms are located either in *fcc* or *hcp* sites, forming periodic domains along the brighter lines. The modulation causes that two more atoms fit per $(22 \times\sqrt{3})$ surface unit cell.

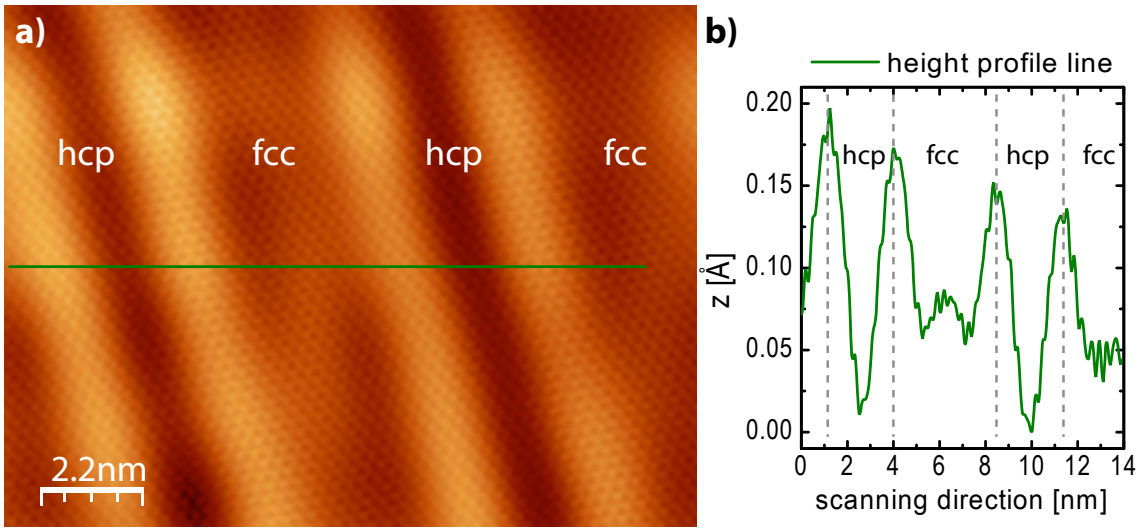


**Figure 1.8:** (a) STM topographic map of a bare reconstructed Au(111) surface. The bright lines are domain walls between areas, where the first atomic layer is stacked in either a *hcp* or *fcc* manner with respect to the underlaying layers. This very stable reconstruction is the reason why two additional atoms fit into a surface unit cell of $22 \times \sqrt{3}$ lattice constants [Nara 92]. The fine corrugation results from individual atoms. The local electron density on the surface, which is probed here, modulates periodically according to the nuclei lattice. From the knowledge about the lattice constant the lateral motion of the STM can be calibrated. (b) Shows the line profile along the green line in (a). The reconstruction is corrugated by $\lesssim$0.2 Å in height the atomic corrugation is of $\sim$0.04 Å height. Scanning condition: $V_B = 303$ mV; $I = 6.7$ nA.

### Superconducting Gap of Lead

Below the critical temperature $T_c = 7.2$ K lead becomes superconducting. In the electronic fingerprint this effect results in an energy gap of $\sim$2 mV width. In the tunnel junction this gap is measurable with double the width, when the STM tip is also covered with lead. Figure 1.9 (a) shows this in a scanning tunneling spectrum using a lock-in modulation of only $V_{mod} = 0.1$ mV. The sharpness of the resonances and the aspect of the gap shows very good signal to noise ratio, proving how sensitive the setup is and what influence the low equilibrium temperature has.

### Inelastic Vibrational Spectroscopy of $C_{60}$

Vibrational spectroscopy detects very small changes in the slope of the current voltage characteristics namely in the range of $\sim$1-10% of the conductance. Thus, for performing IETS measurements very good stability is needed for the tunneling junction, since longer acquisition times improve the signal to noise ratio of the spectra. With the presented STM the vibrational modes of the $C_{60}$ molecule could be studied adsorbed on a Pb(111) surface, as seen in figure 1.9 (b). Seen are nine pairs of peaks and dips that could be associated to a selection of vibrational modes of certain symmetry.

Also this measurement shows that the tunneling junction of the STM is of exceptional stability. For the duration of the spectrum (300 s) the tip probed one

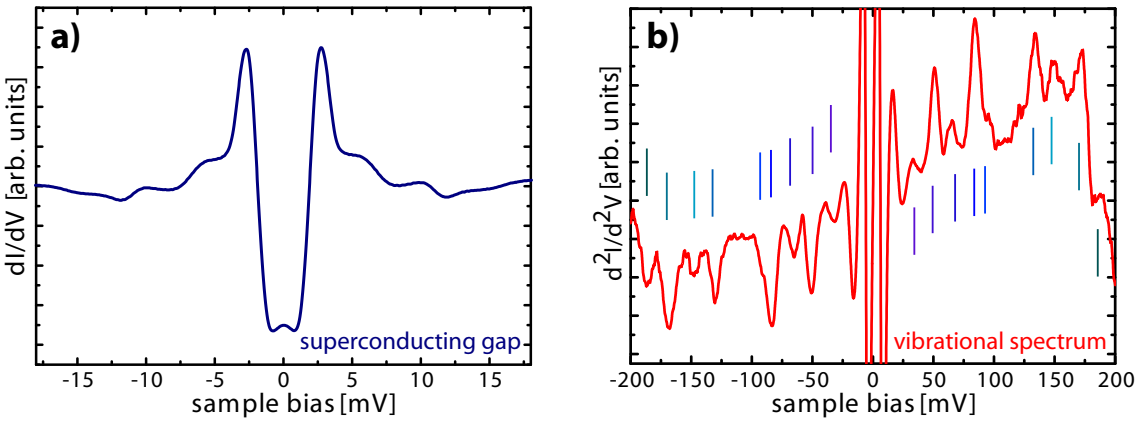


**Figure 1.9:** (a) $dI/dV$ spectrum of superconducting Pb(111) measured with a Pb tip at $4.8$ K. The plot shows a gap of $\sim$5 meV width [Kons 08]. (b) shows a vibrational spectrum of $C_{60}$ adsorbed on Pb. Due to the folding to the LUMO nine vibrational resonances can be obtained in the $d^2I/dV_B^2$ spectrum by lock-in technique [Fran 09].

individual molecule without disturbance. This example proves on the one hand the sensitivity of the apparatus and on the other hand its mechanical stability.

## 1.3 Adsorption Process

The adsorption of molecules is expected to influence many molecular characteristics. The approach of molecular states interacting with states of surface electrons, as described before, is already a complex process. Here we want to focus on this field from a more general point of view. We will classify interaction mechanisms, that come into play upon adsorption, discuss how adsorption potentials change in the interplay of two different species, and return to the aspect, how molecular states get affected upon adsorption.

### 1.3.1 Classification of Attractive Interactions

In order to understand the primary effects of adsorption, we want to classify attraction forces. The corresponding interaction mechanisms may act between surface and molecules, between different molecules or they can stabilize the molecular structure itself. In table 1.2 following they are listed scaling from the weakest to the strongest interaction.

#### Van der Waals Interaction

The weakest interaction is determined by a quantum mechanical effect and called *van-der-Waals* interaction. It is also named induced *dipole-dipole interaction*, *London interaction* or the *interaction of fluctuating dipoles*. The closed shells of valence electrons in noble gases or the fully saturated electron configurations of molecules, cause a spherically symmetric electron density if averaged over time [Ashc 01].

| type of bond | typical length | typical binding energy |
|---|---|---|
| v.-d.-Waals | $\gtrsim$ 4Å | 0.5 - 5kJ/mol $\widehat{\approx}$ 5 - 50 meV/molecule |
| $\pi - \pi$ | $\sim$ 4Å | 5 - 15kJ/mol $\widehat{\approx}$ 50 - 150 meV/molecule |
| hydrogen | $\sim$ 1 - 5Å | 5 - 150kJ/mol $\widehat{\approx}$ 5 - 150 meV/bond |
| metal-organic | $\sim$ 2 - 4Å | 50 - 100kJ/mol $\widehat{\approx}$ 50 - 100 meV/bond |
| covalent | $\sim$ 1 - 3.5Å | 100 - 1000kJ/mol $\widehat{\approx}$ 0.1 - 1 eV/bond |

**Table 1.2:** List of attractive interactions scaling from the weakest to the strongest. The typical bond lengthes scale inversely with the strength of the interaction.

However, small fluctuations of the atomic core and the electron distribution result in induced fluctuating dipoles, which couple to neighboring atoms inducing dipole fluctuations there [Kitt 02]. The dipole fluctuations can be modeled by harmonic oscillators, whose total energy $U$ depends on the square of the dipole moment $\vec{p}^{\,2}$. This does not vanish in the time average (in contrast to $\vec{p}$), and thus causes an attractive interaction

$$\Delta U \propto -\frac{\alpha \vec{p}^{\,2}}{r^6},$$

where $\alpha$ is the polarisability. The typical bond lengthes are larger than 4 Å.

### $\pi$-$\pi$ Interaction

Aromatic compounds usually are planar structures resulting from $sp^2$-hybridized orbitals. The resulting hexagonal phenyl rings show $\pi$-orbitals of delocalized electrons, in both directions perpendicular from the aromatic planes. The interaction to other aromatic units takes place by the overlap of such $\pi$-orbitals, which results in a dispersive attraction [Rapp 00]. On the other hand, the electrostatic repulsion causes a lateral shift from one aromatic layer to the next (parallel-displaced orientation). This $\pi$-$\pi$ interaction strongly acts on polycyclic hydrocarbons and becomes stronger, when the number of participating $\pi$ electrons increases. For supra molecular chemistry as well as for the crystal structures of organic molecules it plays an important role [Fern 06]. Another popular example of $\pi$-stacking occurs in purine or pyrimidine rings, which are positioned almost perpendicular to the length of DNA strands. These neighboring aromatic units of adjacent bases add stability to the supra molecular structure. On surfaces a very similar interaction is found, where a molecular $\pi$-system tends to maximize the overlap with the surface's electron system, by adsorbing in a planar configuration.

### Hydrogen Bond

When the hydrogen termination of one molecule interacts with a non-hydrogen atom, also named *proton acceptor*, hydrogen bonding is observed. The covalent bond coupling a hydrogen atom to a molecule requires the hydrogen's electron to hybridize with molecular states. This causes an electron depletion at the remaining proton, forming a partial positive charge. In distances of up to 5 Å the polarity of

the covalent bond can attract saturated or partial negatively charged moieties. The prominent example of ice shows hydrogen bonding between water molecules. The solid phase of water ($H_2O$) builds a complex crystal of the oxygen atoms, where the hydrogen's protons mediate bonds of $\sim$2 Å [Ashc 01, Kitt 02].

For weakly adsorbed atoms or molecules hydrogen bridges are one of the most common driving forces for self-assembling. Planar adsorbed molecules orient to their counterparts in such a way, that the largest number of hydrogen terminations get saturated by non-hydrogen atoms of neighboring molecules [Henn 08a]. As a result, well-ordered structures of molecules assemble upon thermal activation. The final structure is then stabilized in certain orientations and the number of hydrogen between the molecules usually determines the stability of adsorbed clusters.

### Covalent Bond

When valence electrons of neighboring atoms are shared between two nuclei, reorganization of orbitals occurs, which is called hybridization of the free atomic orbitals. The hybridized orbitals can display a bonding or anti-bonding character and hence act attractive on the two reactant atoms, when the bonding orbital is energetically favored. The resulting covalent or chemical bonds can be classified in $\sigma$ or $\pi$ bonds depending on the character of the initial orbitals. The electron population of bonding orbitals determines the order of a bond (single-, double-, or triple bond) and hence its rotational flexibility and strength.[3] Single bonds are generally of larger extend and weaker than double bonds. Hence, accumulation of charge by means of orbital redistribution is a sign for bond stiffness, charge depletion is a sign for a weak bond. The strength of covalent bonds is given by the electronegativity of its two counterparts.

Covalent bonds are forming molecules and they become important for classifying our adsorbates. When adsorbates *chemisorb* on surfaces strongly the formation of a covalent bond between surface and adsorbate can often be observed.

### Coordination Bond

Between transition metals and ligands, mostly atoms (H, O, Cl, etc.) or molecular fragments coordination bonds can form, building so-called metal-ligand- or metal-organic-complexes [Jean 05]. These complexes can be understood either in the framework of weak covalent-like bond formations or by an interaction of induced ions with asymmetric charge in both counterparts.

Metal atoms tend to the valence electron configuration of noble gases in their period [4]. This trend attracts electrons of non-bonding orbitals (radicals or lone-pair electrons) of ligand units, when the electronic levels of the ligand orbitals and empty metal states are of comparable energy. In consequence the charge at at the metal gets redistributed. All non-interacting metal electrons condense in a $nd^x$-like

[3] Bonds of odd bond order are free to rotate, bonds of even bond order are fairly stiff.
[4] $[nd^{10}(n+1)s^2(n+1)p^6]$-configutation

configuration. The occupied ligand orbitals, such as lone-pair electron orbitals, combine directionally with the free metal states.

Usually the coordination bonds are constrained to octahedral or tetrahedral geometries dependently on the strength of the bond, but also planar triangular or linear arrangements are observed [Shan 75]. They typically present lengthes of $\sim$ 4 Å. This type of interaction is found when, for instance, metal atoms are embedded in molecules (spin-cross-over complexes) or in polymer materials designed with predefined nano-meshes that build for instance membranes for specific reactants [Mena 08]. Also on surfaces such nano-meshes can self-assemble upon co-adsorption of metal atoms and molecular ligands, forming metal-organic complexes [Step 07, Schl 07, Schl 08].

### 1.3.2 Complexity of Adsorption

It has been stated that adsorption is a complex process, when observing individual atoms or molecules. One differentiates between physisorption and chemisorption, the former is a weak interaction and the latter is a rather strong coupling. However, the importance of these two terms lays in understanding qualitatively the different adsorption processes, resulting in consequences for the adsorbing species. The two types of interaction are usually mediated by different interaction mechanisms. Physisorption is usually van der Waals-like, of $\pi$-, or of hydrogen bond character, while chemisorption implies the formation of a covalent bond. There are usually more than one chemisorption states of different strength that might differ in orientation, coordination, or molecular configuration.

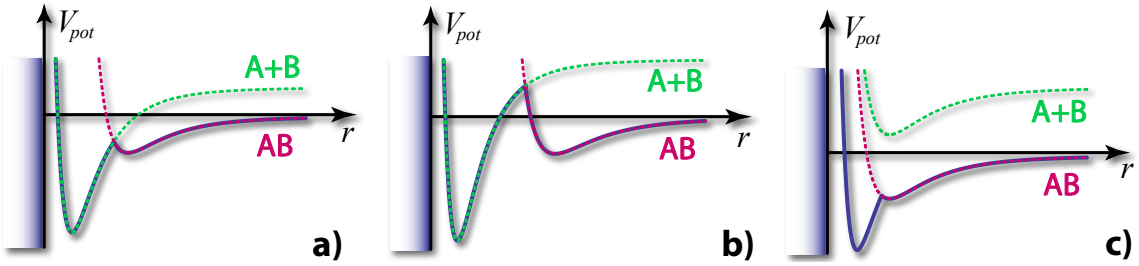


**Figure 1.10:** Schematic diagrams of the potential energy of an adsorbate-substrate complex to three different ground state configurations: (a) dissociative chemisorption; (b) molecular physisorption; (c) molecular chemisorption (Lennard-Jones, 1932) [Zang 88].

The different adsorption processes can be described by *energy* versus *reaction coordinate* diagrams. The energy loss or gain normalized to the total energy of the isolated species (substrate and adsorbate infinitively separated) can be displayed versus the distance to the substrate, versus the internal coordinates of the adsorbate or substrate, or versus a more complex reaction coordinate ($r$). A. Zangwill clarifies this in a simplified model of a two species adsorption process [Zang 88]. Figure 1.10 shows qualitatively three examples of the adsorption modeled by Lenard-Jones

potentials. The dashed lines correspond to the physisorbed potentials of the individual adsorbates (A+B) or the molecular species (AB) respectively. Depending whether the crossing point of both potential curves is below or above zero and depending on the detailed shape of the curves, the ground state of the adsorbates vary.

Figure 1.10 (a) shows that the system gains energy upon spontaneous dissociation as the molecule (AB) approaches the surface. In figure 1.10 (b) the individual species (A+B) form a strong chemisorption with a deep potential minimum, which is not accessible for the compound (AB), unless extra energy mediates this process. In figure 1.10 (c) two molecular states are present, while the dissociated species are not favorable at all. The weaker physisorbed state is the *precursor state* for the strong chemisorbed state, visible in the deep minimum.

Since special chemical reactions can be mediated by the surface in this way, it becomes obvious, why catalysis become an important tool for industry, benchmarked by the Nobel Committee in 1918, 1931 and 2007 [Ertl 90, Ertl 08]. In such complex adsorption processes, the temperature plays an important role, since it delivers energy to the systems, making different adsorption and precursor states accessible.

The complexity of the previous examples for a simple molecule consisting of only two atoms indicates already how challenging the complete understanding of adsorption will be, when more atoms and more degrees of freedom come into play. For instance, in the case of switchable molecules, the adsorption strongly influences the switching ability, even if it is not a matter of dissociation but internal molecular motion. A larger system will have a larger number of stable or semi-stable configurations, adsorption sites or complex precursor states, which may not be simply classified by chemi- or physisorption anymore. Surface interaction hence modifies the characteristics of a pure gas-phase molecule non-trivially by charge screening, energy level alignment and broadening.

### 1.3.3 Electronic Effects upon Adsorption

In the tunneling process through molecules electronic states are probed due to a very short-lived attachment or detachment of electrons, depending on the polarity of the sample bias. The free molecule can be represented by a structured system of electrons distributed in orbitals. Each molecular orbital is related to an energy level. The levels are sharp and well defined in energy, such that the electronic gap of the free molecule is given by the difference between ionization potential (IP) and electron affinity (EA).

The condensation of molecules and the adsorption onto a metal surface have strong influence on the electron system. In polarisable surrounding, mobile charge carriers screen the molecular electron distribution (see figure 1.11 (b)). Due to the coupling to molecules in their vicinity, the level's line shape broadens. This is also reflected, by the reduced life time of electronic resonances with respect to the free molecular case.

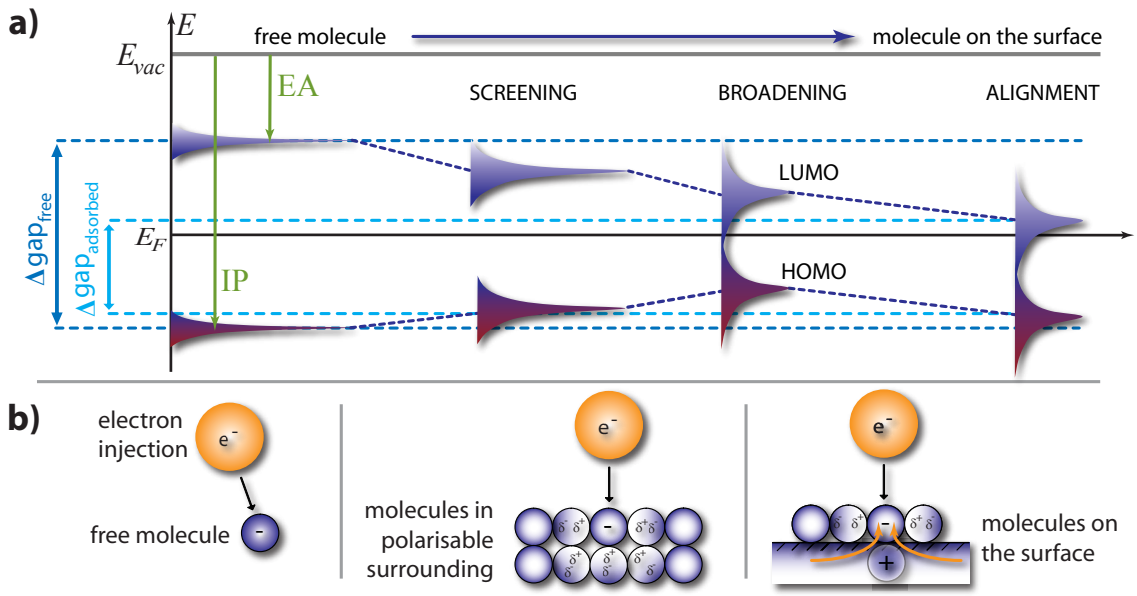


**Figure 1.11:** The adsorption can influence molecular orbital resonances. (a) The resonances of occupied and unoccupied molecular orbitals define an energy gap between ionization potential (IP) and electron affinity (EA). In a polarisable surrounding (such as neighboring molecules or a surface), mobile charge carriers rearrange and screen the adsorbates' states. Consequently, the width of the gap is reduced. When coupled to a metal surface the sharpness of resonances suffer according to short excitation lifetimes. Due to charge transfer into the molecular states, orbitals might get populated or depopulated, which results in the rearrangement of individual states in energy, but also may cause an image charge in the substrate. That further screens the molecular orbitals. (b) Schematic view on the different effects: (*left*) electron injection (extraction) into the free molecule probes the electron affinity level (ionization potential); (*middle*) in polarisable surrounding the local partial charges $\delta^+$ and $\delta^-$ rearrange; (*right*) besides screening, charge transfer occurs, and image charges modify the gap.

On a surface, the molecular orbitals partially donate or accept electrons. The charge within the molecule but also in its surrounding will redistribute until an equilibrium of the affinity levels is reached. Thus the orbital levels will get populated or depopulated and the energy levels levels will align in the electrostatic arrangement with respect to the surface's Fermi level.

The interaction of surface and adsorbate by all these effects causes a redistribution of electronic states. The STM can probe the influence of the molecule on the surface (*e.g.* population or depopulation of surface's states) with local resolution, but not the characteristics of an independent molecule, unless the coupling of surface and adsorbate is weak enough and can be neglected.

## 1.4 Molecular Switches: Example Systems

Molecular switches are an attractive endeavor to control the functionality of a molecule (structure, color of appearance, conjugation, spin) by the use of external stimuli

[Feri 01]. A molecular switch requires two stable configurations and an accessible configurational/electronic pathway connecting them. Therefore, it also represents an interesting workbench to explore fundamental processes regarding the interaction of light, electrons, and external fields with molecular degrees of freedom. Many different molecular species have been proposed as switches and have shown promising results in gas phase or solution. In a brief overview, they are grouped in three different classes, which address completely different switching mechanisms: ring-opening-/-closing-reactions, spin-switching, and *cis-trans*-isomerization.

### 1.4.1 Ring-Opening/Closing Reactions

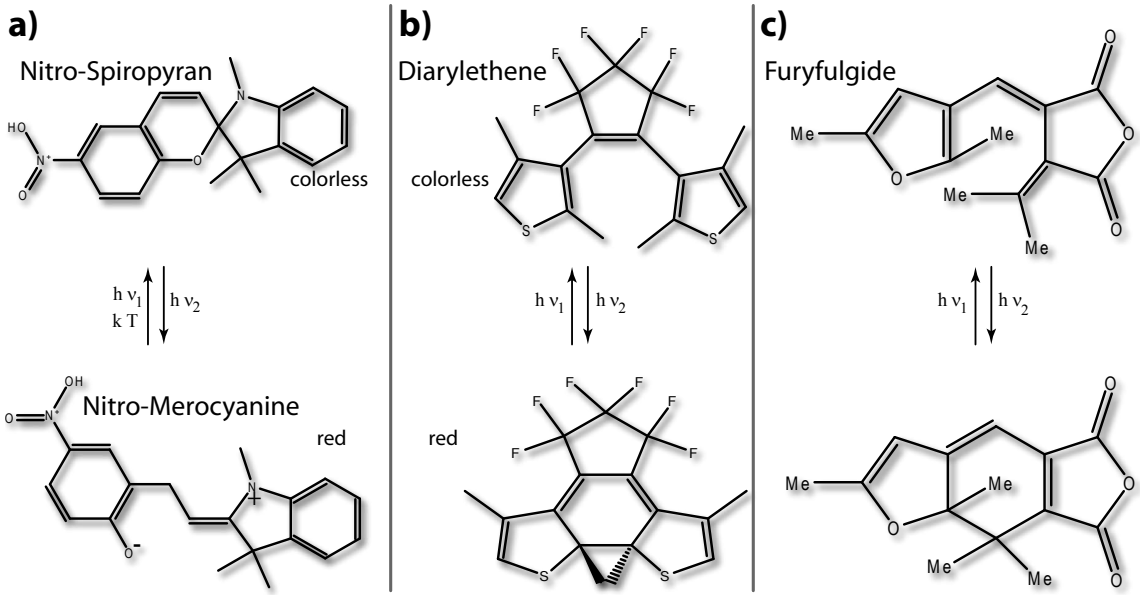


**Figure 1.12:** Ring-opening transformation of (a) spiropyran into merocyanine (b) of diarylethene, (c) and of furyfulgide molecules.

One mechanism that qualifies as molecular switch, implies a small chemical reaction. The cleavage or formation of a bond within the molecule's framework, causes the opening or closing of a molecular ring. The electronic structure changes by such a transformation, such that molecular properties as electron conjugation or color gets affected. In figure 1.12 the isomer spiropyran transforming into merocyanine (a), two conformers of diarylethene (b) and furyfulgide (c) are shown [Irie 88, Mats 04, Amim 05, Pian 09]. In all cases, the molecules are known to switch upon irradiation of light. Their overall size does hardly change during the transformation. Hence, the molecules may qualify as a switch between fixed leads.

### 1.4.2 Switching the Magnetic Moment: Spin State

In analogy to conventional storage media, where data bits are saved in domains of different magnetization, also an individual spin can be used as the smallest unit of magnetic data. The readout of an individual spin has been proven by *e.g.* spin resolved STM technique [Bode 98, Piet 00, Hein 00]. Still, individual spins have rarely

been investigated. A spin bit for instance could be embedded within a molecule, that carries a weakly coupled atom with a singly occupied electronic state [Tsuk 09].

### 1.4.3 *Cis-Trans* Isomerization

*Cis-trans* isomerization is the main field of investigated molecular switching mechanisms in this work. By the example of azobenzene the detailed switching mechanism will be discussed in the next section. Here we briefly introduce the *cis-trans*-isomerizing molecules azobenzene, di-benzene-imine and stilbene.

The term isomerization defines the geometrical change in a molecule's configuration without any chemical change. This internal degree of freedom can be observed, when molecular subunits can align differently with resect to each other. Therefore the bond configuration of one atom must show at least a three-fold symmetry as for instance the $sp^2$-hybridized orbitals do. The possible bonds of such a species span a plane, each bond 120° separated to the next one. The diazo unit (R-N=N-R) is one example of this kind, where the double bond between the two nitrogen atoms (N) is ∼120° aligned to the single bonds of the nitrogen atoms to the rest groups (R), as shown in figure 1.13 (a).

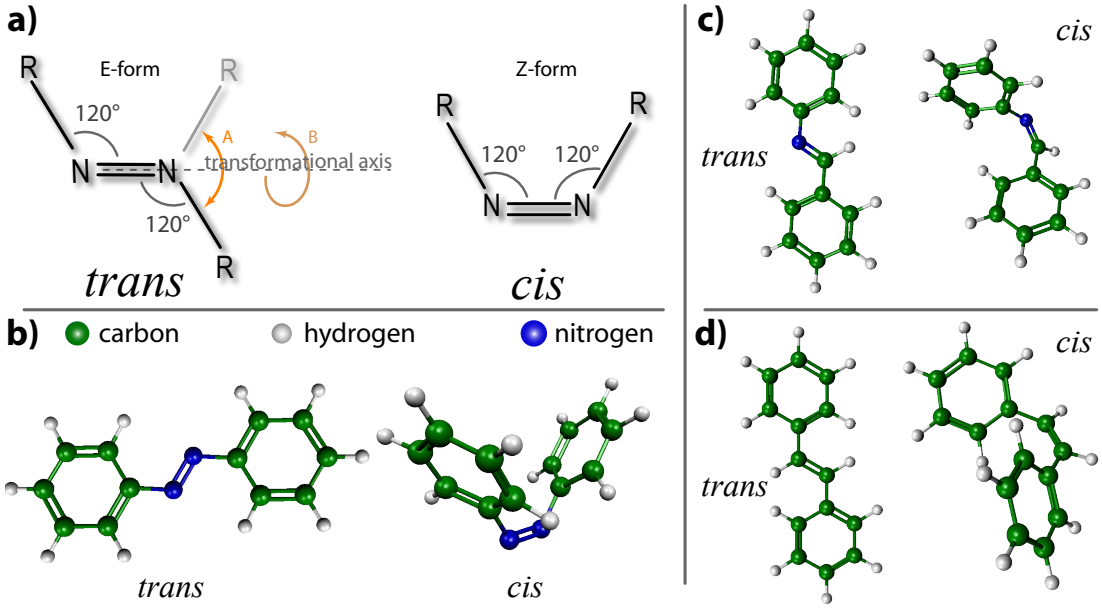


**Figure 1.13:** (a) Scheme of *cis-trans*-isomerization in the diazo unit and examples of (b) azobenzene, (c) di-benzene-imine, and (d) stilbene in their *trans*- and *cis*-configurations respectively.

This constraint allows two possible arrangements of the rest groups with respect to each other. In the *trans*-configuration they are arranged on opposite sites of each other, describing a zigzag shape. This configuration is also named E-form, originating from the German term "entgegen" (= against). In the *cis*-configuration they are on the same side, describing an U-shape, also named Z-form from the

German term "zusammen" (= together). The transformational motion from one configuration to the other is called isomerization and realized by either an in-plane inversion (path A) or a three-dimensional rotation around the axis defined by the nitrogen double bond (path B).

This isomeric unit is embedded in the azobenzene molecule, whose semi empirically minimized structures of the *trans*- and *cis*-configuration are shown in figure 1.13 (b). Fulfilling the constraint that the diazo group is planar, the phenyl rings of azobenzene arrange very differently in the *trans*- and *cis*-configuration. Since the phenyl rings can rotate freely around the single C-N bonds, the *cis*-configuration is three-dimensional. Its three-dimensionality arises from a steric repulsion of the two phenyl rings. In gas phase and solution the molecule transforms upon ∼320 nm light irradiation from its *trans*-form to its *cis*-form via electronic excitation. The thermal inverse reaction can be supported by irradiation of ∼420 nm light.

Replacing one of the nitrogen atoms of the diazo bridge by a carbon atom the molecule changes little. Although locally the atoms at the switching junction change their character and the symmetry of the molecule is broken, the di-benzene-imine molecule exhibits the same *trans*- and *cis*-configuration as azobenzene, shown in figure 1.13 (c) [Lotz 09]. While the diazo bridge has unsaturated orbitals by means of non-bonding lone-pair electrons, in the case of di-benzene-imine the carbon's electron configuration is saturated by a hydrogen atom. Therefrom the molecular resonances are influenced, it is expected that the switching barrier is lower than for the case of azobenzene. Replacing also the second nitrogen atom by a carbon atom, stilbene (figure 1.13(d)) is a third example for a small molecule showing *cis-trans*-isomerization [Schm 07, Schm 08b]. In contrast to the two previous examples, the stilbene's switching barrier is higher. There are many more examples of *cis-trans*-isomerizing molecules, which are larger and hence their mechanical switching results in a large motion of nuclei.

## 1.5 Azobenzene

The process of *cis-trans-photo*-isomerization in solution and in gas phase is one of the best understood [Nobl 56, Feri 01, Beve 66, Wach 04, Sekk 02, Hart 36]. In particular, azobenzene molecules are one of the simplest examples of optical sensitive *cis-trans*-switches, because they combine a high efficiency with a small structure: two photoactive phenyl rings connected through a diazo group. Photoisomerization of azobenzene involves one single excited state, which is populated upon light irradiation, allowing effective control of its structure [Sekk 02, Huge 02, Zhan 04, Elsa 98, Nage 97, Fuch 06].

Extensive research efforts have recently been devoted to the functionalization of surfaces with molecular switches, with the aim of building up a new class of materials with controllable properties. From the fundamental point of view, the interest of many studies lies in exploring, how the structure and the configurational dynamics of molecular switches in general and azobenzene-

based compounds in particular are modified when adsorbed on metal surfaces [Alem 06, Henz 06, Henz 07, Coms 05, Coms 07, Choi 06, Levy 09].

The general geometry of azobenzene has been shown in figure 1.13 (b) and it was emphasized that the diazo unit plays a key role for the *cis-trans*-isomerization. We want to point out, how this important bond configuration influences the intramolecular degree of freedom.

### 1.5.1 Free Diazo-Group

In figure 1.14 the formation of the the planar diazo unit (C-N=N-C) is explained via the $sp^2$-hybridization of orbitals of free nitrogen (N) with carbon (C) atoms. The

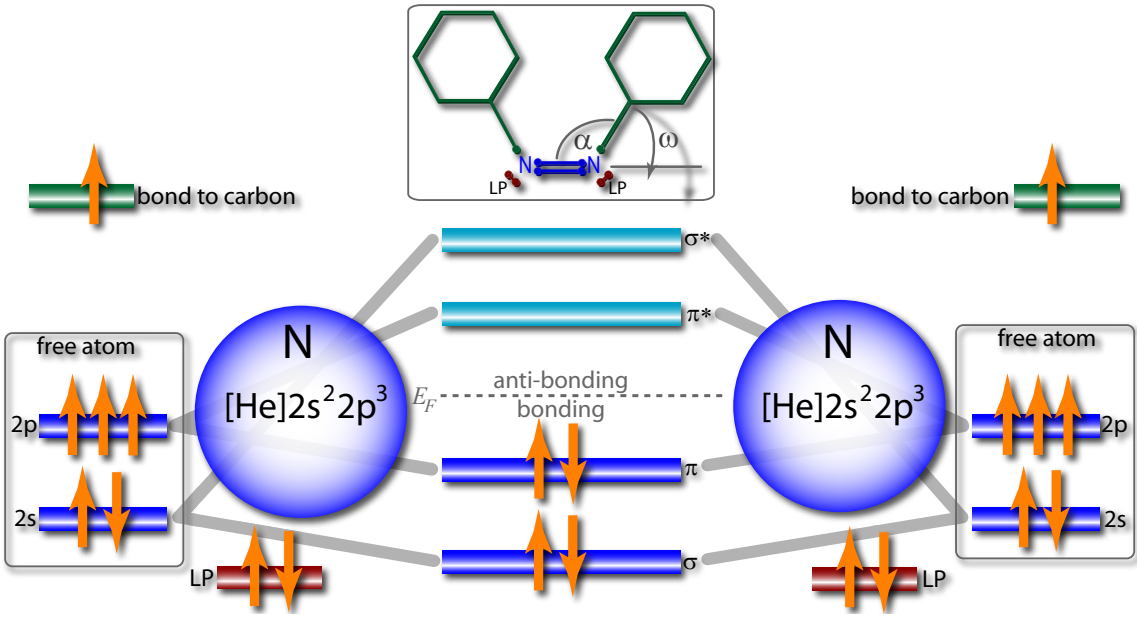


**Figure 1.14:** Energy level diagram of the N=N double bond resulting from the hybridization of the nitrogen's $2s^2 2p^3$ valence orbitals. The resulting bonding ($\sigma$ and $\pi$) and anti-bonding ($\pi^*$ and $\sigma^*$) orbitals with the according energy levels are only half populated and additional localized lone-pair electron orbitals (LP) emerge at each N atom. Furthermore one electron per N is forming a bond to a carbon atom of the adjacent phenyl ring.

nitrogen ground state electron configuration consists of an closed helium shell and five valence electrons occupying the two states of lowest orbital momentum in the $2s^2 2p^3$ configuration [Bran 80]. In the framework of azobenzene, the bonding to a phenyl ring and to the other N atom results in a $sp^2$-hybridization with a three-fold alignment of bonds. One electron couples with the phenyl ring forming a single bond. Two other electrons join to a lone-pair (LP) electrons' orbital and localize in $\sim 120°$ from the direction of the phenyl ring. The two last valence electrons populate the hybridized $\sigma$-, $\pi$-, $\pi^*$- and $\sigma^*$-orbitals with their counterparts from the other nitrogen atom. They form a double bond, which is of strongest character in its ground state, when only the $\sigma$- and $\pi$-orbitals are doubly occupied. It aligns in the same plane as the LP and the C-N bond but further $\sim 120°$ oriented. Symmetry explains

the same structure for the other N atom and determines the molecular structure of the azobenzene's back bone, showing either a planar zigzag-shape (*trans*) or an U-shape (*cis*), as seen in figure 1.13.[5] As a result, the $\pi$-states are delocalized over the molecule and form part of the hole molecule's conjugated electron $\pi$-system.

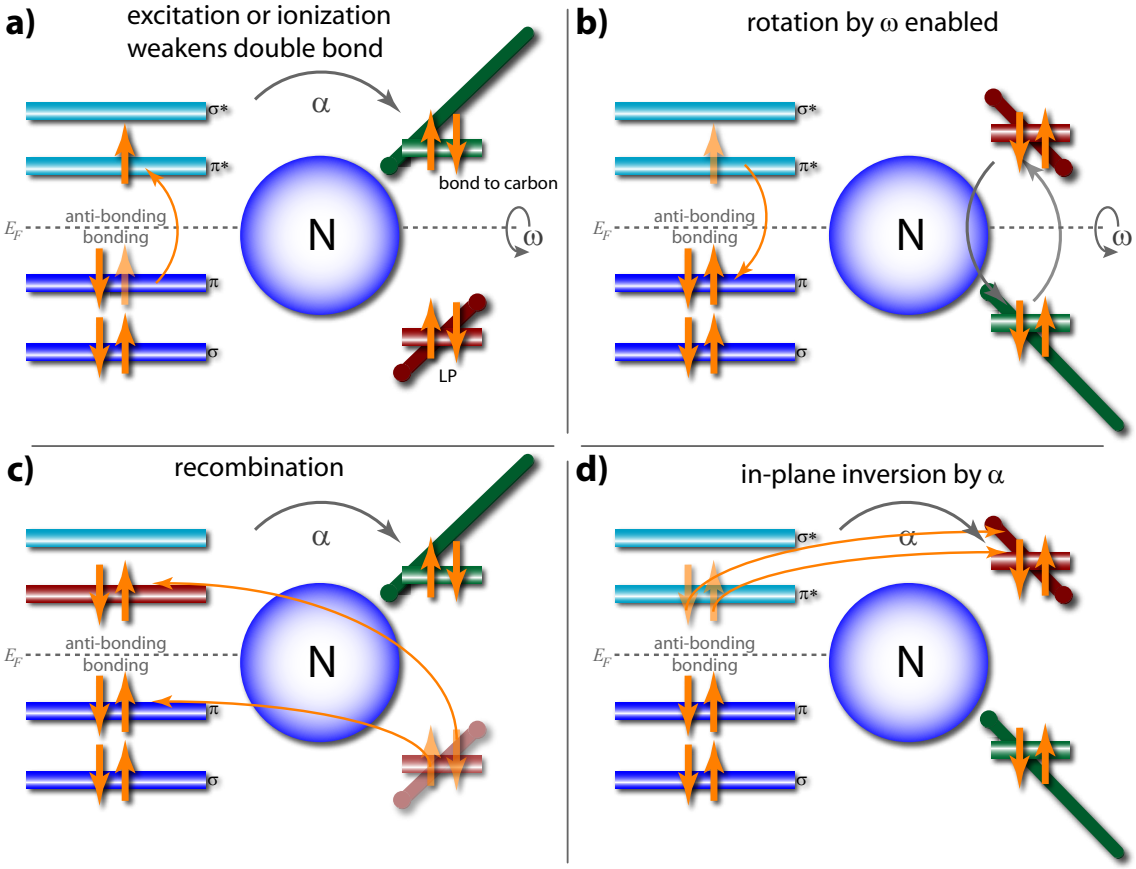


**Figure 1.15:** Different states in the isomerization process following either a three-dimensional $\omega$-rotational transformation, seen in (a) and (b) or an in-plane $\alpha$-inversion, seen in (a), (c) and (d). Starting from the electron excitation (a) the rotation in (b) can occur, because the N=N double bond is weakened. The inversion is caused by (c) the recombination of lone-pair electrons and (d) redistribution of bonding (to carbon) and non-bonding (lone pairs) orbitals.

The *cis-trans*-isomerization can occur in two different ways: rotation or inversion. With the knowledge about the bond configuration the processes determining the two different paths can be explained more in detail by figure 1.15. The initiation process, seen in panel (a) for both paths is described as the excitation of an electron from the ground states ($\sigma$ and $\pi$) into the excited $\pi^*$ or $\sigma^*$ state, by *e.g.* photons of appropriate energy.[6] Hereby the bonding character of the stiff N=N double bond is

[5] Side effects in the electronic structure and influences due to the bulky phenyl rings are present, too and account for small deviations from the described geometry. They may even weaken the bonding character.

[6] Direct electron injection from *e.g.* a tunneling junction would primarily ionize the molecule, but not depopulate the ground state ($\sigma$ or $\pi$) and hence will have not the same effect. Still, the

weakened and a three-dimensional rotation of the phenyl ring by $\omega$ can be seen in panel (b). The inversion can be seen in panel (c) as one lone-pair electron refilling the empty $\sigma$ or $\pi$ ground state, while the excited $\pi^*$ electron recombines with the other LP electron. Both form a new non-bonding lone-pair orbital, which basically has exchanged the site with the bond to the C atom, sketched in panel (d). This motion can be described by an inversion in plane via the angle $\alpha$.

### 1.5.2 Adsorbed Azobenzene

With this detailed view on the diazo bridge we want to focus on how the azobenzene molecule gets influenced upon adsorption on metals. On the one hand, photoactive phenyl rings have an ubiquitous tendency of mixing their aromatic parts with metal states. On the other hand, the lone pairs of the diazo unit can couple covalently to metallic reactants. Thus, the electronic surrounding and the type of surface in particular play important roles in the adsorption process.

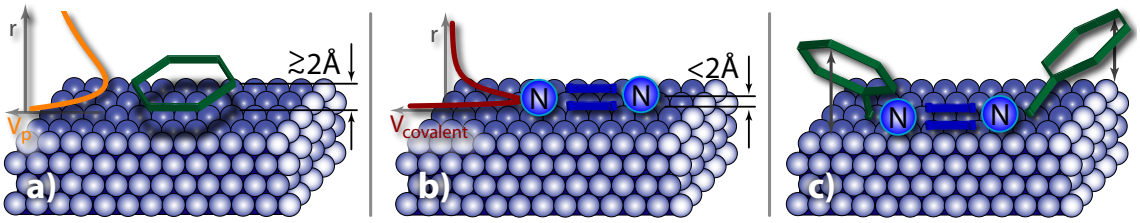


**Figure 1.16:** Interaction mechanisms in the adsorption process of azobenzene conquer such that the planar molecule deforms. The pure phenyl ring adsorbs in larger optimal distance to the surface than an individual covalently bond atom or small $N_2$ molecule.

Both, the covalent bond and the $\pi$-coupling compete with each other in the adsorption. The optimal distance for an individual benzene ring, weakly adsorbed on a metallic surface is about $\gtrsim$2 Å, as illustrated in figure 1.16 (a). In contrast, a covalent bond, which would be established between the nitrogen atoms and a metal atom, usually shows lengths of less than 2.5 Å, as shown in figure 1.16 (b). The discrepancy of both interaction lengths within one molecule has a strong influence on the way of adsorption and highlights that the free molecule structure does not sufficiently describe the geometry of the adsorbed species [Reut 07]. In the optimal distance of the pure covalent bond, the $\pi$-coupling potential is of repulsive character due to coulomb repulsion. As a consequence the molecule suffers from internal stress and eventually deforms, as sketched in figure 1.16 (c). With a deformation usually the molecular symmetry breaks, the orbitals rearrange, and individual bonds change their character. Eventually the switching ability is affected, because orbital redistribution may strengthen or weaken the diazo double bond. It is very probable that one of the configurational states is disturbed differently strong from a deformation than the other state, which results in a different stability and a preferred configuration. In this way the molecular configuration would be

system is expected to react similarly by enhancing the weight of anti-bonding orbitals.

determined by the surface interaction but not by the molecular bi-stability of the *cis*- and *trans*-configuration. Correspondingly a switching may be prohibited.

The $\pi$-interaction is determined by the extent of the $\pi$-orbitals. Hence, the $\pi$-surface interaction component in the cooperative adsorption is mostly independent of the metallic substrate material. In contrast, the strength of a covalent bond intrinsically results from the reactants' electronegativity: the surface atom and nitrogen. Therefore the surface influence on azobenzene depends on the strength of the covalent bond. Correspondingly the reactivity of the surface can tune the molecular geometry of *trans*-azobenzene in a large variety: from an almost planar to a strongly bent structure.

Also the strength of coupling determines dynamics of the excited states. The lifetime of excited states is reduces in well-coupled systems and hence molecular excitation that may lead to configurational changes are quenched rapidly [Duli 03]. So the choice of substrate is crucial for tuning molecular characteristics or for preserving its gas phase characteristics.

### 1.5.3 Azobenzene in Surface Science

Recently, the interest in molecular photoswitches in condensed matter has grown following the rapid development of precise molecular epitaxy tools for the "bottom up" growth of molecular devices. One approach is the fabrication of self-assembled monolayers (SAM), where switching units are predominantly vertical arranged. Here, photoemission studies have obtained successfully switching events in ensembles of molecules [Dela 96, Webe 03, Schm 08a]. Also surface properties, may be switched when the switching units are oriented vertically on the surface and its characteristics can be changed by selectively addressing of switches.

Various studies have been published in the last years on the results of fundamental research of azobenzene derivatives, adsorbed planar on metal surfaces. STM studies have demonstrated that excitations of azobenzene molecules in the tip-surface junction, induced by tunnel electrons [Henz 06, Henz 07, Choi 06, Gaud 00, Henn 07], by photons [Coms 07, Levy 09], or by large electric fields [Alem 06, Qiu 04a, Ianc 06], can induce switching between two molecular configurations. In most of the works, weak surface interaction or a decoupling of the aromatic moieties with inert bulky groups, like tert-butyl terminations preserve the free molecule characteristics [Alem 06, Coms 07, Ovar 07, Hage 07, Tege 07].

Also, the coupling of azobenzene to its surrounding has been investigated. In contact to carbon targets (or carbon tubes) is expected to modify the target's characteristics respectively to the configuration of the attached switching unit [Ai 08].

# Chapter 2

# Ordering Processes of Azobenzene Derivatives on Metallic Surfaces

Besides the functionalization of surfaces by switchable molecules and characterizing their switching phenomena, it is important to understand why and how these characteristics can be affected by the metal substrates and the neighboring molecules. Hence, the main aspect of this chapter is to describe different adsorption and ordering phenomena of azobenzene molecules with different end group functionalization and on different surfaces of coinable metals. Beforehand, the azobenzene derivatives investigated in this study will be introduced. The following sections deal about how molecular assembly is mediated by the formation of hydrogen bond networks and how these lateral interactions compete with vertical interactions between molecules and surface. Herein the aspects of surface reactivity, molecular packing density, and temperature play crucial roles, which eventually support a configurational change. In one special case of supra-molecular building blocks the molecular adsorption configuration can be switched by tunneling electrons from a semi-stable into a structure of minimal adsorption energy. The chapter will close with a brief comparison of two very similar types of molecules, whose electronic structure could be explained in an intuitive way by a one-dimensional quantum well.

## 2.1 Molecular Architecture of Azobenzene Derivatives

For many different purposes the switching molecule azobenzene can be functionalized with end groups or embedded in larger molecular compounds. In the present work all molecules are of comparably small size, which is a restriction to the used sublimation technique. In general, a functional unit can act as linkage to other molecules, it can couple the molecule to a surface, or decouple it from the surface, and it can accumulate or donate charge and hereby also affect the molecule's switching capability. The three functional end groups employed in this study, are listed in the following. The corresponding molecular Lewis-Structures are shown in figure 2.1.

- **Cyano** (CN) end groups are used in two different positions of the azobenzene's phenyl rings forming Di-Meta-Cyano-Azobenzene (**DMC**) and Di-Para-Cyano-Azobenzene (**DPC**). Nitrogen (N) has the highest bond

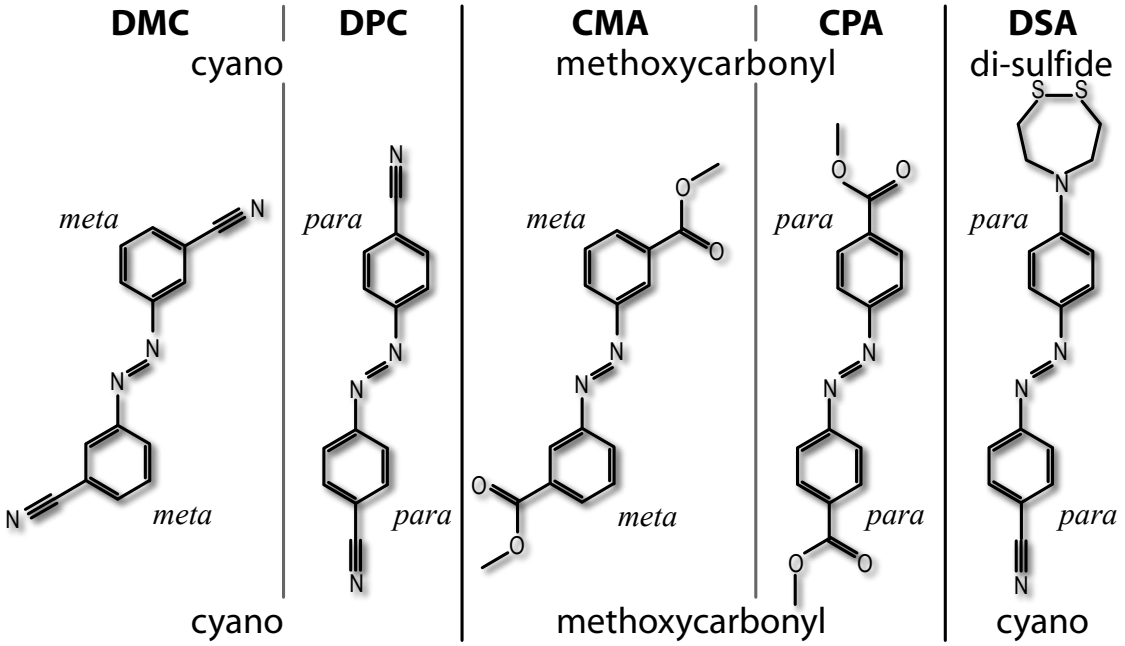


**Figure 2.1:** Lewis structures of the molecular species in their *trans*-configuration investigated in this work: Di-Meta-Cyano-Azobenzene (**DMC**) and Di-Para-Cyano-Azobenzene (**DPC**) with the electrophilic cyano (CN) moiety in meta and para sites of the phenyl rings; Di-Meta-Methoxycarbonyl- (**CMA**) and Di-Para-Methoxycarbonyl-Azobenzene (**CPA**) with bulky functional groups in meta and para positions of the phenyl rings; Para-Cyano-Para-Di-Sulfide-Azobenzene (**DSA**) with the cyano group attached at one side and the reactive di-sulfide pentagon at its opposite side, making the molecule appearing asymmetric.

enthalpy among all elements and hence, has a very electrophilic character. In combination with one carbon atom a cyano group establishes with a characteristic triple bond. It accumulates a non-bonding lone-pair electron orbital and can be used as optical spectroscopical marker [Pian]. In STM topographies, the orientation of cyano moieties is visible, because the charge accumulation lowers locally the work function of the supporting metal. In consequence faint depressions in STM topographies are observed in the proximity of the cyano groups. The small size of the cyano functionality allows comparative studies of **DMC** and **DPC** with theoretical results, obtained for instance by Density Functional Theory (DFT). Quantum chemistry calculations for these species have been performed by G. Füchsel *et al.*, [Fuch 06].

Cyano groups are characteristic anchoring points for metal atoms in coordination complexes and hence can have stabilizing effects on molecules upon adsorption as it will be seen in chapter 4, when **DMC** is co-adsorbed with cobalt atoms.

- **Methoxycarbonyl** ($CO_2CH_3$) end groups are attached to azobenzene molecules in two different orientations, forming Di-Meta-Methoxycarbonyl-Azobenzene (**CMA**) and Di-Para-Methoxycarbonyl-Azobenzene (**CPA**). This end group is larger, which allows to clearly identify its position in STM

topographies. Also, the functional unit offers various possibilities for hydrogen bond formations, which will stabilize adsorption structures. Even if *cis-trans*-isomerization is not assisted, we will show, how these molecules dynamically undergo a different intra-molecular conformational change upon adsorption [Henn 08a]. Furthermore we will analyze the electronic structure of these molecules and the self-organization of the molecules under various adsorption conditions.

- **Disulfide Ring** functionalization ($NC_4H_8S_2$), forming Para-Cyano-Para-Di-Sulfide-Azobenzene (**DSA**) is expected to locally anchor strongly onto a gold substrate by either directly the disulfide unit or upon a dissociation process. In both cases the cyano moiety would be free, acting as switchable part. The plausible observation of a complex adsorption geometry let us speculate about an interlocking process between molecules leading to the formation of supra-molecular building-blocks.

## Orientation of Functional Groups

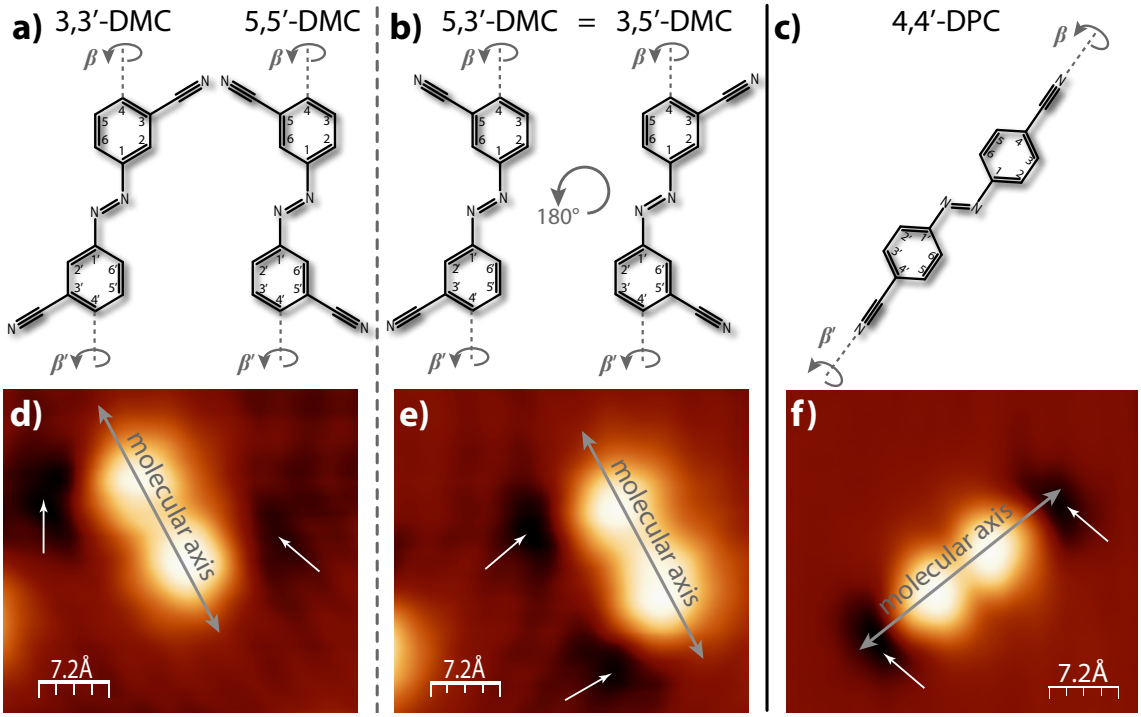


**Figure 2.2:** Structure of (a) 3,3'-*trans*-DMC transferred into (b) 3,5'-*trans*-DMC by rotation around the CN-single bond ($\beta$). The structure of (c) 4,4'-*trans*-DPC does not cause such an conformational change. Topographic STM images of individual (d) 3,3'-*trans*-DMC and (e) 3,5'-*trans*-DMC molecule when adsorbed on a Ag(100) surface. The STM image (f) of 4,4'-*trans*-DPC adsorbed on Ag(100) shows the only possible *trans*-conformation of this molecule. Scanning conditions: (a) $V_B = 686$ mV, $I = 2.8 \times 10^{-10}$ A; (b) $V_B = 686$ mV, $I = 2.3 \times 10^{-10}$ A; (c) $V_B = 217$ mV, $I = 9.3 \times 10^{-11}$ A.

Recent experiments on a different molecular species found that intramolecular rotation of phenyl end-groups can occur erratically after thermal excitation [Weig 06].

A change of the position of functional groups influences the molecule's aspect as shown in the molecular Lewis structures 2.2 (a)-(c). Hence, this determines whether a molecular internal degree of freedom like such phenyl ring rotation is seen or not. By comparing the positions of the functional groups between **DMC** and **DPC** molecules, the term *"para"* refers to a straight shape, while the term *"meta"* refers to molecules appearing in a zigzag shape. The two terms define the carbon sites of functional units attached to a phenyl ring with respect to one reference, in this case the diazo bridge (C-N=N-C). In figures 2.2 (a) and (b) the carbon sites are enumerated anti-clockwise, for the example of the **DMC** molecule. Thus the *meta* position defines the $3^{rd}$ or $5^{th}$ site in a benzene ring, and can be transferred into each other by rotation around the angle $\beta$. On the other hand, the *para* position is defined as the opposite site from the diazo reference ($4^{th}$ site).

Adsorbed on surfaces we can observe the rotation of one phenyl ring in the *meta*-functionalized molecules (**DMC** and **CMA**) but not on the *para*-functionalized ones (**DPC** and **CPA**). The planar confinement of phenyl rings due to $\pi$-surface coupling allows only two orientations with respect to the $\beta$-rotation ($\beta'$-rotation) for each end group in *meta* position. That results in total in four different geometries, shown in figure 2.2 (a) and (b) for the example of DMC:[1] 3,3'-*trans*-**DMC** and 5,5'-*trans*-**DMC** show the cyano groups on opposite sites of the molecule and cannot be transferred into one another by simple symmetry operations in the molecular plane. 5,3'-*trans*-**DMC** and 3,5'-*trans*-**DMC** can be transferred into each others upon an in plane 180° rotation and hence they are considered to be actually equal. On the contrary the para-functionalized **DPC** with the cyano groups in position 4 and 4' is shown in figure 2.2 (c). Its geometry is not affected upon a phenyl ring rotation by the angle $\beta$.

**DMC** and **DPC** were sublimated onto a ∼100 K cold Ag(100) surface, such that the molecules can hardly diffuse, as shown in figures 2.2 (d)-(f). By inspection of the STM images an azobenzene molecule is seen as a pair of two round protrusions. They result from the delocalized density of states in the two planar phenyl rings, describing well the molecular shapes. Faint depressions, indicated by white arrows, clearly evidence the orientation of cyano groups, resulting from a local lowering of the surfaces' work function. The STM images reveal that two different molecular shapes can be observed. In contrast, the preparation of **DPC** on the same substrate in figure 2.2 (f), reveals only one shape.

In **DMC** the cyano termination can place upon adsorption by chance in two different orientations with respect to its counterpart: on opposite side of the molecule's main axis (given by the two bright protrusions in figures 2.2 (d)), or on the same side of this axis (figure 2.2 (e)). The orientation of the inner N=N bond, the diazo bridge, cannot be resolved by STM technique. Accordingly we cannot differentiate between the 3,3'- and 5,5'-conformations nor between the mirror images of all the enantiomers. Hence, we label them in the following as

[1] Strictly speaking, there are actually eight different configurations, if one includes the mirror images of the displayed enantiomers.

the 3,3'-*trans*-conformation, when the functional units are on opposite sides of the molecule's axis and as the 3,5'-*trans* conformation, when the functional groups are positioned at the same side of the molecule.

## 2.2 Self-Ordering Processes Mediated by Molecular End Groups

Molecular self-assembly at surfaces proceeds through complex selective pathways involving the recognition of molecular structures based on lock-and-key interactions and by effective methods of dynamical search and trial [Lehn 02]. Despite of plenty of studies in this field, the driving mechanism of self-ordering is not yet fully understood. In the following we will focus on several derivatives of azobenzene (**DMC**, **DPC**, **CMA** and **CPA**) showing various types of ordering and self-recognition. The lateral interaction between molecules is affected by the functional groups and competing with interactions of the molecules to the surface. For example, small diazo derivatives have been investigated on Au(111) by Y. Wang *et al.*, forming different structures of few molecules. In the study the molecules form tetramers chains, dimers and trimers in a chain or star-like assemblies [Wang 08].

### 2.2.1 Stabilization in 2D islands

Upon adsorption of molecules on a surface the total energy is reduced due to molecular crystallization in two-dimensional highly ordered structures. This is the case, when either a three-dimensional growth is not favored or when the interaction between adsorbates is strong enough to overcome local barriers of the surface potential. Under the condition of weak surface interaction and the correct dosing of adsorbates, ordering is often observed on Au(111) single crystal surfaces.

In figure 2.3 we present three independent experiments of the two azobenzene derivatives with the methoxycarbonyl functionalization (**CMA** (a) and **CPA** (b)) and of the previously described **DMC** (c). They were all deposited on a Au(111) surface at room temperature. Highly ordered structures could be obtained in all three systems. The interlocked molecules all adsorb in a planar configuration on the metal surface, as the superimposed structural models indicate (lower panels). The assembly in all cases is highly selective by the molecules' structures, showing homogenous patterns. All islands are built up by rows of molecules, in which they all are oriented in the same direction.

**CMA** shows two prochiral appearances of exclusively the 3,3'-rotamer, alternating from row to row in panel (a). The intermolecular interaction hence drives a recognition process, establishing a rectangular lattice of molecules on an hexagonal oriented surface.

In the case of the **CPA** features (panel (b)), the orientation of molecules alternate

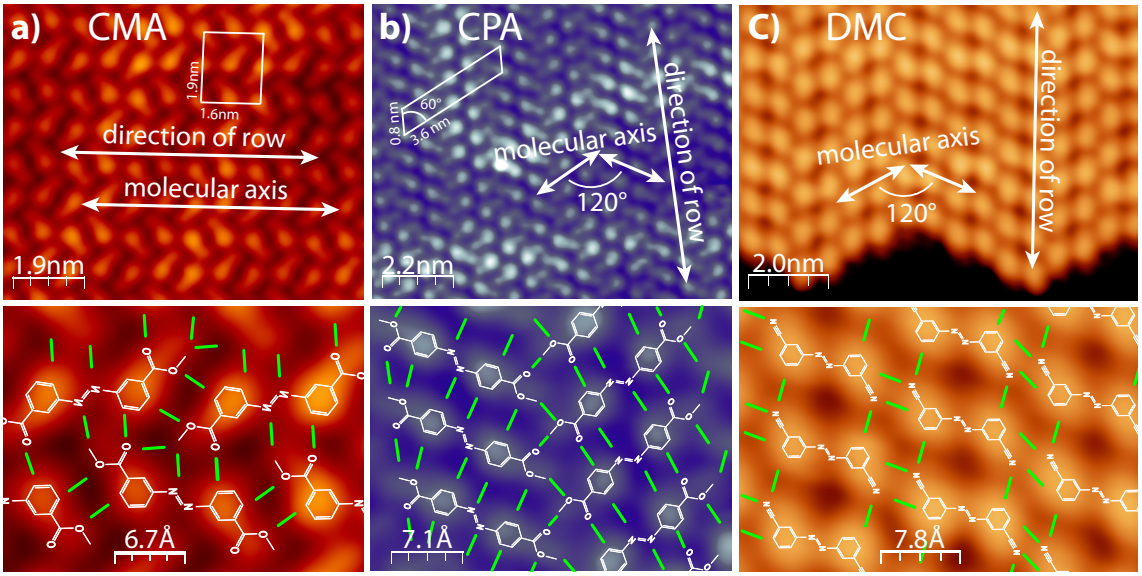


**Figure 2.3:** Self-assembled molecules in homogenous 2D islands: (a) **CMA** (b) **CPA** and (c) **DMC** on Au(111). Lower panels are close-up images of the upper ones with molecular models superimposed. The planar molecules all grow in highly ordered domains of rows, consisting of a single orientation In (a) and (b) the molecular unit cell is included. In all cases the molecular orientation is determined by the direction of lateral hydrogen bond attraction emerging from functional units. Possible patterns of hydrogen bonds are indicated by green lines. Scanning conditions: (a) $V_B = 322$ mV, $I = 8.9 \times 10^{-11}$ A; (b) $V_B = 482$ mV, $I = 5.5 \times 10^{-11}$ A; (c) $V_B = 1.87$ V, $I = 1.5 \times 10^{-10}$ A.

from one row to the next by $\pm 120°$. The three-fold symmetry of the (111) surface is reflected in this structure. While the rows evolve along one direction the orientation of the molecules within each row reflects the other two surface directions.

**DMC** crystallizes in exclusively its 3,3'-conformation, forming a compact two-dimensional layer. The molecules create small domains of homogenous orientation following two of the high symmetry directions of the Au(111) surface, oriented 120° with respect to each other. Two or three rows of molecules with the same orientation are seen next to each other along the third high symmetry direction of the supporting material.

In the case of *meta*-functionalized molecules (**CMA** and **DMC**), the selection of exclusively 3,3'-rotamers can be explained, because the 3,5'-species disturbs the ordering. It is favorable that internal flexibility by $\beta$-rotation enables a conformational change into a 3,3'-specie. This type of transformation will be explicitly studied in the case of **CMA** in section 2.3 [Henn 07].

Now we focus on the mechanism of stabilization in theses structures. By studying the close up images (lower panels of figure 2.3) one can see how the functional groups predominantly face to hydrogen atoms, which saturate the phenyl rings of adjacent molecules (CH$\cdots$N and O$\cdots$HC). All potential hydrogen bonds are indicated by green lines between molecules, forming networks with

the molecules. The sum of all contributing hydrogen bonds stabilizes the structures.

Despite the similar growth of the different molecules in two-dimensional domains formed by rows, the individual structures of the methoxycarbonyl functionalized molecules (**CMA** and **CPA**) have an evident difference. While the **CMA** (a) rows grow along a line parallel to the molecules' main axis, the **CPA** (b) molecules grow in an angle to the 120° alternating molecular main axis. This effect results from the orientation of sidewise pointing inter-molecular hydrogen bonds, which are determined by the functional groups. Correspondingly, they can only favor an on-axis growth (**CMA**), if the functional groups are off-axis (in *meta*-position) and vice versa, they favor an off-axis growth (**CPA**), when the functional unit is on-axis with the molecule (*para*-position).

The orientation of hydrogen bonds between the **DMC** molecules (in panel (c)) is defined by the cyano units. Hence, their off-axis site (*meta*) must favor the off-axis growth of homo chiral rows. In all three cases the design of the functional units thus determines the structure of the highly ordered densely packed domains.

### 2.2.2 Assembly in Clusters

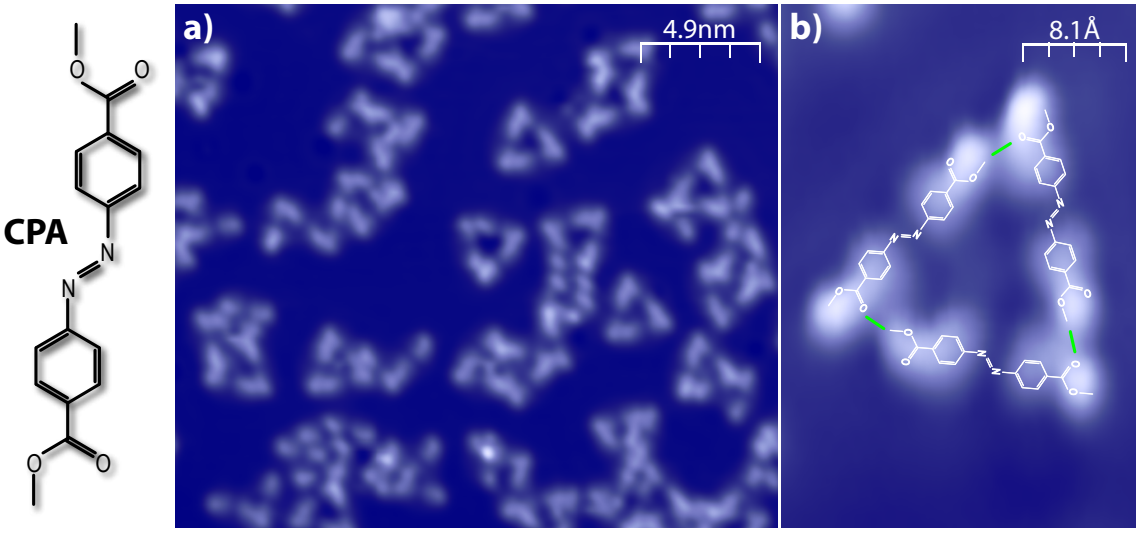


**Figure 2.4:** (a) Self-organized triangular structures of **CPA** molecules (right: its Lewis structure) on Cu(111). The zoom (b) shows one individual molecular cluster with the molecular models superimposed. One hydrogen bridge per molecule is indicated by a green line. Scanning conditions: (a) $V_B = 1$V, $I = 4.5\ 10^{-11}$A; (b) $V_B = 1.9$V, $I = 6.9\ 10^{-11}$A.

Molecular assembly can be controlled by the orientation of functional units, but also the strength of their interaction to the surface plays a crucial role. Increasing the surface reactivity of the supporting metal by replacing the previously studied gold substrate with a Cu(111) single crystalline surface, the **CPA** molecule changes its aspect in STM topographies.

Figure 2.4 shows the example of **CPA** molecules, when they are adsorbed in a sub-monolayer coverage onto a Cu(111) surface, also at room temperature. Small triangular clusters are now formed, which are built from three molecules as seen in the close-up image 2.4 (b). Short range interaction dominates the dilute assembly, which is reasoned by hydrogen bonds between the functional units (O$\cdots$CH), as indicated by green lines. The three-fold structure reflects the surface orientation and emphasizes that a stronger interaction with the surface is present in this preparation with respect to the previous preparations. The surface interaction is most likely originated in a strong bond between diazo's nitrogen and copper atoms from the surface [Henn 08b]. This also causes a larger diffusion barrier for the molecules on the surface. Thus it explains why a long range order in homogenous islands cannot establish. Hence, an interplay of surface-molecule and lateral inter-molecular interaction stabilizes this system [Bart 07, Schl 08].

### 2.2.3 Assembly in Networks

It has been shown that the cyano functional group causes ordering in a closed packed fashion on Au(111) due to hydrogen bonds (remind figure 2.3 (c)). When the azobenzene derivative with the cyano functionality in *para* position (**DPC**) is adsorbed on Cu(111) at room temperature a fairly different structure can be observed.

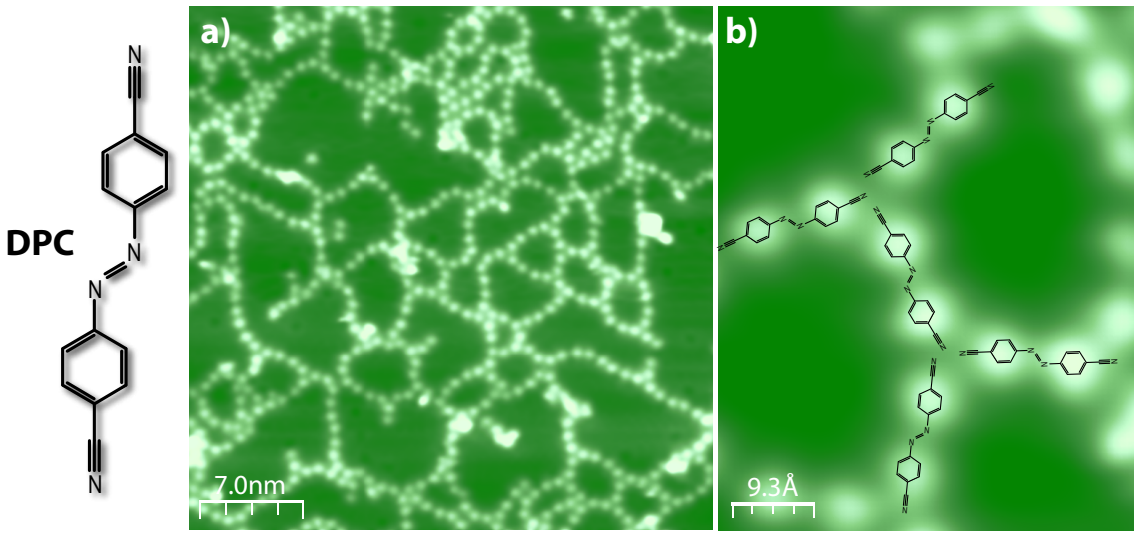


**Figure 2.5:** (a) Network of **DPC** molecules (right: its Lewis structure) on Cu(111). The scale up STM image (b) reveals individual molecular structures. Scanning conditions: $V_B = 1$ V, $I = 2.4 \times 10^{-11}$ A.

In figure 2.5 (a) a continuous network of molecules spans over the surface. The molecules form long chains following the main directions of the hexagonal surface structure. Since the cyano groups are aligned with the molecular main axis, the coupling of molecules is realized via these terminations in two-fold and three-fold

geometries, seen from the superimposed molecular models in the close-up image 2.5 (b). Surprisingly the two electron rich end groups do not repel each other but join with their antipodal local dipole moments.

One possible explanation for the coupling would involve surface Cu atoms, that mediate coordination bonds to cyano groups [Schl 07, Step 07, Step 08]. The charge between the Cu atom and the cyano moieties would then require to redistribute between metal and molecular ligand and form bonding orbitals of *sp*- or $sp^2$-like character, accordingly with two- or three-fold geometry, which fits to the observed structures. A comparable molecular interlocking may be achieved, when metallic ad-atoms, for instance Co atoms, are co-adsorbed with this species.

## 2.3 Role of the Surface Material, Temperature and Molecular Density in the Self-Assembling Process of Azobenzene Derivatives

It has been shown, how the intrinsic parameters of molecules and surface properties can influence the surface growth of molecules. In this framework, molecular behavior varies for different substrate materials, at different preparation temperatures, or when so many molecules are available, that the free diffusion in a surface potential is hindered. These preparation conditions hence have a major influence on the self-assembled structures.

### 2.3.1 Surface Reactivity

In figure 2.6 various assembly structures of **DMC** are shown adsorbed in different amounts on a Au(111) surface (a)-(c) and on a Cu(100) surface (d)-(e) (in all cases prepared at room temperature). The coverage has been increased in three steps, and significantly different behavior is observed for the two substrates.

At a low coverage ($\ll$0.1 monolayers (ML)) the molecules form small clusters on Au(111) (panel (a)) but are quite arbitrary spread in the case of Cu(100) (panel (d)). This hints to a lower diffusion barrier on Au(111), contrasting to a little mobility on Cu(100). When dosing larger amounts of molecules on Au(111) it is confirmed that the molecules interact with each other on Au(111) (panel (b)) but not on Cu(100) (panel (e)). Since **DMC** selectively forms ordered domains of exclusively the 3,3'-*trans*-rotamer on Au(111), we suppose that even a transformational change from 3,5'-*trans*- to 3,3'-*trans* rotamers may occur on Au(111). In contrast, on the copper substrate, the molecular interaction does not show order, as it is seen in the incomplete film in (e). Here **DMC** adsorbs in the proximity of other molecules and creates shortly ordered rows, which grow arbitrarily over the surface, and contain both, 3,3'- and 3,5'-conformations.

For a fully saturated ML this trend is preserved. The Au(111) surface is completely and homogenously covered by the 3,3'-*trans*-species of **DMC** (c), as it was shown

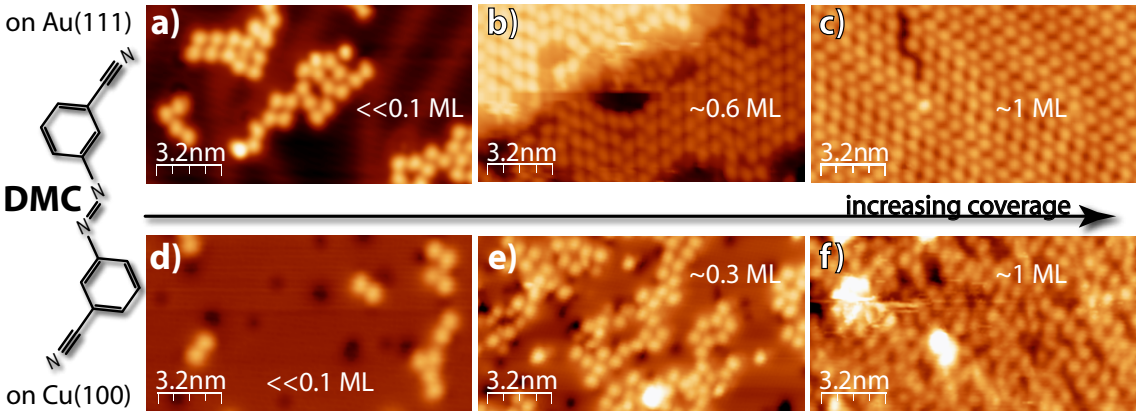


**Figure 2.6:** Coverage depending adsorption behavior of **DMC** molecules on Au(111) (a)-(c) and on Cu(100) (d)-(f). On Au **DMC** develops a highly ordered structure of only 3.3'-*trans*-rotamers, as seen when the coverage increases in (b) and (c). Most likely the molecules undergo a $\beta$-rotational transformation. (d) Little order is observed, when **DMC** is adsorbed on Cu(100). (e) Higher packing forces the molecules to form dimers or small chains. (f) At very high packing density, shortly ordered chains are observed while a second monolayer growth starts. Scanning conditions: (a) $V_B = 1.2$ V, $I = 1.9 \times 10^{-10}$ A; (b) $V_B = 1.9$ V, $I = 1.5 \times 10^{-10}$ A; (c) $V_B = 1.0$ V, $I = 3.8 \times 10^{-11}$ A; (d) $V_B = 0.6$ V, $I = 2.1 \times 10^{-10}$ A; (e) $V_B = 0.6$ V, $I = 1.1 \times 10^{-10}$ A; (f) $V_B = 0.3$ V, $I = 2.0 \times 10^{-10}$ A.

previously in figure 2.3. On the Cu(100) surface, the saturated layer (f) still has many defects. Between short rows of parallel molecules three dimensional clustering is observed, which cannot be resolved in detail, but is clearly seen from the appearances of higher protrusions.

XPS[2] measurements of M. Piantek *et al.* and DFT[3] calculations of R. Rurali agree that **DMC** undergoes a chemisorption on Cu(100) at room temperature, while it adsorbs weakly on Au(111) [Pian, Henn 08b]. On the one hand, diffusion of the weakly adsorbed molecular system supports ordering on Au(111). On the other hand the locally anchored molecules on Cu(100) hinders diffusion and hence, their assembly. This observation emphasizes the different character of both surfaces, namely that copper is more reactive for organic molecules than gold.

### 2.3.2 Active Intramolecular Conformational Dynamics

Similar homogenous structures, than those of **DMC** on Au(111) were already observed for **CMA**, the azobenzene derivative, functionalized by methoxycarbonyl groups in *meta*-position of its phenyl rings. Again, the $\beta$-rotation in this molecule results in two different planar adsorption geometries, which are shown in figures 2.7 (a) and (c). However, in the highly ordered film only one species was present, namely the 3,3'-*trans*-conformer. In the following we want to track, how the conformational dynamics of molecules with internal flexibility depend on the preparation conditions and how they form different supra-molecular assemblies.

[2]X-ray photoemission spectroscopy
[3]Density Functional Theory

We will present thermally activated conformational changes and those resulting from a close packing. Both will be identified at the single-molecule scale, and statistically interpreted, which implies that internal degrees of freedom may be active during the recognition and growth of molecular thin films at surfaces [Miwa 06, Ling 07, Wang 08]. We speculate that they play a crucial role in the mesoscopic ordering and phase separation. Because this phenomenon requires a strong intermolecular interaction, a Au(111) substrate is employed, leading to weak molecular adsorption [Fern 06].

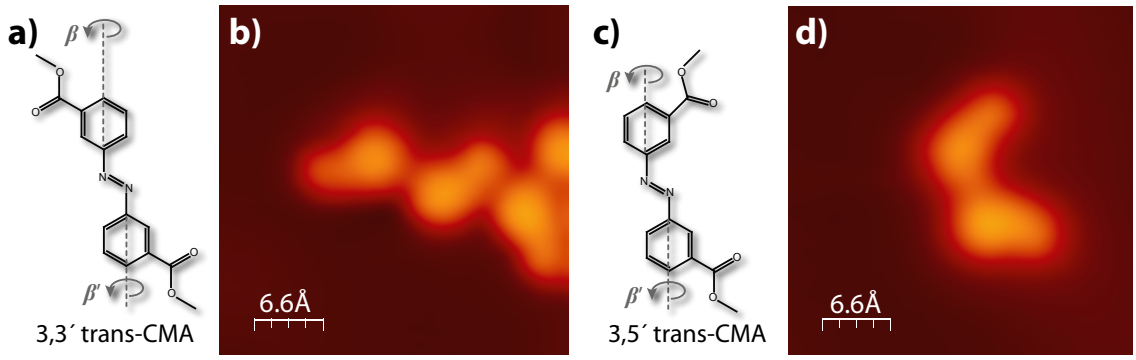


**Figure 2.7:** (a) and(c) Lewis structure of the effectively two possible rotamers of *trans*-**CMA** on a surface. (b), (d) STM images of the two shapes found on a Au(111) surface. Each pear-like protrusion corresponds to a phenyl ring, to which an carboxymethyl group is attached; (b) is associated with the 3,3'-*trans*-rotamer shown in (a), whereas (d) corresponds to the 3,5'-*trans*-rotamer in (c). Scanning conditions: (b) $V_B = 75$ mV, $I = 4.3 \times 10^{-11}$ A; (d) $V_B = 1.3$ V, $I = 3 \times 10^{-10}$ A.

Figure 2.7 shows the methoxycarbonyl functionalized molecule **CMA** in structure and, for comparison, the STM topographies of individual planar *trans*-molecules in panel (b) and (d) [Prie 05, Prie 06]. The methoxy ($O\text{-}CH_3$) part of the end groups are large and can be easily identified in the STM images by topographic protrusions, while the carbonyl moieties (carrying oxygen), which are strongly active in the formation of intermolecular hydrogen bonds, are in charge of the recognition, selection, and locking to specific molecular shapes in ordered domains.

On a cold Au(111) substrate ($T_S = 70$ K), both zigzag-shapes (3,3'-*trans*-) and bow-shapes (3,5'-*trans*-rotamers) of **CMA** are found with the same probability in the STM images. (52% are 3,5'-rotamers.) At low substrate temperatures, their thermally induced mobility is small and only molecular islands with disordered structures are found, shown in figure 2.8 (a). If **CMA** is deposited instead on a substrate held at room temperature, the thermal mobility is sufficient, to induce molecular self-assembly in two types of characteristic molecular assemblies: one-dimensional (1D) chains (figure 2.8 (c)) and two-dimensional (2D) homogenous islands (figure 2.8 (d)). Both structures are seen in the overview 2.8 (b). Interestingly, each type of assembly nucleates rotamers of exclusively one kind. The zigzag-shaped 3,3'-molecules assemble in highly ordered two-dimensional domains with alternating rows of the two prochiral forms of the 3,3'-conformers (panel 2.8

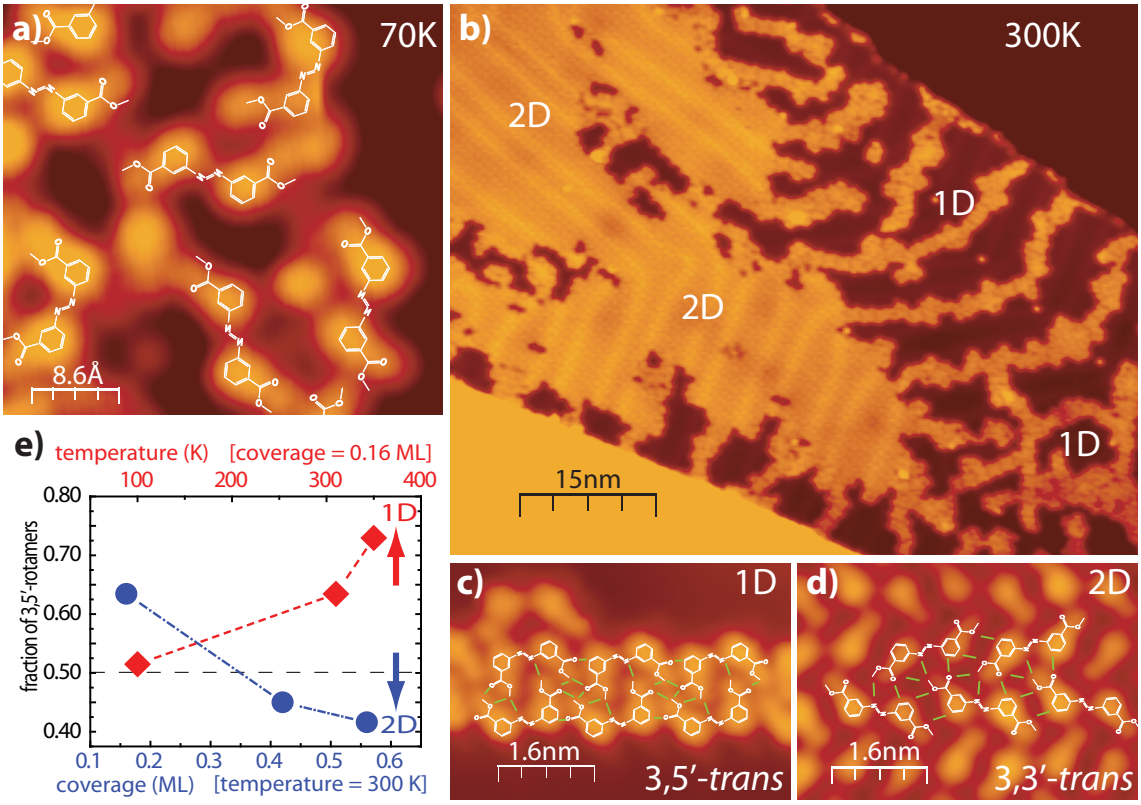


**Figure 2.8:** (a) Highly resolved STM image of **CMA** on Au(111), which was kept at 70 K for the preparation. Besides the **CMA** molecules in different rotamer conformations (structures superimposed), the topography shows many defects and molecular fragments. (b) STM image of the Au(111) surface covered with 0.42 ML of **CMA**. Two distinct regions are identified: the one labeled with "2D" is a defect-free two-dimensional packed island of **CMA**; "1D" indicates regions where molecular rows and disordered clusters along the Au(111) reconstruction are seen. (c, d) close-up images of the two-dimensional and one-dimensional domains. The images include proposed models of **CMA** and intermolecular hydrogen bonds. (e) shows the fraction of the 3,5' rotamer as a function of coverage and annealing temperature, obtained from the identification of about 10.000 molecules over several statistically representative regions for every coverage and temperature. The fraction of 3,5'-**CMA** increases with temperature, which indicates a larger stability of this bonding configuration and decreases with coverage due to its lower packing density.

(d)). High-resolution STM images reveal an alignment as already described in section 2.2.1. The stabilization is enforced by up to 15 possible inter-molecular hydrogen bonds per molecule (O···HC and CH···N). Instead, the bow-shaped 3,5'-**CMA** molecules are connected in a zipper fashion to form straight molecular chains (figure 2.8 (c)). In these one-dimensional chains we estimate that each molecule is linked by nine potential hydrogen bonds to its neighbors. The different hydrogen bond patterns of host sites in every domain determine the recognition of each of the rotamers through a lock and key strategy.

Both types of structures occupy large surface areas: the two-dimensional domains form defect-free compact regions, while the rows of U-shaped rotamers appear with short lengths, as they are emerging from disordered regions. The massive

ordering in large regions reveals the existence of an effective mechanism for the phase separation in mesoscopic regions formed by only one rotamer. Instead of pure thermal mobility for large distances across the surface, we consider here a mechanism based on a stochastic search of multiple conformations by thermal activation of intramolecular dynamics. We note that the transformation between the two rotamers at the surface is possible through the rotation of one phenyl ring. Recently, it has been shown that this transformation can be achieved at the surface via electron-induced excitation [Henn 07].

As each of the **CMA** structures apparently involves a different number of hydrogen bonds, we expect that they require different energies of formation. To probe whether a simple thermally induced conformational transformation between the two rotamers mediates the phase separation and the formation of large **CMA** domains, we analyze the fraction of each rotamer on the surface as a function of the substrate temperature, shown in graph (e) of figure 2.8. In the limit of low **CMA** coverage (0.16 ML), an equilibrated mixture of both rotamers (deposited at low sample temperature) evolves with the annealing temperature (red scale) towards the exclusive formation of zipper chain domains formed by the bow-shaped molecules. As a consequence, the fraction of 3,5'-**CMA** molecules increases monotonously with the annealing temperature. After annealing to 350 K, 75% of the molecules correspond to the 3,5'-conformer. This finding demonstrates that the chains of bow-shaped rotamers are indeed the most stable structures and that their formation involves the internal rotational dynamics of the phenyl rings of Azobenzene.

At a higher **CMA** coverage, this simple picture breaks down. Molecular density becomes an issue, and the two-dimensional domains of zigzag-shaped molecules pack **CMA** more efficiently. Correspondingly, at a coverage of 0.4 ML, 19% of the sample is covered by two-dimensional domains of 3,3'-**CMA** (at room temperature), and this fraction increases at larger coverage, as also shown in the blue scale of graph (e) in figure 2.8. The formation of two-dimensional structures takes place through an overall decrease in the fraction of 3,5'-rotamers on the sample. The percentage of these rotamers is reduced to 45% for 0.4 ML and 40% for 0.57 ML. The chain structure, albeit more stable, is less efficient for packing **CMA** molecules in two dimensions. Thus, at a higher coverage the two-dimensional structure becomes gradually more favorable due to its larger packing density. The monotonous change in the fraction of each rotamer at the surface, influenced by temperature and coverage, demonstrates that the large-scale organization of the molecular thin film necessarily involves thermally activated internal rotations of the **CMA** phenyl rings and hence, the change of its conformation.

The energy required to activate the internal rotational dynamics presumably increases due to the planar interaction of the phenyl rings with the metal surface. However, non-covalent interactions add up, when multiple connection points exist between molecules and stabilize ordered structures. Also they may cooperatively overcome the adsorption barriers and mediate a conformational change [Fern 06]. In our case the internal molecular motion requires the three-dimensional lifting of

a phenyl ring. Thus, we believe that only through the effective mediation of multiple hydrogen bonds (in addition to thermal energy) the out-of-plane conformational dynamics of **CMA** can overcome the rigidity imposed by the metal surface.

## 2.4 Formation of Supra-Molecular Building Blocks

Sulfur (S) is an element showing characteristic interaction to gold atoms, when embedded in molecular structures [Ohar 06, Gron 00]. Thiols (R-SH) and disulfide groups (R-SS-R) attached to organic molecules have been intensively studied as anchoring units to gold surfaces in self-assembled-monolayers. In the scope of studying azobenzene derivatives, this particular interaction opens the possibility for anchoring also individual molecules or small clusters to avoid molecular diffusion in the manipulation process. For instance, it has been shown how individual dimethyldisulfide molecules ($CH_3SSCH_3$) on a Au(111) surface could be dissociated into two thiol units by STM [Maks 08]. Therefore, as one switchable compound, the *para*-cyano-*para*-disulfide-azobenzene derivative (**DSA** shown in figure 2.9 (a)) could be synthesized in the work group of K. Rück-Braun. The adsorption to a gold surface is expected to act via the di-sulfide moiety either by direct coupling or by a dissociation of the disulfide ring into two thiol arms. Both types of adsorption may offer the cyano functionalized part of the molecule for STM induced switching, while the other part is not perturbed. However, in the following pages it will show that disulfide units do not dissociate but interact strongly to other disulfide units, forming supra-molecular clusters.

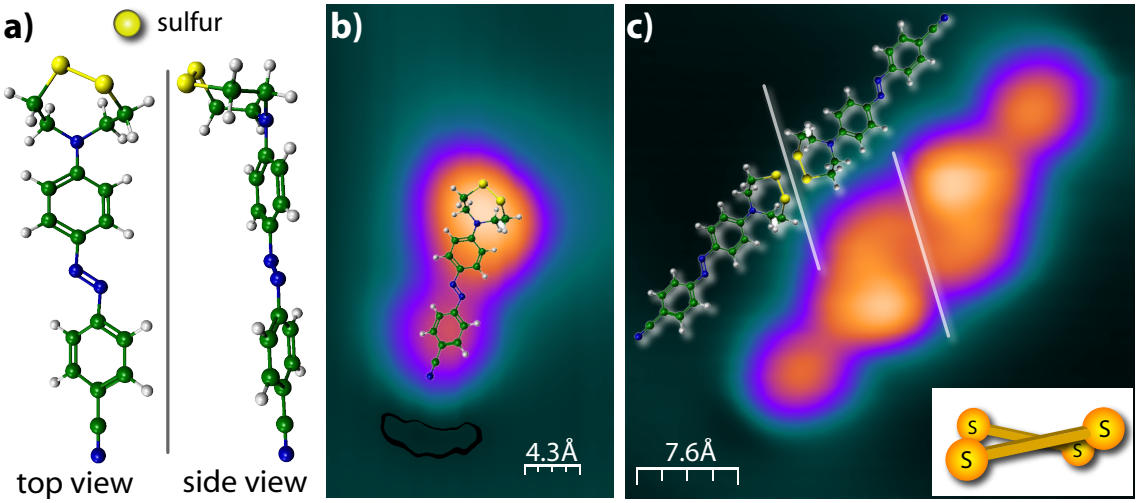


**Figure 2.9:** (a) Gas phase structure of a **DSA** molecule minimized by the semi empirical MOPAC method, in top- and side view. (b) Single molecule adsorbed at room temperature onto a Au(111) single crystal, the minimized structure is superimposed. (c) frequently observed dimer building block of **DSA** and its parallel displaced molecular dimer structure showing how the recognition is caused by interaction of four sulfur (S) atoms. Scanning conditions: (b) $V_B = 800$ mV, $I = 1.2 \times 10^{-10}$ A; (c) $V_B = 680$ mV, $I = 3.4 \times 10^{-10}$ A.

Figure 2.9 (b) shows the STM topography of an individual **DSA** molecule adsorbed

on a Au(111) surface, consisting of two protrusions. As the super imposed molecular structure suggests, the lower one can be associated to the cyano functionalized phenyl ring. A faint depression enclosed by the black contour line in the bottom left of the molecule gives the orientation of the cyano group, resulting from a lowering of the metals work function in the proximity of electron rich cyano group. Consequently, the higher protrusion is interpreted as the molecular moiety with the disulfide-heptagon attached.

The super imposed molecular structure and the ones shown in panel (a) of figure 2.9 are the results of a minimization of the total energy of the free molecule by the semi-empirical MOPAC algorithm. The top and side view of the obtained structure show that the disulfide moiety adopts a three-dimensional structure and is oriented out of the molecular main plane (in contrast to the planar Lewis structure in figure 2.1). The computed structure fits from its size comparably well to the obtained features in the STM topography.

The bright diffuse feature of the molecular disulfide side shows some asymmetry. This may arise from the alignment of the disulfide unit as one can learn from the top view structure. Still the data do not clarify whether the disulfide unit points downwards and anchors to the surface or whether it points upwards from the surface. In the latter case, the nitrogen atom joining the ring with the azobenzene's main body most probable would couple to the surface.

In Figure 2.9 (c) a topography of frequently observed dimer structures of **DSA** molecules is shown. Two molecules are interconnected in a head to head fashion via the disulfide group. Surprisingly, only in these cases the STM can reveal intra-molecular resolution of the disulfide parts, while the cyano sides are mapped the same as in the single molecule case. The intra-molecular resolution of the disulfide part consists of a higher protrusion and a lower one extending further in the direction of the counterpart molecule and interlocking with it. The different heights confirm that the two sulfur atoms of one molecule are aligned in different ways parallel to a nodal line (indicated in the topography 2.9 (c)) but most probable at different heights. This interpretation is supported by the theoretically minimized molecular models, superimposed to the image.

The interlocking of the molecules causes a larger stability for dimers than for individual molecules. Most probable the interlocking results from hydrogen bonds between sulfur atoms and hydrogen terminations. A dissociation of the disulfide bond upon adsorption is not observed since the matching of sulfur positions in the molecular model and the topography agrees well. Also a dissociation would cause thiol arms of high flexibility ($C_2H_4SH$), which would have various adsorption conformations.

Inspection of larger scanning areas reveals larger clusters that consist of assemblies of dimers, shown in figure 2.10 (a) and (b). The complex structures are composed of up to four but usually two dimers laying parallel, as it is shown in the frames 1 and

2 in panel (a) of the figure. The high resolution STM image in panel (b) clarifies that the cyano end groups are terminated by additional dimers perpendicular to the former ones. In panel (c) a suggested molecular model is shown, that fits to STM topography and reveals possible hydrogen bonds, as indicated by orange lines (S···H and N···H).

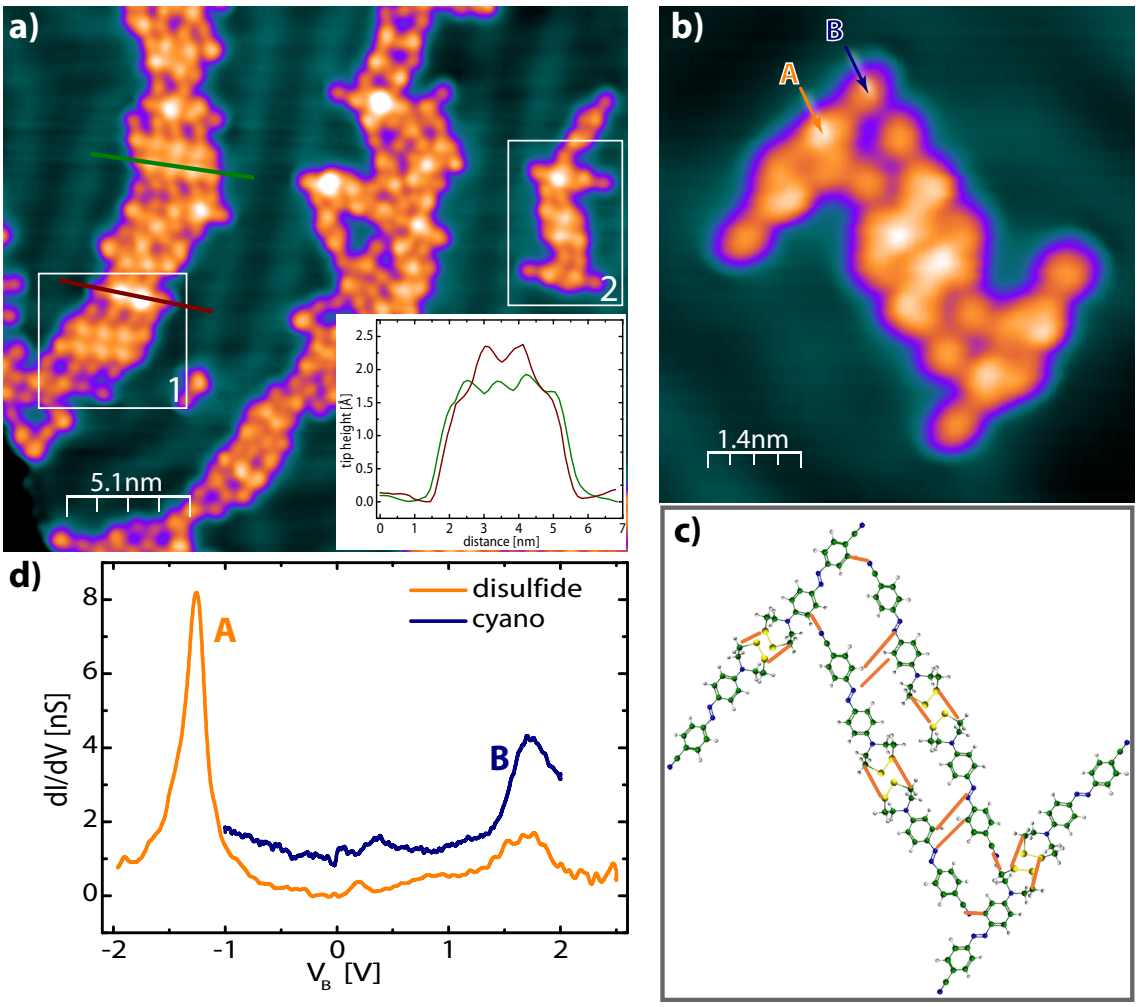


**Figure 2.10:** (a) Overview STM image of **DSA** adsorbed at room temperature onto a Au(111) single crystal, indicated areas in frame **1** and **2** show characteristic supermolecular arrangements. The inset shows the height profiles of a normal disulfide moiety (green line) and a high one (red line). In (b) a high resolution image of a typical molecular organization is shown with the characteristic site of the disulfide moiety (arrow **A**) and the cyano side (arrow **B**) indicated. Panel (c) represents the according molecular structure. Tunneling spectra in (d) reveal characteristic line shapes for the disulfide (**A**) and the cyano part (**B**) of **DSA**. Scanning conditions: (a) $V_B = 553$ mV, $I = 1 \times 10^{-9}$ A; (b) $V_B = 0.18$ V, $I = 2.1 \times 10^{-9}$ A.

We assume that these structures assemble upon a selective recognition of hydrogen bond patterns at two different levels: While the sulfur-hydrogen interaction drives the formation of molecular dimers into molecular building blocks, a slightly weaker interaction evolves from nitrogen with hydrogen atoms, which mediates the parallel

alignment and perpendicular oriented dimers.

Tunneling spectroscopy (STS) depict different fingerprints for the phenyl ring with the disulfide heptagon (**A**) and the one with the cyano group (**B**) attached to it. Both sites are indicated by yellow and blue arrows respectively in panel (b) and the spectra are shown in panel (d) of figure 2.10. At the disulfide side, a sharp resonance at −1.3 V (orange spectrum) in the occupied energy region is observed and a weak signal at +1.7 V above the Fermi energy. At the cyano moiety (blue spectrum) the latter is seen more prominent than in the disulfide side, but no other resonance is observed. The +1.7 V peak is related to the lowest empty molecular orbital (LUMO) of the molecule, delocalized over the molecule, in agreement with data for the **DMC** molecule, which will be presented in section 3.1 of the next chapter. The additional feature at the disulfide side must result from a localized state. Its sharpness indicates that this state is well decoupled from the surface.

As in the large scale STM topography of figure 2.10 (a), higher protrusions are often seen in molecular clusters. For instance in the upper part of frame 1 two protrusions are seen with heights of around 2.5 Å, while the typical molecular heights are 1.7 Å. These higher features are only observed at the disulfide moiety of the dimers. The inset shows the different heights by two height profiles along the red and green lines for the higher features and typical molecular corrugation respectively.

In figure 2.11 (a) we can focus on a cluster of dimers that has two of the high protrusions in the upper part and another high protrusion in the lower part, where two molecules dimerize. The asymmetric height profile along the latter is shown by the red line in panel (b) of this figure. Non-destructive tunneling spectroscopy could be performed on these protrusions, in the limit of small electrical fields. Hence, we show in panel (c) STS data, performed with the feed back loop of the STM electronics switched ON (constant current of 0.5 nA). Here we have performed spectroscopy in the positive and negative range individually, shown by the purple lines.[4] A sharp resonance is observed at +0.5 V above the Fermi level.

When applying voltage pulses of ∼2 V onto the higher protrusions they change their aspect in topography and spectroscopy. The result of such manipulation is shown in panel (d) of figure 2.11. The high protrusion has changed into the typical scenario with a height of 1.7 Å as seen from the green height profile in panel (b). The spectroscopy at position **B**, shown by the yellow lines in panel (c) reveals now the typical fingerprint with the sharp resonance of the occupied state at −1.3 V and the LUMO resonance at +1.7 V.

Since this manipulation process was not observed reversibly, we attribute the high protrusion of 2.5 Å at the disulfide moiety to a semi-stable configuration of the molecule, procuring the adsorption. The lower molecular feature in the typical scenario with 1.7 Å height, is hence the fully relaxed molecular structure. Existence

[4]The STM tip would approach for zero bias voltage to contact, causing diverging conductance and most probable destruction of the molecule.

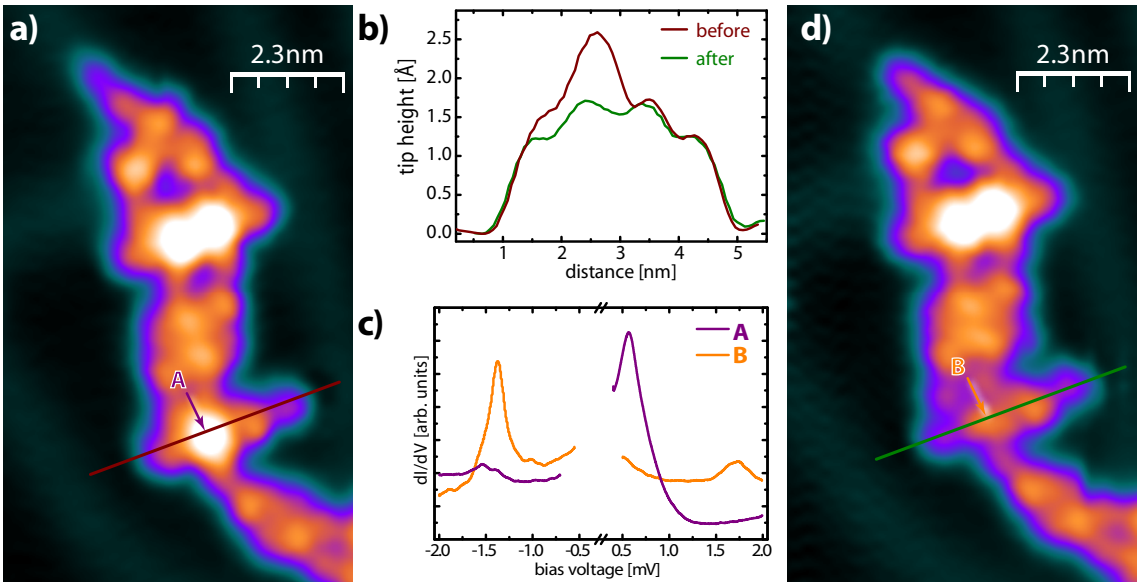


**Figure 2.11:** (a) Close up image of an ordered **DSA** cluster with higher features at two disulfide moieties. One is manipulated, resulting in the fully relaxed molecular geometry, shown in (d). The different topography of both structures is reflected in the height profiles (b) of both clusters according to the indicated red and green lines. The different molecular geometry correlate with different spectroscopic fingerprints shown in (c), taken before and after the transformation in site **A** and **B** respectively. Scanning conditions: (a, d) $V_B = 1.03$ V, $I = 2 \times 10^{-10}$ A.

of multiple adsorption states is very likely for complex molecules. In this case they can be caused by different intermolecular hydrogen bond configurations between the sulfur atoms and hydro-carbons or by different atomic adsorption sites of the disulfide unit on the surface. The activation of the molecular relaxation is induced via tunneling electrons above the LUMO energy. Hence, we assume that electron attachment triggers this process.

The different spectroscopic fingerprints reveal weak surface coupling of the involved resonances in both cases. Surprisingly the resonance of the precursor state is above, the one of the fully relaxed structure below the Fermi level. Accordingly, the molecular relaxation may involve electron transfer between molecule and surface.

## 2.5 A Molecule as one-dimensional Quantum Well

The spectroscopic fingerprint of the two methoxycarbonyl-functionalized azobenzene molecules (**CMA** and **CPA**) will be compared. The two species differ geometrically only by the orientation of the functional groups: *meta*-orientation for **CMA** and *para*-orientation (**CPA**). The topographic maps (figure 2.12 (a) and (c)) show, how the individual molecules have two different options to adsorb in the case of **CMA** but are restricted to one geometry in the case of **CPA**. Both topographies show the molecules adsorbed on a Au(111) surface at room temperature.

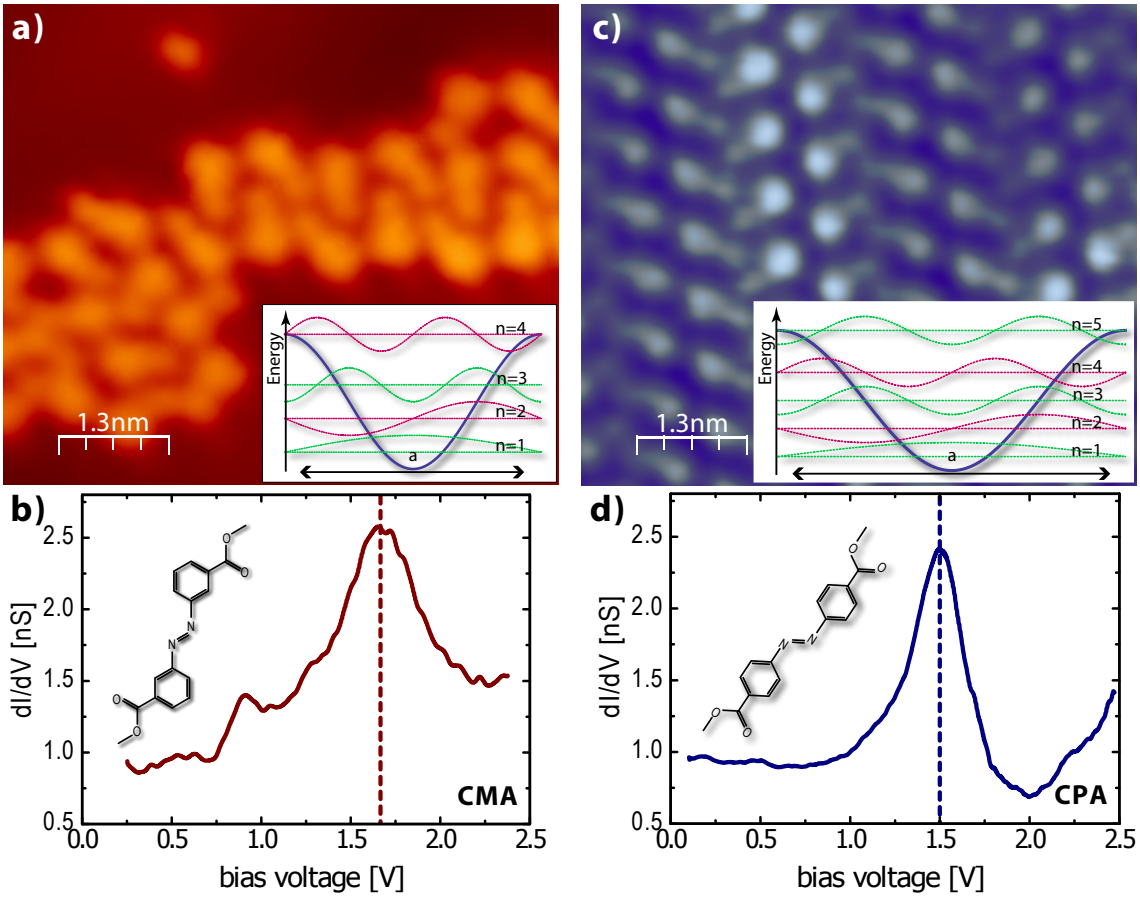


**Figure 2.12:** (a) **CMA** and (b) **CPA** molecules adsorbed on a Au(111) surface. **CMA** shows two different conformations, **CPA** only one. $dI/dV$-spectra of (c) **CMA** and (d) **CPA**. Scanning conditions: (a) $V_B = 396$ mV, $I = 1.2 \times 10^{-10}$ A; (c) $V_B = 482$ mV, $I = 5.5 \times 10^{-11}$ A.

For a delocalized electron system of an organic molecule, the *meta*-position of a phenyl unit is known to be *non-conjugated*. Consequently, a functional group linked in such sites is decoupled from the molecules' $\pi$-electron system. This is the case of **CMA** molecules. On the other hand, the *para*-position is *conjugated*, and hence the **CPA**'s functional group is well coupled to the molecule's $\pi$-system. This results in a larger effective length for the delocalized electron system in **CPA** compared to **CMA**.

The electrons in each molecule can hence be considered as confined in a bound state of different size. In the most simple approximation this can be described by a quantum well and solved as a text book example by the Schrödinger equation when employing standing waves. The energy eigenvalues $E_n$ scale with the square of the main quantum number $n$ and with the inverse square of the lateral delocalization length $a$ (width of the quantum well).

$$E_n = \frac{\hbar^2 \pi^2}{2 m_e a^2} n^2 \tag{2.1}$$

The plots in figure 2.12 (b) and (d) show two scanning tunneling spectra obtained from **CMA** and **CPA** by STS. **CMA** shows an electronic resonance at 1.7 eV while **CPA** displays a strong feature at 1.5 eV. Associating this discrepancy to an energy shift of the standing waves inside a quantum well, a difference of 0.067 Å can be computed for the effective molecular lengths between both molecular species. Hereby we assume that the total molecular size is 17 Å and the $14^{th}$ electron state dominates the conjugated $\pi$-system because 7 electron pairs describe the $\pi$-state. Although the computed difference in length does not compare well with the geometrical structures, it quantitatively confirms that an energy level scales up, when the system size shrinks. Also the crude approximation of the potential shape by a rectangular box limits this comparison.

# Chapter 3

# Conformational Switching of DMC-Azobenzene on Noble-Metal Surfaces

The investigation of molecular systems that show internal flexibility on a surface and hence, can be employed as molecular switch is one of the main challenges in the scope of this thesis. The azobenzene molecule with its two states, very different in their aspects, is a promising candidate for this goal, because its switching characteristics are well understood from theoretical and experimental studies in gas phase and solution [Tsuj 00, Tsuj 01a, Tsuj 01b, Wach 04, Feri 01, Sekk 02, Drr 90, Fuch 06]. Nevertheless, the adsorption on surfaces strongly influence the molecules characteristics and hence, their ability for switching. Covalent anchoring, steric hindrance of the surface, and charge rearrangement are the major reasons, why a surface prevents a switching of molecular adsorbates and why a decoupling from the surface in many studies allowed successfully isomerization [Alem 06, Coms 07]. In this chapter we deviate from this approach and systematically focus on the influence of different surfaces (Au, Cu, and Ag) on the azobenzene derivative **DMC**. This molecule has been introduced before: an azobenzene molecule, functionalized with cyano groups in the *meta*-position of each phenyl ring (see figure 3.1). We reveal that the coupling of surface and molecule can be utilized for tuning the switching ability of the diazo unit.

We study first how the weak surface interaction of Au(111) allows a $\beta$-rotational transformation, but no *trans-cis*-isomerization is observed on this surface. The understanding of rotational switching is substantiated by quantum chemical calculations. On Cu(100), the *cis*-isomer can be achieved upon STM manipulation on a *trans*-isomer, but no reversion of this process could be found. A stronger bond is established between the *cis*-isomer and the surface than in the *trans*-one, which is supported by DFT calculations. When the molecule is adsorbed on Ag(100), an intermediate interaction strength allows to observe reversible *trans-cis-trans*-isomerization.

## 3.1 Ring-Rotation of *trans*-DMC on Au(111)

Gold, known to be the most inert noble metal, is expected to hardly influence the molecular structure upon adsorption [Alem 06]. The weak adsorption via $\pi$-surface

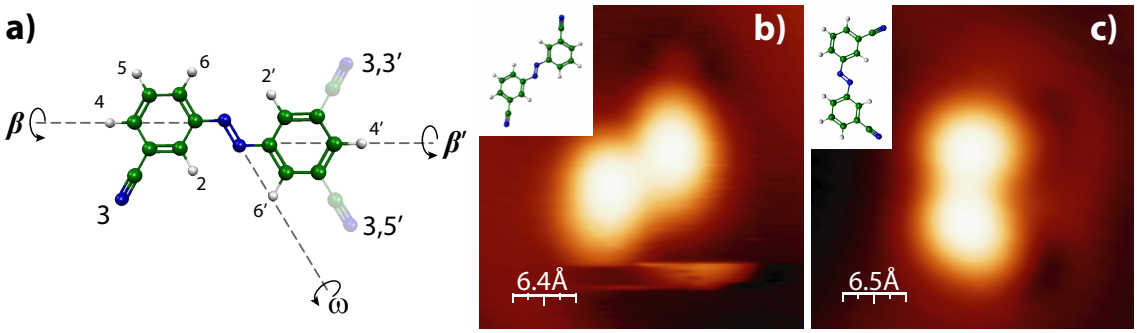


**Figure 3.1:** (a) Atomic model of the **DMC** molecule indicating the reaction angle $\beta$ for the rotation of a phenyl ring (from 3,3'- to the 3,5'-conformation) and the dihedral angle $\omega$, which mainly describes the *cis-trans*-isomerization. STM images of (b) the isolated 3,3'-*trans*-DMC and (c) 3,5'-*trans*-DMC isomers on the Au(111) surface with their molecular structures, respectively in the insets. Scanning conditions: $I = 0.48$ nA; (b) $V_B = -1$ V; (c) $V_B = +1.2$ V.

interaction hence is expected to preserve the **DMC**'s gas phase characteristics to a great extent, when adsorbed planar. Still, the *cis*-isomer, involving a three-dimensional molecular structure, is not observed, because its $\pi$-electron system does not stabilize the molecule on the surface.

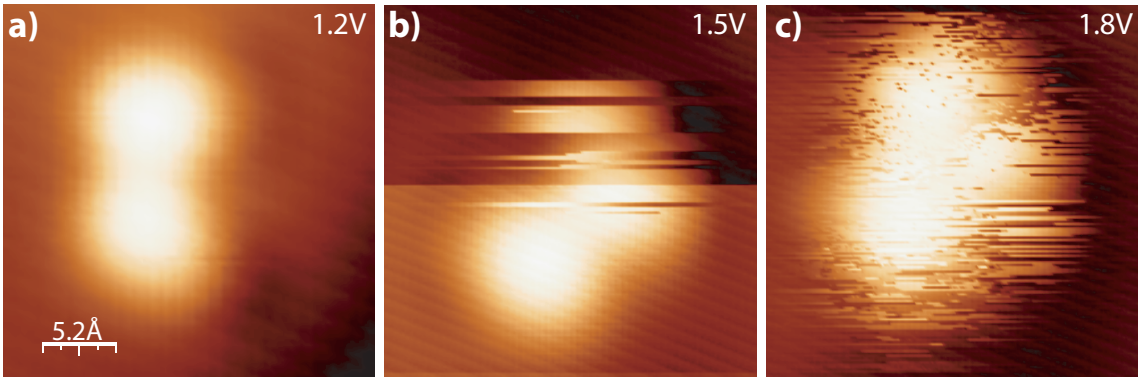


**Figure 3.2:** (a) STM images of an isolated molecule scanned with several sample bias values. (a) For $V_B = 1.2$ V the molecule lies stable on the Au(111) surface in a 3,5'-*trans* conformation. (b) For $V_B = 1.5$ V molecular motion between two configurations is excited. (c) For $V_B = 1.8$ V the molecule moves faster than the scanning process can map it, thus it appears in a fuzzy shape. All images were scanned at a feedback current of $I = 0.21$ nA.

At low temperatures ($\sim$100 K) **DMC** adsorbs on Au(111) forming mostly disordered islands and a few number of monomers (as seen in figure 2.6 (a)). We find the two characteristic configurations, which are associated to the 3,3'-*trans* and the 3,5'-*trans* $\beta$-rotamers as shown by the STM topographies in figure 3.1 (b) and (c).

Both can be described by two ellipsoidal lobes separated by $0.74 \pm 0.05$ nm one from the other. Each lobe corresponds to one of the phenyl moieties. The cyano groups induce a weak elliptical deformation of the lobes in the STM topographs. In isolated molecules, it is also possible to observe the faint topographic depressions close to the location of the cyano end groups, resulting from the high electrophilicity, as explained in section 2.1 for the case, when **DMC** is adsorbed on Ag(100) [Spag 71].

As expected, **DMC** adsorbs weakly on the Au(111) surface. In general, imaging of islands and monomers becomes unstable, when the sample bias is raised above a threshold value of about 1.5 V. Molecular motion (diffusion, rotation) is frequently induced by the STM tip during scanning. Figure 3.2 shows a series of STM images of an isolated molecule showing that the successive increase of the bias voltage ($V_B$) is accompanied by an instability of the molecule. In figure 3.2 (a) a **DMC** molecule with a 3,5'-conformation lies stable while scanned with $V_B$=1.2 V. When the sample bias is increased to $V_B$=1.5 V horizontal lines in the image indicate erratic changes of the molecule during scanning. As the bias is increased to $V_B$=1.8 V the rate of these erratic "switches" becomes faster ($\sim$ 7 Hz), and the STM is only able of imaging a superposition of hopping protrusions.

On some occasions the induced motion of the whole molecule is accompanied by a change in molecular conformation between the 3,3'-*trans*- and the 3,5'-*trans*-isomers. Figure 3.3 shows one example, where a 3,5'-*trans*-conformer (a) appears in the 3,3'-*trans* conformation (b) after applying a current pulse of 10 nA for 4 seconds ($V_B$ = 1.7 V). Since both lateral motion and conformational changes are induced simultaneously, we tentatively ascribe this phenomenon to the existence of a transient highly mobile state, which is excited by tunneling electrons and that is characterized by the lifting of at least one phenyl ring from the surface. Curiously, on rare occasions, a double ring-flip could be detected after a single pulse event, leading to an apparent change in the chiral aspect of the molecule in the STM image (figure 3.3 (c) and (d)). Since we cannot differentiate between the 3,3'-*trans*- and the 5,5'-*trans*-conformation, nor between the enantiomers of all the conformations from the STM topographies, a complete inversion, a rotation or a flip of both phenyl rings by $\beta$-rotational transformations can explain the change of the molecule's aspect after the manipulation.

Similar motion can also be observed on bi-dimensional (disordered) molecular islands during scanning with similar high bias values, or by applying voltage pulses, as it is shown in figure 3.4. **DMC** molecules coalesce easily in islands interconnected probably through hydrogen bonds between CN and HC terminations, increasing their stability against the effect of tunnel electron activated mobility. The figure shows a cluster of **DMC** molecules (a) before and (b) after applying a 1.7 V pulse. In this case only one single molecule changes from the 3,5'-*trans*- to a 3,3'-*trans*-conformation. In most cases, the result of electron injection in one molecule is the collective motion of several molecules in a cluster, indicating that their interaction is strong enough to couple their motion. This coupling between molecules generally quenches the manipulation, thus the shown example is one of

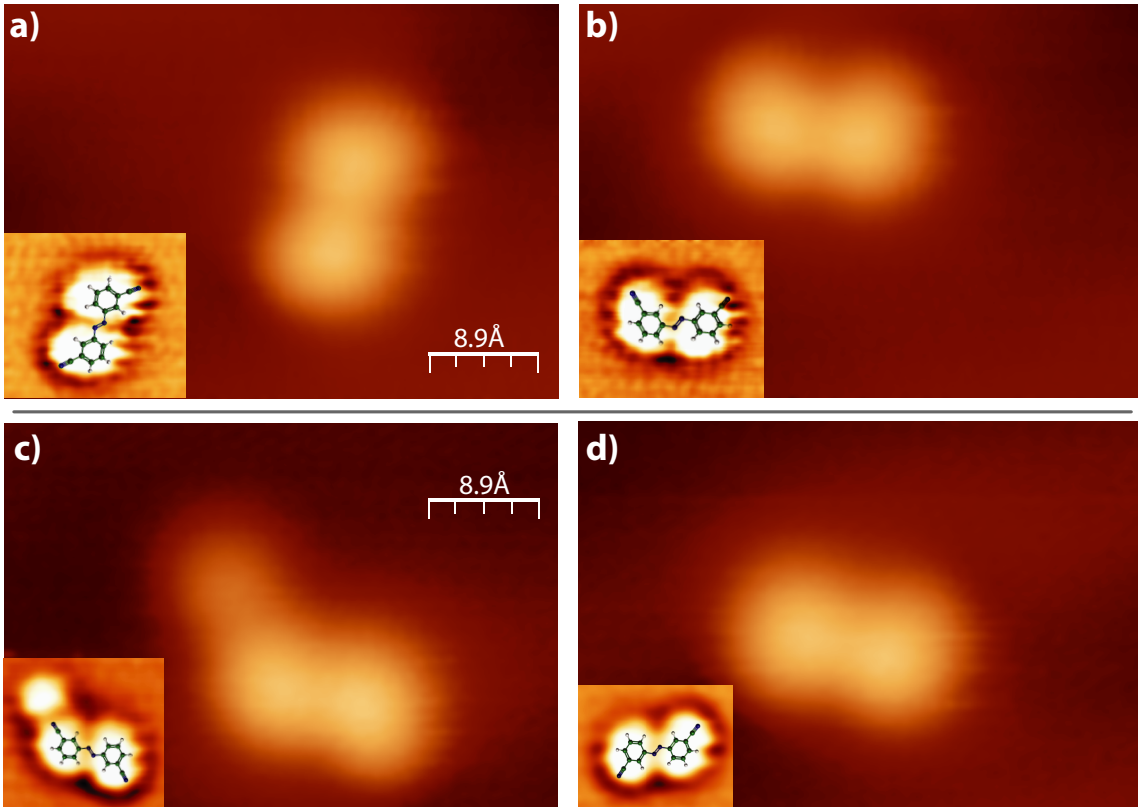


**Figure 3.3:** STM images of isolated **DMC** molecules before and after applying current pulses with the STM tip on top of one of the phenyl rings. The inset in each figure shows the STM topographs with a laplace filter [Horc 07], and a model of their conformation. (b) shows the same molecule as in (a) after applying a 4 seconds bias pulse of $1.8$ V with a current of $10$ nA. A combination of translation, rotation and a change from the 3,3'-*trans* to the 3,5'-*trans* conformation can be seen. In (c) and (d) the same procedure (now a $0.5$ s. pulse) leads to inversion of both cyano groups. Either rotation of the whole molecule or the flipping of both phenyl rings can cause this. The additional feature in (c) is ascribed to an impurity of unknown nature. Scanning conditions: (a, b) $V_B = 821$ mV, $I = 1.3{\times}10^{-11}$ A; (c, d) $V_B = 1.1$ V, $I = 8.9 \times 10^{-12}$ A.

the rare clear examples, where a conformational change occurs, but the neighboring molecules remain unchanged. Image processing allows us in the third image to display the difference between color scale values of the previous two images ((a)-(b)). Hence, the green depression and the red protrusion indicate the rotational change of one individual cyano group, evidencing an isolated $\beta$-rotation, while the rest of the molecules remains unchanged.

The quantum yield for inducing molecular motion (diffusion, rotation or ring-flip) in **DMC** islands is roughly estimated as $Y_R = 5{\times}10^{-10}$ $events/electron$ and shows in figure 3.5 (a) a certain increase at 1.7 V, where it remains at a constant value for larger sample bias. The value is approximately 10 times larger in the case of single molecules. This value, however, is an average of various molecular islands and for each case it will depend on the number of hydrogen bonds locking the molecules in the clusters. The threshold value for such changes of about 1.7 V determined in

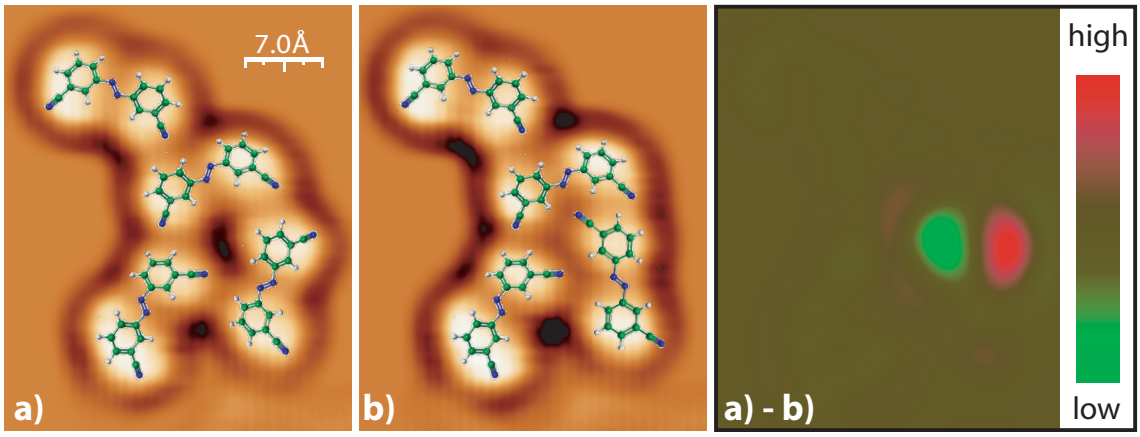


**Figure 3.4:** (a) and (b) show two successive STM images of a **DMC**island before and after a 4 seconds pulse of 1.7 V and 6 nA was applied. (a)-(b) shows the difference between the two images. The red to green motion reveals a change in one of the lobes of a molecule from the 3,5'-*trans* to the 3,3'-*trans* conformation. (a) and (b) are laplace filtered [Horc 07] to emphasize the molecular conformation. Scanning conditions: (a) and (b) $I = 3.2$ nA; $V_B = 0.5$ V.

molecular islands is similar to the behavior found in single molecules.

### 3.1.1 Tunneling Spectroscopy

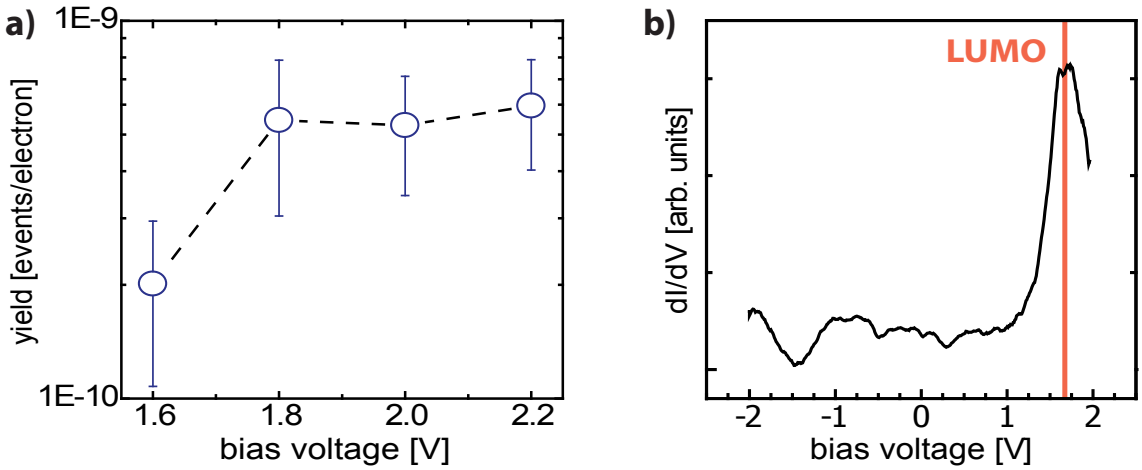


**Figure 3.5:** (a) function of the quantum yield of observed switching events versus the sample bias. It shows a strong increase, when the threshold value of 1.7 V is overcome and remains constantly for larger voltages. (b) tunneling spectrum of a **DMC** molecule. The resonance at 1.7 eV is associated with the first unoccupied molecular $\pi^*$ orbital (LUMO), which seems to initiate the conformational change.

The threshold bias of ∼1.7 V found in our experiments is a fingerprint for the type of molecular excitation leading to both molecular motion and phenyl ring rotation. Electron-induced processes may involve either the electronic excitation of transient molecular states [Mull 98, Stok 98, Sloa 05, Ianc 06] or the excitation of molecular vibrations through inelastic scattering [Ho 02, Kome 02, Pasc 03]. Both types of processes can also activate conformational changes in molecules [Fuch 06, Gaud 00, Tana 02]. To figure out which of the two mechanisms applies

here, we compare the threshold voltage for switching with the energy alignment of molecular states obtained from **DMC** on Au(111), measured using scanning tunneling spectroscopy (STS). The spectrum in figure 3.5 (b) is acquired on top of a **DMC** molecule forming part of a molecular cluster to hinder the fast motion of the molecule during the measurement. The spectrum shows a clear enhancement of the differential conductance at 1.7 V and is interpreted as resonant electron tunneling through the molecular state associated to the lowest unoccupied molecular orbital (LUMO) of the **DMC** molecule. The good correspondence of the energy of this molecular resonance with the ∼1.7 V threshold for switching strongly supports that the switching dynamics is activated by electron scattering with this unoccupied molecular state.

### 3.1.2 Intramolecular Dynamics

The energy position of the resonance found in the tunneling spectrum can be interpreted based on first principle calculations by Füchsel *et al.* [Fuch 06]. For a free *trans*-**DMC** isomer, the authors find an electron affinity (EA) of about 1.9 eV. The vertical excitation energy to an anionic state of **DMC** adsorbed on Au(111) can be estimated from $\Delta E = \Phi - e^2/4Z^2$, where $\Phi = 5.1$ eV is the Au(111) work function. The last term accounts for the stabilization of the excitation energy due to image charge screening. The peak alignment of about 1.7 V, found in figure 3.5 (b), requires an image charge stabilization energy of 1.5 eV, which is fully consistent with typical molecule-surface distances $Z$.

In gas phase, the electron population of affinity levels (*e.g.* electron attachment) is an efficient method to induce chemical reactions [Ingo 96]. For adsorbates on metal surfaces, electron tunneling is generally a fast process, much faster than nuclear motion (see section 1.1.4). Therefore, electronic excitations are not an efficient way to induce molecular transformations. However, the topology of excited potential energy surfaces (PES) can help, to accelerate the nuclei along specific reaction coordinates, which eventually leads to a transformation after quenching to the ground state [Fuch 06]. It is thus important, to question about the PES topology and the intramolecular dynamics in the electronic excited state, to rationalize our result of the observed $\beta$-ring-rotation.

On Au(111), **DMC** is presumably adsorbed in two planar conformations because the physical interaction with the metal is governed by the phenyl $\pi$ states and hence it is comparably weakly coupled. The two ground state conformations 3,3'-*trans* and 3,5'-*trans* are supposedly connected through a potential energy barrier essentially composed of the free molecule's $\beta$-rotation energy barrier and the potential energy due to the interaction of the phenyl rings with the Au(111) surface. From our experiments we conclude that electron tunneling through the anionic resonance is able to initiate the rotation of one of the **DMC** phenyl rings along the $\beta$ reaction coordinate. This rotation necessarily implies the existence of a non-planar intermediate precursor state, having the ring lifted from the surface,

which justifies to introduce a second reaction coordinate: the dihedral angle $\omega$ (see figure 3.1) describes the rotation of half the molecule around the axis given by the diazo center (N=N), when the other half is fixed. This angle is also important for the *trans*- to *cis*-isomerization. Due to the molecule's geometry, for our case the $\omega$-rotation evidently results in the desired lifting of one phenyl ring. The detailed structure of the transition state can only be described, after knowing the intramolecular pathway, followed during the excitation. This is a complex motion, even if only a motion by two coordinates ($\beta$ and $\omega$) is allowed and having neglected the interaction to the existing electric field in the tunneling junction.

Supported by a theoretical approach, we aim to rationalize, how a fast electronic excitation of on a free planar molecule can couple to internal motion out of the planar structure of *trans*-**DMC** with and without an electric field [Fuch 06]. Therefore it is helpful to argue about the time scale for a ring rotation based on the experimental quantum yield $Y_R$. For the individual molecule on the Au(111) surface, we estimate roughly $Y_R = 10^{-9}$ *events/electron*. This low value is a consequence of the short excitation lifetime $\tau_e$ with respect to the time required to rotate the ring. From the line width ($\Gamma \approx 450$ mV) of the LUMO resonance in the STS data (figure 3.4(c)), we may approximate $\tau_{LUMO} = \hbar/\Gamma \approx 1.5$ fs. This excitation life time is much shorter, than needed for typical atomic motions. It is then reasonable to expect that the complete internal dynamics, leading to the ring rotation, occurs in the electronic ground state, eventually triggered by the fast electron scattering with the LUMO resonance.

### 3.1.3 Quantum Chemical Calculations

The scenario of a negative ion resonance-mediated reaction is supported by the quantum chemical calculations, which have been performed in this context by J. Dokić in the research group of P. Saalfrank. Her calculations revealed fully optimized structures of the **DMC** molecule and two-dimensional potential energy surfaces $V(\beta, \omega)$ were computed. Both, the structures and potential surfaces were calculated for the neutral **DMC** and the anionic charged $\mathbf{DMC}^-$ with and without an external electrostatic field, as depicted in figure 3.6. The electric field represents a simplified model for the tunnel junction between the surface (+) and the STM tip (-).

In the panels (e)-(h) of figure 3.6 the restricted, two-dimensional potential energy surfaces $V(\beta, \omega)$ for the four different situations are shown, according to the fully optimized molecular structures, which are shown in panels (a)-(d). For **DMC** without an electrical field in panel (e) one finds two minima, corresponding to the 3,3'-*trans*- and 3,5'-*trans*-conformations. The former is slightly more stable than the latter (by 0.01 eV), because of the favorable antiparallel dipole moments originating from the cyano groups. The corresponding fully optimized structures of the 3,3'-*trans*-form is shown in figure 3.6 (a).

When attaching an electron to the free **DMC** (figure 3.6 (g)), the major effect

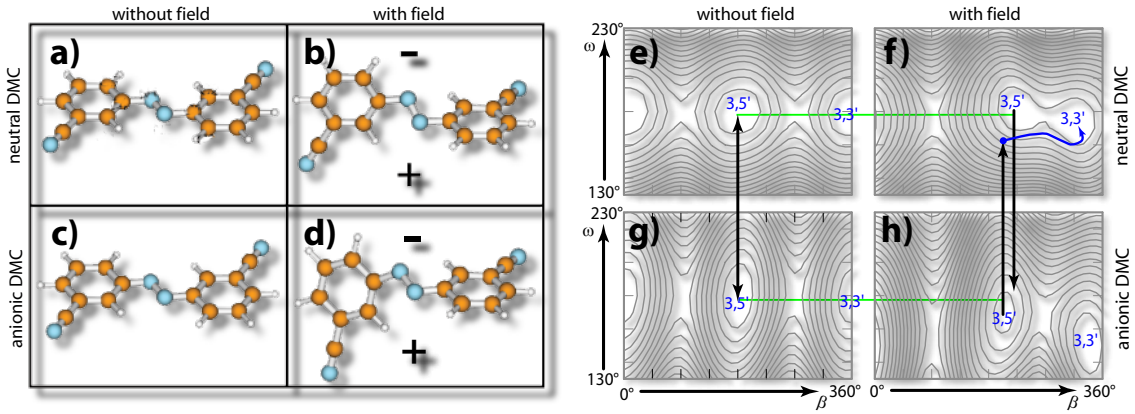


**Figure 3.6:** (a)-(d) optimized structures of neutral 3,3'-*trans*-**DMC** without (a) and with electrical field (b) and of its anionic species 3,3'-*trans*-**DMC**$^-$ without (c) and with (d) field. The field is oriented perpendicular to the right N-phenyl-CN ring, directed from the surface (+) to the tip (-). (e)-(h) Contour plots of potential energy surfaces $V(\beta, \omega)$ of **DMC** without (e) and with (f) external electrostatic field and of the anionic species **DMC**$^-$ without (g) and with (h) a field. All contours are separated by 0.1eV. The black arrows indicate the process of sudden, vertical electron attachment/detachment processes. In the field free case (left) no energy is gained during these processes, because the 3,5'-*trans* and 3,3'-*trans* minima for the neutral and anionic species are at the same position. In contrast, in the case with electric field the sudden discharging can gain enough energy to overcome the barrier for a change in configuration from the 3,5'-*trans* towards the 3,3'-*trans* (blue arrow) minimum in (f).

is an increase of the ismerization barrier to about 0.61 eV. The minima positions as well as the geometry of the fully optimized **DMC**$^-$ (in figure 3.6 (c)) remain the same. The increased energy barrier for the anionic **DMC**$^-$ results from the bonding character of the LUMO at the central N atoms to the neighboring C atoms. Consequently, the attachment of electrons into this orbital will quench a rotation.

However, the larger barrier for the anionic state is not *per se* counterproductive for the 3,3'-*trans* to 3,5'-*trans*-isomerization, if the reaction predominantly proceeds in the neutral state, following an attachment and rapid detachment of a tunneling electron. This is possible since the electron migration is much faster than the nuclei motion. For successful isomerization upon the ionization-and-relaxation process it is obligatory that energy is gained by this process. Since the topologies of the energy surfaces of **DMC** and **DMC**$^-$ in figure 3.6 (e) and (g) are almost the same, no energy gain results here and no torque along the $\beta$-coordinate is created by the attachment-detachment process, hence the molecule will remain ideally flat and non-rotating.

In the presence of an electric field a geometrical rearrangement, by means of changes in $\beta$ and $\omega$, occurs. As seen in figure 3.6 (b) for the neutral and (d) for the anionic case, the molecular structure changes, inducing a $\beta$-tilt of the right phenyl ring. The optimized structures adopt a more three-dimensional geometry than in the field free case. Thus, the energy minimizes in the external field by orienting the CN group of the mobile phenyl ring towards the surface. This maximizes the

attractive Coulomb interaction between the partially negatively charged Cyano moiety with the positive surface underneath.

Seen from the potential energy plots in panel (f) and (h), the minima redistribute and the neutral energy surface (f) has a much lower isomerization barrier. When attaching an electron and entering the anionic system (h), the molecular coordinates tend to the minima in this state gaining kinetic energy, because the anionic minimum energy is shifted with respect to the neutral case. This is an essential difference to the field-free case: Since the minima in the energy surfaces are in different positions, the electron attachment will induce a (coupled) motion along the $\beta$ and $\omega$ coordinates, towards the shifted minimum in the ionic potential (h). Detachment of the electron from the anion $\mathbf{DMC}^-$ (h) brings the system back to neutral **DMC** (f) by a vertical fast process. The mismatch with respect to the local minimum of the neutral potential indicates a gain of kinetic energy, which eventually is released by the change into a different conformation, as exemplarily indicated by the blue arrow.

An upper bound of the energy gain by attachment and subsequent detachment of an electron can be estimated as following: After geometrical optimization of the neutral **DMC** and anionic $\mathbf{DMC}^-$ with a set of coordinates defined by $Q_{DMC}$ and $Q_{DMC^-}$ with corresponding energies $E_{DMC}(Q_{DMC})$ and $E_{DMC^-}(Q_{DMC^-})$, the energies of the anion being in the geometry of the neutral **DMC** $E_{DMC^-}(Q_{DMC})$ as well as $E_{DMC}(Q_{DMC^-})$, which is the energy of the neutral molecule in the optimized coordinates of the anionic $\mathbf{DMC}^-$. The maximum energy gain is the sum of two contributions: firstly the energy difference between an anion, suddenly created by electron attachment to the neutral **DMC** in minimized coordinates and the energy minimum of this anion $\mathbf{DMC}^-$; secondly a corresponding energy difference term for the subsequent electron detachment process, thus the potential of the neutral molecule in the coordinates of the anionic minimum minus the energy of the neutral minimum:

$$\Delta E = [E_{DMC^-}(Q_{DMC}) - E_{DMC^-}(Q_{DMC^-})] + [E_{DMC}(Q_{DMC^-}) - E_{DMC}(Q_{DMC})]\,. \qquad (3.1)$$

The maximal energy gain $\Delta E$ according to equation 3.1 is about 0.45 eV for the field-free and about 2.1 eV for the case with an active electric field. In particular, this last value shows that a substantial amount of energy may be gained during an electron attachment-detachment process, in fact, enough to overcome a typical $\beta$-rotation barrier. This effect remains valid, even if additional distortions due to surface interactions arise.

It needs to be noted, that only detailed calculations of the multidimensional dynamics as well as explicit inclusion of the surface can prove that the excess of energy is channeled into conformational motion and thus whether the suggested mechanism is operative.

## 3.2 Irreversible *Trans-Cis* Isomerization on Cu(100)

In the following paragraphs we report on the irreversible configurational change of **DMC** adsorbed on a Cu(100) single crystal (see figure 3.7 (b), (c)) [Prie 06, Prie 05]. The adsorption is mediated by a strong chemical bond between the central diazo unit of **DMC** and Cu surface atoms. The previous study of **DMC** on Au(111) revealed that only the *trans*-form is stable, presenting various conformers depending on the relative rotation of their phenyl rings [Henn 07]. Yet, a *cis*-**DMC** configuration was not found on Au(111). This is attributed to the large stability of the *trans*-isomer, which at the gold surface is predominantly caused by the coupling of the molecule's $\pi$-states with the metal surface. However, copper surfaces are more reactive to organic molecules than gold surfaces. Here we show that a three-dimensional molecular structure, closely resembling the gas phase *cis*-configuration, can be stabilized after manipulation using the STM tip.

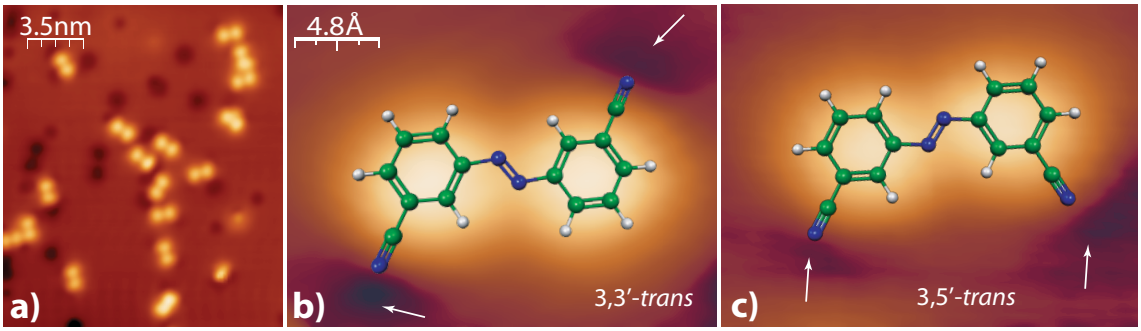


**Figure 3.7:** (a) STM overview image of the planar *trans*-**DMC** adsorbed on Cu(100), dark spots arise most probably from CO contaminations. (b) and (c) close up images of the two rotamers as indicated by the superimposed model: (a) 3,3'-**DMC** and (b) 3,5'-**DMC**. The location of the CN end groups are detected as faint depressions (indicated with arrows). Scanning conditions: (a) $I = 0.1$ nA, $V_B = 351$ mV; (b) $I = 0.26$ nA, $V_B = -0.72$ V; (c) $I = 0.12$ nA, $V_B = -0.5$ V.

STM inspection after **DMC** deposition onto the 80 K cold sample finds that all molecules appear isolated and not ordered, as seen from panel (a) in figure 3.7. The panels (b) and (c) show the two typical appearances of **DMC**, in the (a) 3,3'-*trans*-conformation and (b) the 3,5'-*trans*-conformation, superimposed with the molecular structures. Both planar rotamers can be distinguished by the faint depression arising from the electron rich cyano group. They are indicated by white arrows. These appearances agree well with the previously seen, where this molecule is adsorbed on Au(111).

R. Rurali from the Universitat Autònoma in Barcelona (Spain) simulated the atomic structure of **DMC** on Cu(100) by means of plane wave DFT calculations, in the framework of the generalized gradient approximation (GGA) as parameterized by Perdew and Wang [Perd 92, Henn 08b]. Herein, the Cu(100) surface has been incorporated with a slab of four copper layers. A $6 \times 5$ supercell has been used to fit the adsorbed molecule and to neglect the spurious interactions with the periodic

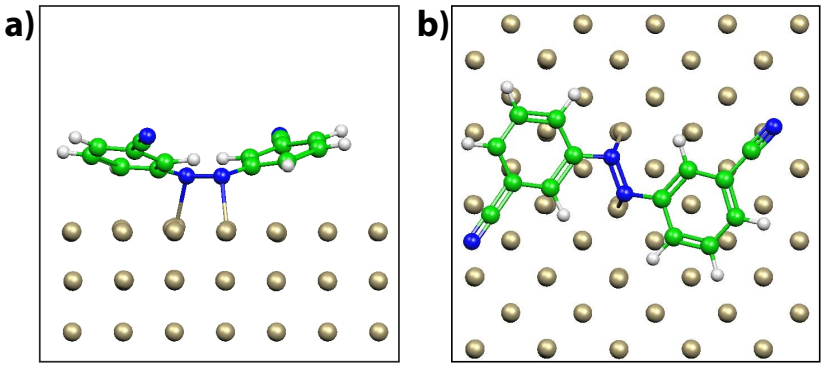


**Figure 3.8:** Relaxed geometries of *trans*-**DMC** on Cu(100) obtained by DFT first-principles calculations in (a) side and (b) top views. The surface-adsorbate interaction is dominated by the bonds formed from the N lone-pairs with the Cu surface.

images. The top layers and the adsorbate have been relaxed until all the forces on the atoms were lower than 0.03 eV/Å.

According to these calculations, the planar structure of *trans*-**DMC** is distorted on the Cu(100) surface, as shown in figure 3.8 (a). This distortion can be explained by the balance of the participating interactions. **DMC** chemisorbs on Cu(100) through the formation of local bonds between the two N atoms at the central backbone and two copper atoms. The N-Cu distance is ∼2 Å. Van der Waals forces are not described by the GGA exchange correlation functional. However, the small N-Cu bond length lies already in the repulsive part of the interaction potential between phenyl rings and the copper surface. Hence, both aromatic parts of **DMC** are pushed upwards, lying at an angle of ∼12° from the planar configuration. The distortion from the planar configuration reduces partially the $sp^2$-character of the central N=N bridge, thus weakening this bond, on the one hand, and strengthening on the other hand the bond to the surface. DFT gives a chemisorption energy of 0.29 eV, which probably reflects the balance between energy gained by the formation of local N-Cu bonds and energy employed to bend the molecular structure [Fran 08].

The chemisorption of **DMC** on Cu(100) suggests that configurational changes of the molecule will involve also changes in the Cu-N bond strength and hence, the whole **DMC**-metal system has to be analyzed in order to interpret atomic motion. It also poses doubts about the possibility of using molecular excitations (either induced by photons or by electrons) to drive this motion, since the hybridization between N and Cu atoms is probably quenching any excitations very rapidly [Henn 07]. To deal with these issues we have carried out further experiments trying to manipulate the shape of single **DMC** molecules on the Cu(100) surface.

### 3.2.1 Isomeric Manipulation

On Cu(100), **DMC** monomers remain stable upon STM imaging indicating that the strength of their bonds to the surface is larger than observed on Au(111), where

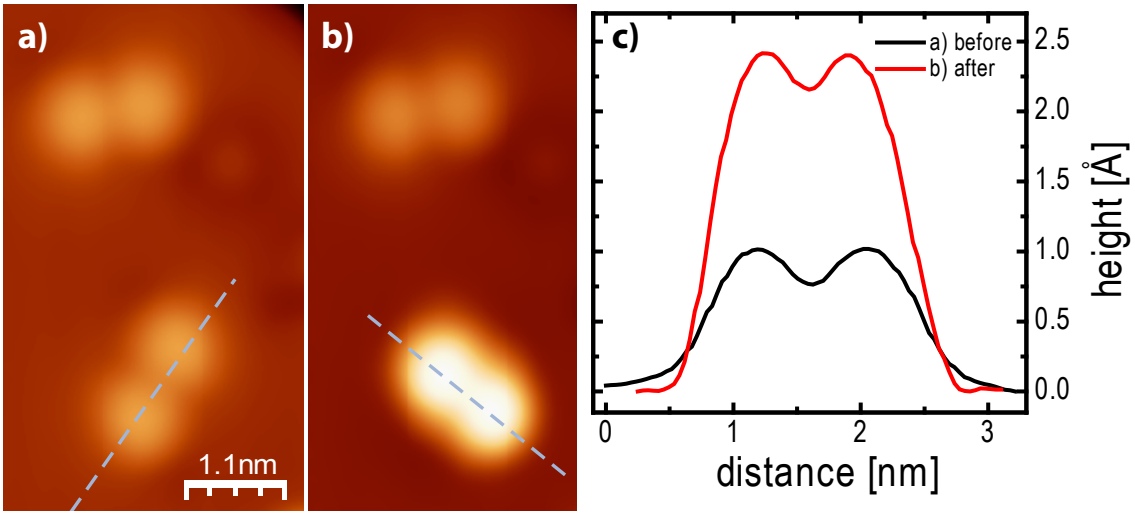


**Figure 3.9:** STM image of a sample region with two *trans*-DMC molecules (a) before and (b) after positioning the tip on the left molecule and slowly increasing the sample bias in the negative polarity. At about $V_B = -2$ V, a sudden increase in the tunneling current (not shown) indicates a transformation event. (c) shows the line profiles along the indicated dashed blue lines. Scanning conditions: (a) $I = 0.54$ nA, $V_B = -0.72$ V; (b) $I = 0.12$ nA, $V_B = -0.5$ V.

diffusion of isolated monomers was easily induced by the tunneling current. On Cu(100) it is possible, however, to induce changes in their structure by increasing the sample bias above a few volts, at either polarity. Figure 3.9 shows the effect of applying a negative voltage ramp to one single molecule, while the STM tip is positioned above the central neck of the **DMC** molecule. During the ramp, a sudden change in the tunneling current occurs, indicating an irreversible change in the adsorbate. This is confirmed by subsequent imaging of the same region. The probed molecule appears much brighter, with a height of 2.5 Å, still showing two protrusions, now separated by 6.8 Å. Neighboring molecules remain unperturbed in the image, with a height of 1 Å. Hence, we can exclude any effect due to tip changes.

In some cases, the topographic features resulting after applying a voltage pulse appear with an asymmetric shape. Figure 3.10 shows two STM images of a **DMC** molecule (a) before and (b) after performing a scan on the surface region using a bias voltage of +3 V. In the latter image (b), one lobe appears higher in the STM image than the other, which is only slightly lifted as seen in the corresponding height profiles in panel (c) of this figure.

A possible origin of the manipulated **DMC** molecules appearing with different shapes in the STM images is the partial fragmentation of the molecular structure. Tunneling electrons may activate the dissociation of an intramolecular bond and consequently change the apparent molecular shapes in the STM images [Lauh 00]. For **DMC** we would expect to find multiple fragments, most of them with a smaller size than the original molecule. However, we note that the brighter lobes of the modified **DMC** molecule appear repetitively with double the height of

original *trans*-**DMC** and a similar separation distance. We suggest that, instead of degradation, the molecular structure has evolved towards a different configuration. A tempting possibility to explain would be that either the symmetric or the asymmetric constellation in the STM topographs is a three-dimensional configuration resembling the free *cis*-isomer known from gas phase.

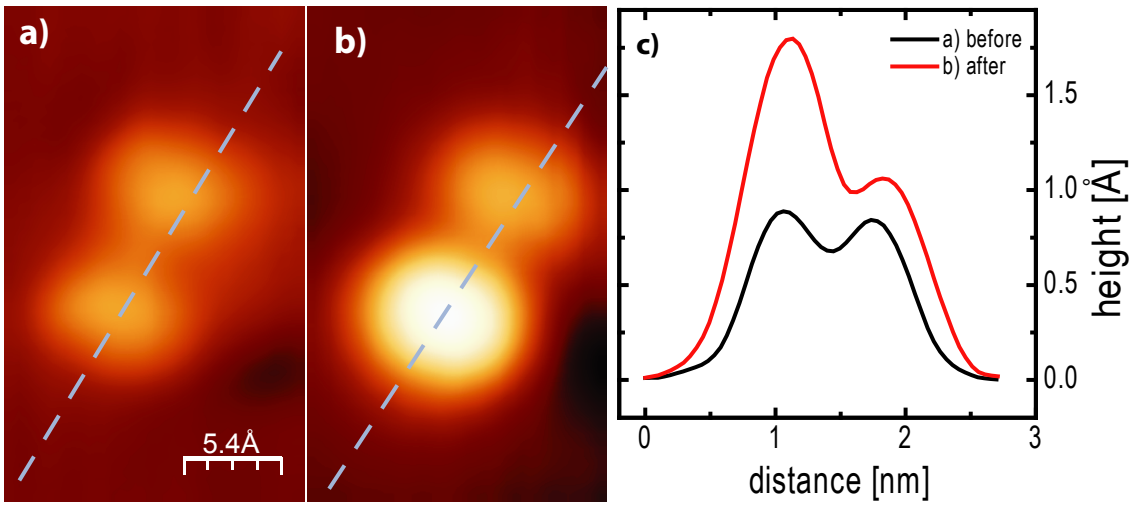


**Figure 3.10:** STM image of one **DMC** molecule (a) before and (b) after scanning with a bias voltage of $V_B = 3$ eV. (c) Line profiles along the indicated dashed lines. One of the two lobes of an *trans*-**DMC** molecule appears with double the height after the manipulation. Scanning conditions: (a) $I = 1.7$ nA, $V_B = 1.3$ V; (b) $I = 0.97$ nA, $V_B = 1.2$ V.

Recalling the previous findings of **DMC** adsorbed on Au(111), the molecules were never found in their *cis*-configuration, even after similar attempts of tip induced manipulation with the STM [Henn 07]. The important difference between these two systems is the adsorption state of **DMC**. On Au(111) a purely physisorbed state is found, where the bonding is dominated by the interaction of the $\pi$-states with substrate electrons leading to the flat stabilization of the *trans*-isomer. In contrast, on Cu(100) the chemical bonds between N and Cu atoms (as found for the *trans*-isomer, *i.e.* figure 3.8) may well provide sufficient rigidity to stabilize a three-dimensional configuration of **DMC**. In order to prove this, R. Rurali relaxed the gas phase atomic structure of the *cis*-**DMC** isomer on the Cu(100) using DFT calculations as described previously. This simulation finds a stable three-dimensional form of **DMC**, which closely resembles the free-molecule *cis*-isomer, as it is shown in figure 3.11. This configuration is characterized by the two phenyl rings pointing upwards from the surface by an angle of $\sim 55°$. The molecule forms local N-Cu bonds of approximately 2 Å length, in a similar fashion as the *trans*-**DMC** but slightly stronger bound to the surface (figure 3.8). In fact, the central N=N bridge remains with respect to the surface essentially in the orientation as observed in the case of the previous *trans*-**DMC** relaxation.

This relaxed structure agrees well with the observed topographical features in the STM data (figure 3.9 (b)): Firstly, the lifted phenyl rings coincide with the

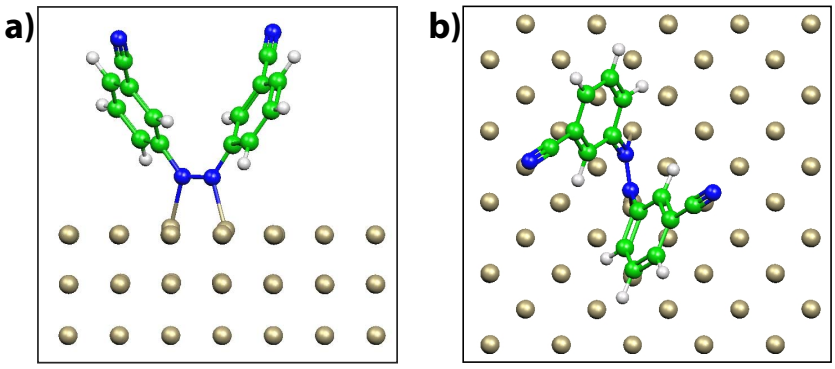


**Figure 3.11:** (a) Side and (b) top views of the relaxed geometries of *cis*-**DMC** on Cu(100) obtained by DFT. The surface-adsorbate interaction is dominated by the bonds formed by the N lone-pairs with the Cu surface.

higher and closer protrusions in the modified molecule (figure 3.9). Secondly, the top view in figure 3.11 (b) resolves that due to the lifted orientation, the phenyl rings appear rotated ∼45° with respect to the relaxed *trans*-structure (figure 3.8 (b)). If we take into account that during a transformation event the N=N bond can rotate to an equivalent mirror orientation around the {001} surface directions, we find that rotations of ∼90° can be expected, too. This agrees well with the situation usually found in the experiments: the orientation of *trans*-**DMC** on the surface always changes, when transformed to the *cis*-like configuration by an angle typically multiple of 45° (*e.g.* figure 3.9).

### 3.2.2 Electronic Structure

Further insight in the stabilization of a *cis*-like isomer is provided by the projected density of states (pDOS), obtained by projecting the DFT derived total density of states of the adsorbed system (substrate plus adsorbate) on the molecular orbitals of a free **DMC** molecule (figure 3.12). The acceptor character of the molecule is confirmed for both the *trans*- and *cis*-configurations, with the lowest unoccupied molecular orbital (LUMO) being partially filled and lying pinned close to the Fermi level. The LUMO is dominated by the $\pi^*$-orbital, having large weight at the N=N moiety [Fuch 06]. As this state has anti-bonding character (compare to figure 1.14), the charge transfer is accompanied by a weakening of the central N=N bond (bond length 1.38 Å vs. 1.26 Å for a free **DMC** molecule). This may effectively contribute to the distortion of the planar configuration at the surface. However, it cannot explain the larger bending angle of the *cis*-isomer, because here the charge transfer is smaller, as we can deduce from the shifted position of the LUMO resonance. In accordance with this, the N=N bond length is shorter in the *cis*-**DMC** isomer (1.32 Å). Hence, the *cis*-form is not stabilized by the partial cleavage of the $sp^2$-hybridized N=N bond.

The chemisorption is driven by the non-bonding N orbitals, as we can deduce by comparing the shape of the occupied resonances in both isomers. *Trans*-**DMC**

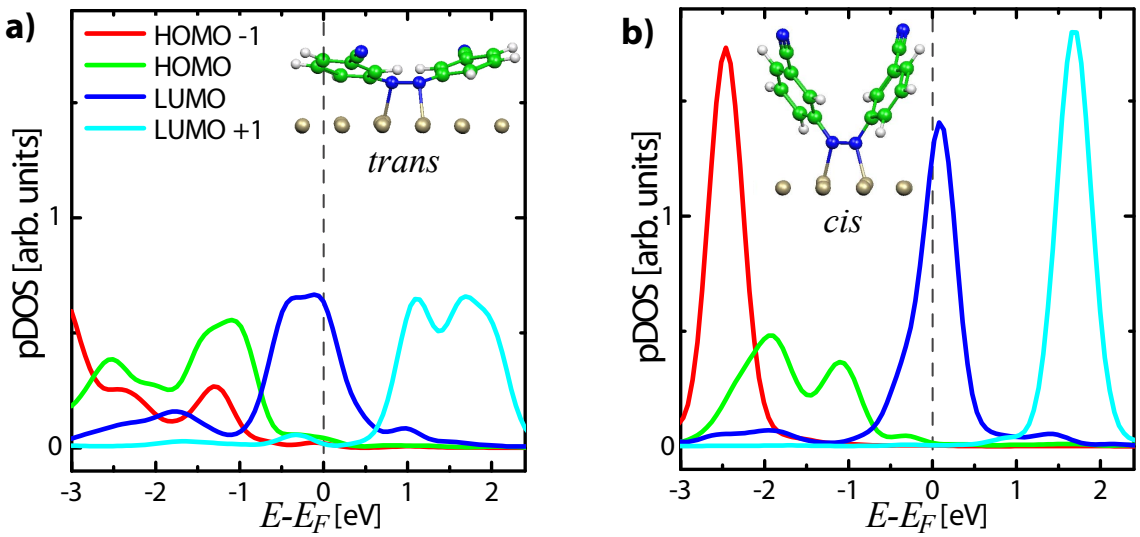


**Figure 3.12:** Density of states of (a) *trans*- and (b) *cis*-**DMC** isomers adsorbed on Cu(100) projected on molecular orbitals of the free species. Charge transfer from the surface to the molecule is revealed by the partial occupation of the LUMO-derived resonance. The broadening of the peaks indicates a larger hybridization of the molecular orbitals with the surface states in the case of the *trans*-conformer. The HOMO state is associated to non-bonding lone-pair electron orbitals, which couple in the *trans*- and in the *cis*-configuration strongly to the surface. The other sharp resonances in the *cis*-configuration evidence little surface interaction.

shows a significant distortion and broadening of all molecular states around the Fermi level. However, all these states but the HOMO appear sharp in the *cis*-form, indicating that the lifted ring geometry reduced the distortion of $\pi$- and $\pi^*$-states by the metal surface. The HOMO corresponds then to the non-bonding state, as it is also the case for the free molecule [Klam 08].

Thus, the three-dimensional *cis*-form is essentially stabilized by the hybridization of the HOMO (mainly located on the N atoms of the diazo group) with substrate states. The larger bending angle of the central bridge in the *cis*-isomer allows a closer – and thus stronger – interaction of these N lone-pair electrons with the Cu(100) surface, resulting in an overall increase of stability with respect to the *trans*-isomer. Flattening the molecule (*i.e.* *cis*- to *trans*-isomerization) requires the weakening of this N-Cu bond and the motion of phenyl rings in the repulsive regime of the phenyl's adsorption potential. Furthermore we cannot exclude that $\pi - \pi$ attraction between the phenyl rings also contributes to the stabilization of the *cis*-like configuration. Altogether a *cis*- to *trans*-back-manipulation is forbidden.

### 3.2.3 Discussion

Figure 3.13 shows the direct energy comparison for the two configurations on the Cu(100) substrate. The stronger N-Cu bond for *cis*-**DMC** results in a larger chemisorption energy of 1.03 eV with respect to 0.29 eV for the *trans*-**DMC**.

Hence, a stability reversal occurs: while in gas phase the *trans*-configuration has a lower energy than the *cis*-configuration, the adsorption results in a lower energy for the *cis*-like configuration in comparison to the adsorbed *trans*-state. The large bending angle of the *cis*-isomer confers a better stability on a Cu(100) surface by N-Cu chemisorption. In agreement with this, we have not succeeded to induce the reverse isomerization (*i.e.* *cis* to *trans*) by manipulation with the STM tip. In spite of the stronger chemisorption of *cis*-**DMC**, all molecules appear as *trans*-**DMC** after deposition. This is however not surprising, because in solid and in gas phase **DMC** adopts its *trans*-form [Prie 06, Prie 05]. Furthermore, since chemisorption on Cu(100) requires intramolecular bending, an activation barrier for this chemisorption process exists [Fran 08]. Hence, we expect that, upon its arrival on the Cu(100) surface, **DMC** first populates a transient precursor *trans*-like state; and can be activated into the chemisorbed *cis*-like state by STM manipulation.

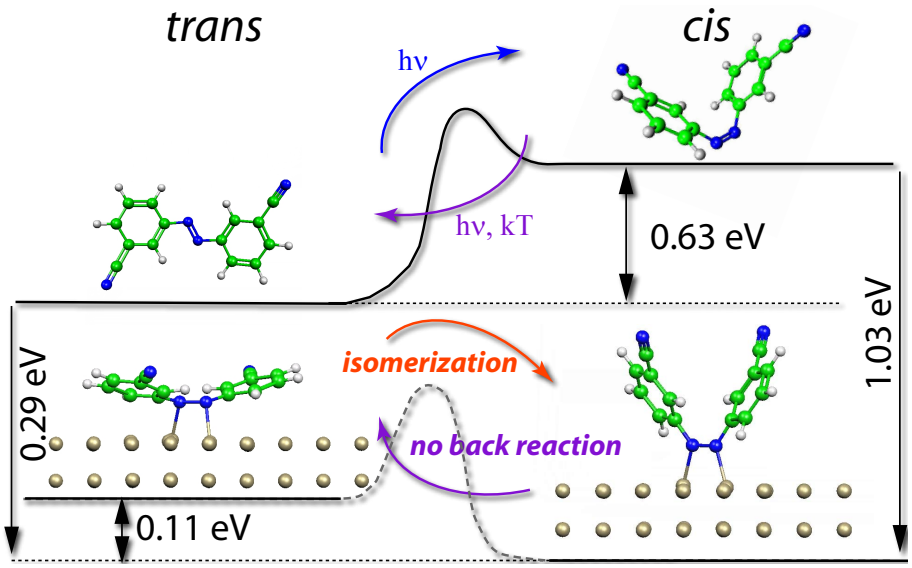


**Figure 3.13:** Relative stabilities of the DMC molecule in the gas phase (top) and adsorbed on the Cu(100) surface (bottom). The calculated chemisorption energies for every conformer and their relative energy difference (as free molecule and chemisorbed) are indicated.

It is interesting to note that, in spite of the larger chemisorption energy of the *cis*-like conformer, its electronic structure is less perturbed. Both the stronger localization of molecular $\pi$-states (figure 3.12 (b)) and the shorter N=N bond length indicate that this isomer maintains, to a large extent, the character of the *cis*-**DMC** molecule, but stabilized at the surface.

Finally, we argue about the possible excitation mechanism inducing the configurational change. Previous works reported that single-molecule *cis-trans*-isomerization of azobenzene can be induced by inelastic excitation of vibrational states in the ground electronic state [Henz 06, Henz 07]. An increase in the electric field at the tip-sample junction can also lead to similar configurational changes [Alem 06]. Here, we note that the non-planar structure of the initial *trans*-**DMC** molecule offers a

resulting dipole moment component perpendicular to the surface. This can increase the effect of an electric field on the molecule and can activate intramolecular motion. In addition to this, the quantum chemistry calculations, presented in the previous section 3.1.3, of the free **DMC** molecule found that a non-planar geometry is essential to couple **DMC** anionic states with a three-dimensional configurational change [Henn 07]. The low success rate of the isomerization events makes it difficult, to provide a certainty on the leading dynamical mechanism. Most probable, it entails a combination of various effects such as the impact of the electric field and various excitation mechanisms (electronic, vibrational, thermic).

## 3.3 Lifting and Reversible Isomerization of DMC on Ag(100)

The properties of a molecular switch change a lot, when adsorbed on a metallic substrate: On the one hand, the surface sterically hinders intra-molecular motion. On the other hand, surface valence electrons often interact with the molecular electronic states, such that ionization/charging, screening, hybridization, or energy level alignment occurs (figure 1.11). In all the latter processes, many molecular properties are affected. For example, orbital excitation and related switching processes are quenched or forbidden. In particular, the rearrangement of electronic states influences the configurational energy barriers, as well as the ionization potential and consequently changes the stability and accessibility of the possible configurations (*e.g.* when **DMC** adsorbs on Cu in figure 3.13).

In the previous two sections adsorbate surface systems were presented, which did not show reversible isomeric molecular switching. The nature of the substrate shows a strong influence on the stability of the two molecular states [Henn 07, Henn 08b]. On Au(111) the planar *trans*-configuration of **DMC** was the only observed, although a phenyl ring rotation revealed two distinguishable states. On Cu(100) the three-dimensional structure, resembling the *cis*-configuration, turned out to be the most stable one. There the planar *trans*-configuration could be manipulated in the *cis*-like isomer, but no reversible switching could be proven. In the following, we present our studies of **DMC** on the Ag(100) surface, whose character is known to be of intermediate reactivity between gold and copper surfaces. Thus it will be shown that the molecule can partially be lifted upon a contact formation with the STM tip and that reversible *trans-cis-trans*-isomerization could be induced by tip manipulation.

Silver, copper and gold condense in the *fcc* bulk lattice structure. The lattice constant of silver is only 21% larger than the one of copper and, as noble metals, they both have the same valence electron configuration consisting of ten $d$-electrons and one unpaired $s$-electron. Nevertheless, silver is known to be less reactive for organic compounds than copper, meaning covalent bonds to copper are generally shorter and stronger than to silver.

It has been shown that the two important interaction components defining the adsorption of **DMC** are the weaker $\pi$-surface interaction, dominating the adsorption

on Au(111) and the stronger bond formation between the nitrogen- and surface atoms, very prominent in the *cis*-configuration, stabilized on Cu(100). The N-Ag bond is expected to be weaker and longer than the N-Cu bond. Consequently, the strong geometrical constraints of the chemisorbed *cis*-state are weakened and hence $\pi$-interaction to the surface will gain importance. This will favor the *trans*-state in comparison to the adsorption behavior on copper and the stability of both states are expected to become similarly stable on the silver-surface. As result also reversible switching will be observed.

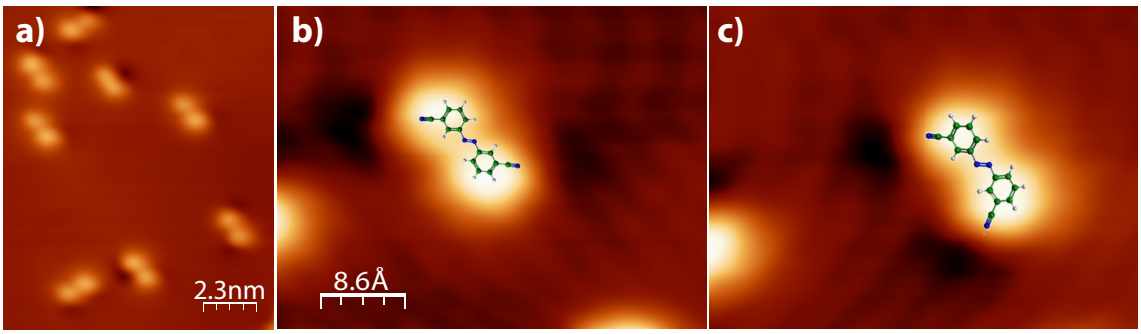


**Figure 3.14:** STM topographies of *trans*-**DMC** when adsorbed Ag(100). (a) Overview scan showing the alignment of molecules in the high symmetry direction of the (100) surface. High resolution STM images of an individual molecule (b) before and (c) after a tip induced $\beta$-rotational manipulation. Scanning conditions: (a) $V_B = 1$ V, $I = 2.9 \times 10^{-10}$ A; (b) $V_B = 686$ mV, $I = 2.8 \times 10^{-10}$ A; (c) $V_B = 686$ mV, $I = 2.3 \times 10^{-10}$ A.

Panel (a) of figure 3.14 shows the overview topography of **DMC**, when adsorbed on Ag(100). After preparation at room temperature both planar *trans*-$\beta$-rotamers are distributed on the surface in equal amounts. The molecules align along the two high symmetry directions [110] and [101] of the *fcc* crystal. The close-up images in panels (b) and (c) show, how tip induced manipulation changes the $\beta$-rotamer from the 3,3'-*trans* to the 3,5'-*trans* conformation. The orientation of the cyano groups is seen by small depressions, resulting from the electron rich cyano groups [Henn 07].

### 3.3.1 Lifting a Molecule

By establishing a stable contact between an individual **DMC** molecule and the STM tip, we can illustrate that the molecule is partially lifted and hence we can classify its internal flexibility. Figure 3.15 shows the example experiment on one individual **DMC** molecule on Ag(100). In panel (a) the highly resolved STM topography of one 3,3'-*trans*-**DMC** shows the initial condition with two depression in the left top and the right bottom of the molecule, indicating the orientation of the two cyano end groups. The STM tip approaches towards the cyano group as indicated by the blue arrow and as sketched in panel (b). During this process the typical exponential increase in the current could be observed (figure 3.15 (e); reading from right to left). At 2.6 Å an erratic step in the current occurs and another stable state of conductance is obtained. Moreover, while retraction, at

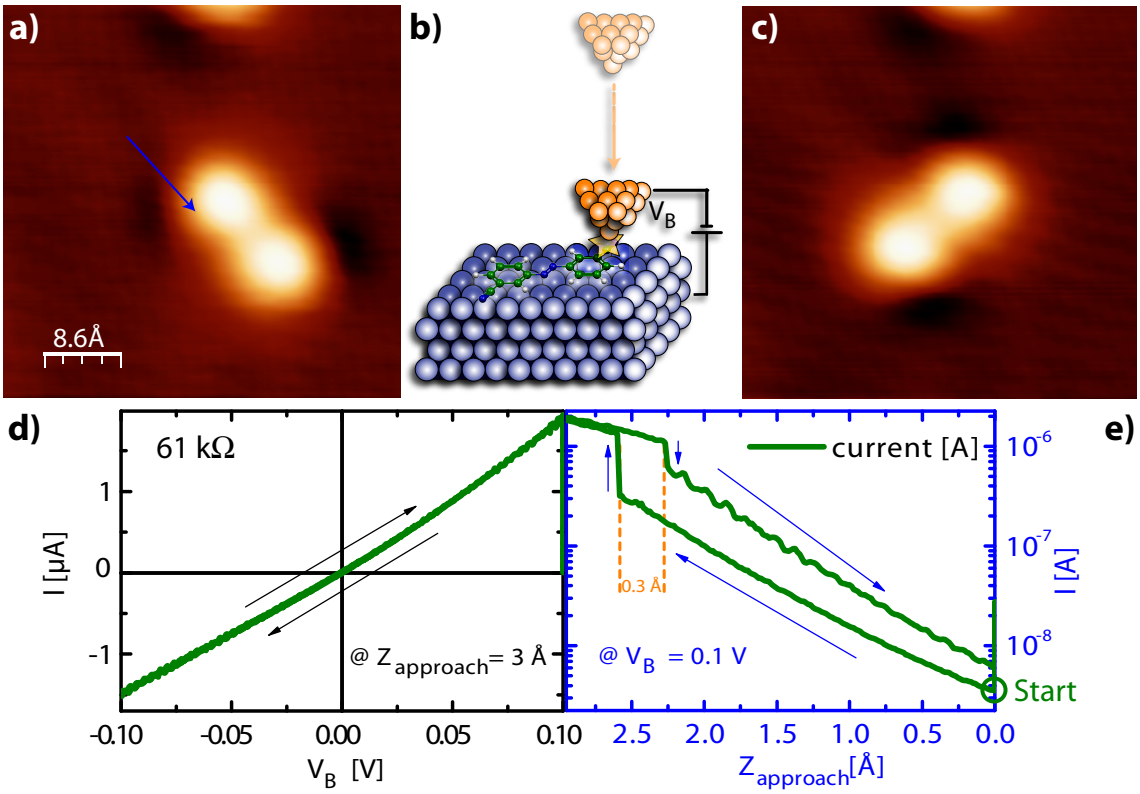


**Figure 3.15:** STM images (a) before and (c) after a manipulation of DMC, by the STM as sketched in (b). The molecule is lifted at its functional group and forms a conductive path between sample and STM tip. This is seen from the tunneling current plots (e) and (d). When the tip is approached to the **DMC** as seen from the a current-distance curve (e) an erratic step indicates the formation, the erratic drop, while the tip is retracted indicates the cleavage of the contact. In the meanwhile the current-voltage characteristic curve (d) shows an almost linear behavior for the contact. Scanning conditions: (a, c) $V_B = 128$ mV, $I = 2 \times 10^{-11}$ A.

2.3 Å the step back to a lower current occurs. We attribute the jumps in the current to the formation and cleavage of a contact between the adsorbed molecule and the STM tip. The $Z$ discrepancy between the steps in the approach and retraction curve is interpreted as a lifting of the cyano moiety by 0.3 Å. Motions of up to 0.5 Å have been observed, too. In the contacted situation the sample bias was ramped, as seen from the characteristic $I(V_B)$-curve in panel (d). In the interval of $[-0.1$ V, $0.1$ V$]$ the current shows reversible almost linear behavior, corresponding to $\sim$60 kΩ. The graph highlights that the contact is particular stable for the duration of 20 sec, without influencing the conductivity nor fracturing the molecule. In panel (c) a STM topography shows the identical sample area after the molecule treatment. The molecule has rotated by 90° being now aligned in the different symmetry direction of the Ag(100) surface. Despite the strong tip interaction, by means of an high electron current ($\sim$2 $\mu$A), this image proves that the molecule stays intact.

The maximum lifting of 0.5 Å is a small value compared to the molecular size, it is hence reasonable to ask, what kind of internal molecular motion is associated to the lifting of the end group. We assume that the motion is dominated by the rotational

motion of the phenyl ring by the angle $\beta$ as defined in figure 2.2. In the planar geometry the cyano group can be lifted very efficiently upon $\beta$-rotation. Also, this motion is expected to be not restricted for the free molecule in the ground state and only sterically hindered by the surface, as stated in section 3.1.3.

### 3.3.2 Reversible Isomerization

The attractive interaction of STM tip and functional unit, which lifts **DMC** partially, can also be used to isomerize it. Therefore it has to be considered, that the isomeric motion is not only vertical but involves a three-dimensional trajectory for the cyano unit.

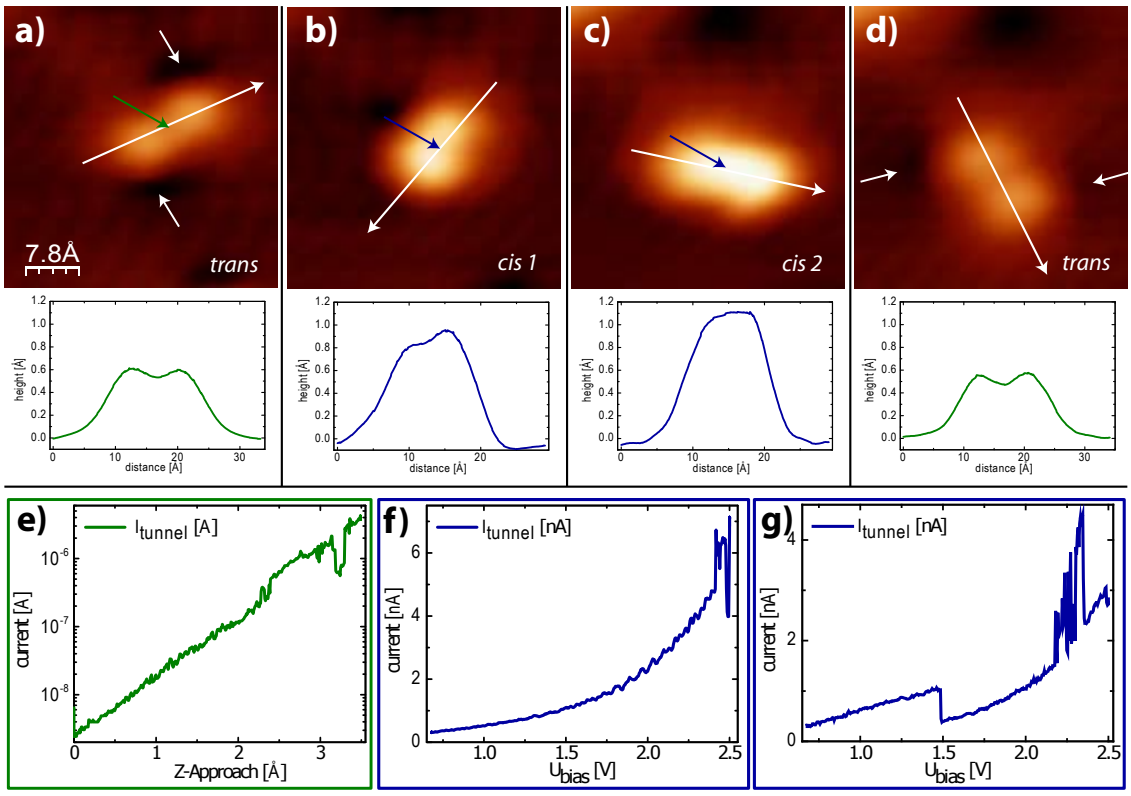


**Figure 3.16:** Cycle of **DMC** isomerization: the (a) *trans*-molecule was switched into the (b) *cis-1*-configuration then into the (c) *cis-2*-configuration and finally back into the (d) *trans*-isomer. The line profiles underneath show the apparent heights of the molecule. The current-distance (e) and current-voltage characteristics (f) and (g) show the manipulation processes applied to the molecule subsequently between acquisition of the STM topographies. Scanning conditions for all images (a-d) $V_B = 686$ mV, $I = 3.2 \times 10^{-10}$ A.

This explains why a configurational change, seen from the manipulation series in figure 3.16, from the *trans*- to *cis*-isomer and backwards can be observed, when the STM tip is positioned above the center of an individual molecule, depicted by the green arrow in panel (a) of this figure. The sample bias of 680 mV is applied and the tip approaches the molecule by 3.5 Å. The current, recorded in panel (e), rises

exponentially to 4 $\mu$A, becoming instable at a distance of 2.4 Å. Successive mapping in panel (b) of the same sample area reveals a different characteristic aspect of the molecule in the topography, which we name "*cis-1*"-configuration. The overall height has risen from 0.6 Å to 1.1 Å, as seen from the height profiles below the topographies of panel (a) and (b). Moreover, the shape changed into a pear-like protrusion with a prominent lobe at the bottom left and an extrusion to the top right. This shape looks similar to the one observed during the measurements of **DMC** on Cu(100) (figure 3.10 (b)), although the difference in the effective height is not as prominent.

In a next step the tip is positioned again above this molecule, indicated by the blue arrow in figure 3.16 (b). Now the the voltage successively rises from 0.68 V to 2.5 V. The recorded current, plotted in panel (f), shows an exponential increase until ∼2.4 V, where instability is seen. Resulting from this, the next topography (panel (c)) displays another appearance of the molecule. Now the molecule appears with a symmetric double lobe even higher (1.1 Å) than in the previous image and narrower than in the first one. Also such a shape has been observed on Cu(100) previously and was assigned to a *cis*-like shape, supported by DFT calculation (figure 3.9(b)). Here, we name it "*cis-2*".

In a third step the latter experiment is repeated (blue arrow in panel (c)) and also this time a clear indication of the transformational process is seen in the recorded current signal (figure 3.16 (g)). The clear drop in the current signal at 1.5 V evidences that the molecule changed its adsorption geometry. As seen from the subsequent topography (panel (d)), the **DMC** molecule resembles the original planar *trans*-configuration. The topography of the molecule is a little broadened and diffuse, probably because the tip structure has changed in the contacting experiment (panel (e)). Nevertheless, the dark depressions, indicating the cyano orientation, are still visible and the height and width in the first and the last height profiles agree. So we can exclude a fragmentation of the molecule during the whole series of manipulations and consider this as a reversible *trans-cis-trans*-isomerization of one individual **DMC** molecule.

The three different shapes of **DMC** on Ag(100), the planar *trans*, the asymmetric *cis-1* and the more symmetric *cis-2* can be observed frequently upon such manipulation processes. We attribute to the two *cis*-like configurations two different bond formations of the diazo group to the surface. Because the two adsorption mechanisms, the weaker $\pi$-surface interaction of the phenyl rings and the strong covalent N-Ag bond, compete with each other, it is probable, that **DMC** adopts many different stable adsorption structures. We assume that the asymmetric *cis-1* state results, when only one N atom of the diazo unit is well coupled to the surface and stabilizes the directly attached phenyl ring, while the second N atom is weaker adsorbed. Due to the $sp^2$-hybridization of the two N atoms this results for the two phenyl rings in very different orientation, seen in the asymmetric topography of the *cis-1* structure. On the other hand, the symmetric *cis-2* structure resembles well the *cis*-like configuration, known from adsorption on

Cu(100) (figure 3.11). Here both nitrogen atoms in the diazo unit are bound to equivalent surface sites resulting in a symmetric appearance in the STM topography.

The reader might recognize the discrepancy in heights between the *cis* configurations on Cu(100) (figure 3.9 and 3.10) and on Ag(100) (figure 3.16). We attribute this difference, to the different coupling of molecule and substrate. The effective heights, measured by STM, result from the local conductivity and hence from the local density of states of the combined system: substrate and molecule. The formation of the stronger covalent bond in the case of Cu(100) hence results in a higher electron transmissivity than on Ag(100), which is directly reflected in the different apparent heights.

## 3.4 Conclusion

**DMC** molecules are found on Au(111), Cu(100) and Ag(100) in two stable conformations (3,3'-*trans* and 3,5'-*trans*), which are connected through a the rotation of a phenyl ring. We have demonstrated that the switching between these conformers can be induced by electrons tunneling through the LUMO resonance, located at 1.7 eV above the Fermi level on Au(111). Also on Ag(100) this rotational switching could be observed. The activation of this process can be explained, if a fast electron scattering with a negative ion resonance induces a temporary change in geometry (transition state). The coupling to rotational motion is possibly linked to structural relaxation in an electric field, which causes a non-planar molecular geometry. The internal rotation probably occurs in the molecule's ground state, which is consistent with the short lifetime of electronic excitations in molecules on metal surfaces. Hence, a phenyl ring $\beta$-rotation becomes possible and leads to a change between the 3,3'-*trans* and 3,5'-*trans* structures on the surface.

The steric hindrance of the Au(111) surface, where the molecule adsorbs planar in the *trans*-configuration upon $\pi$-surface interaction, forbids an isomeric switching into the *cis*-state. Tuning the $sp^2$-hybridized N atoms by means of an interaction to the Cu(100) surface, after a tip induced manipulation the *cis*-like configuration could be observed being more stable than the *trans*-configuration. The formation of strong bonds to the surface evolves via lone-pair electron orbitals of the diazo bridge, as confirmed by DFT calculations. The interplay of covalent and $\pi$-surface interactions could further be tuned in order to gain a reversible switching system. This is realized by a third substrate material. On Ag(100), lifting of an individual functional end group and reversible isomerization between the *cis*- and *trans*-configuration is proven.

In contrast to other strategies, here we show that the decoupling of switching molecule and substrate is not necessarily needed to preserve gas phase switching characteristics on the surface [Alem 06]. The study reveals that the choice of substrate reactivity is important for functionalization of surfaces with switchable molecules. The competing contributions in the adsorption process of **DMC**, the $\pi$-surface coupling and the covalent diazo-surface bond formation, could be tuned such that both

isomeric states become equally stable on Ag(100) and could be switched reversible. We claim that also further structuring of surfaces by kinks, ad-atoms or further tuning the surface reactivity by *e.g.* passivation will help to fundamentally understand switching mechanisms on surfaces.

# Chapter 4

# Chemical Fingerprint of Coordination Bonds

The formation of metal-organic complexes has demonstrated to efficiently synthesize supra-molecular network structures in one, two, and three dimensions by means of coordination bonds [Step 07, Mena 08]. The interaction of molecular ligand orbitals with metal states can result in a stabilization and ordering of molecules, charge redistribution in the metal and ligand, and may cause some structural rearrangement within the molecule, due to the metal's electrophilic character. However, non-interacting electronic states are expected to be predominantly preserved.

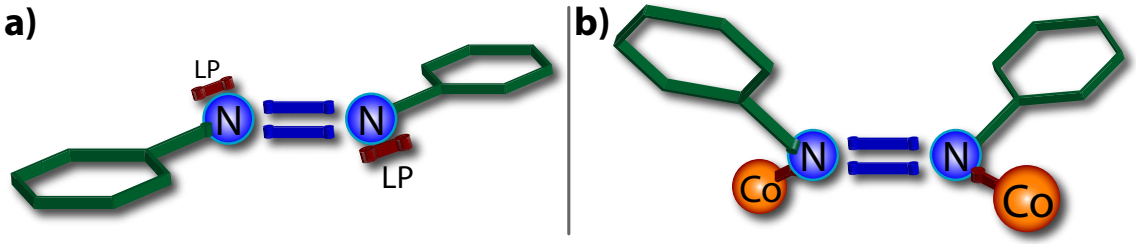


**Figure 4.1:** Sketch of desired coupling between the diazo-bridge and Co ad-atoms. The interaction is expected to modify the molecular structure from a planar molecule (a) to a three dimensional one (b), where the diazo bridge's strong bonding character is weakened.

In this chapter we want to take advantage of the exceptional Co-N interaction, in order to modify the adsorption condition of the azobenzene derivative **DMC**. This azobenzene derivative is known from section 3.1 to be weakly coupled to the Au(111) surface, preserving its gas phase geometry (see figure 4.1 (a)). The molecule's planar geometry on this substrate and the $\pi$-coupling dominating its adsorption cause that no *cis-trans*-isomerization was observed. Upon co-adsorption with Co, the molecule is expected to dock to the surface (see figure 4.1 (b)). In particular, the lone-pair orbitals at the diazo bridge are expected to undergo hybridization with Co states, such that a three-fold $sp^2$-hybridization forces the phenyl rings slightly upwards. Hereby the molecule may weaken its switchable diazo double bond permitting *cis-trans*-isomerization.

## 4.1 Planar Metal-Organic Networks

Various studies on cyano-functionalized molecules performed by U. Schlickum, S. Stepanow *et al.* show that metal organic complexes stabilize polymer networks on a Ag(111) surface. [Schl 08, Schl 07, Step 07, Step 08]. The honeycomb meshes, emerging from 1,4';4',1"-terphenyl-4,4"-dicarbonitrile (CN-$(Ph)_3$-CN) molecules co-adsorbed with Co atoms are shown in 4.2 (a), taken from reference [Step 07]. Depending on the length of the molecules defined via the number of phenyl rings, the meshes vary in size. Usually they nucleate by threefold nodes. The nodes are interpreted as adsorption sites of Co atoms, where electron rich cyano moieties assemble in three-fold orientation around it.

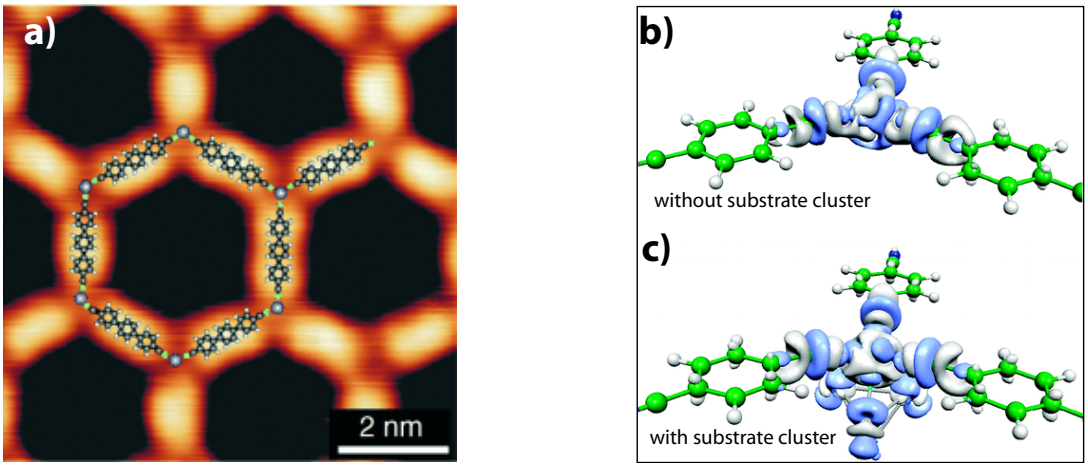


**Figure 4.2:** (a) Honeycomb mesh, built up from cobalt centers with 1,4';4',1"-terphenyl-4,4"-dicarbonitrile (CN-$(Ph)_3$-CN) molecules on Ag(111), taken from reference [Step 07]. (b) and (c) DFT calculated isosurfaces of the mesh's node, showing induced charge density around the cobalt in a three-fold coordination, without (b) and with (c) a $(Ag)_4$ cluster, that represents the surface. The light blue color stands for charge depletion, the grey color for charge accumulation. Figures (b and c) are taken from reference [Schl 07].

DFT calculations explain this observation as formation of metal-organic complexes, exposing directional coordination bonds, shown in figures 4.2 (b) and (c), which are taken from reference [Schl 07]. The charge in the proximity of the Co adsorbate is redistributed, under the influence of three ligands with cyano functionality. This effect basically affects the lone-pair electron orbitals at the cyano functionality. The overall charge distribution of the molecule is hardly disturbed, with respect to the free molecule, as seen from the charge density plots (light blue color represents charge depletion, grey color represents charge accumulation). In the picture of a covalent-like bond, the three-fold geometry in the STM topography can be explained. It results either from an $sp^3$- or $sp^2$-like orbital hybridization depending whether the the surface is included or not.

## 4.2 Cobalt Clusters on Au(111)

When Co atoms adsorb on a clean Au(111) surface at room temperature, the atoms nucleate in three-dimensional clusters of different heights. The higher clusters of up to 6 Å are exclusively located in *fcc* domains of the reconstructed gold surface, predominantly in the corners of the reconstruction. In the corners of *hcp* domains smaller clusters of Co are observed. In figures 4.3 (b) and (c) a small cluster and one of intermediate size are shown, displaying no particular ordering. From the comparably large height we estimate this cluster to consist of at least three Co layers.

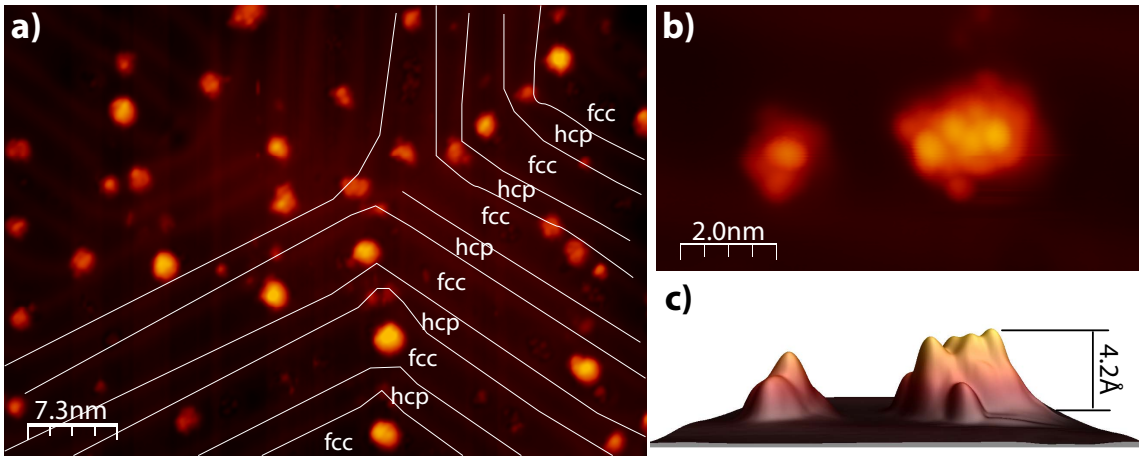


**Figure 4.3:** (a) Large scale STM topography of Co clusters, adsorbed on a clean Au(111) crystal at room temperature. The clusters show heights of up to 6 Å. In (b) and (c) the high resolution image in (a) top and (c) side view reveals two clusters of a textured assembly with an exemplary height of 4.2 Å. Scanning conditions: (a) $V_B = 356$ mV, $I = 2.5 \times 10^{-11}$ A; (b, c) $V_B = 495$ mV, $I = 1.4 \times 10^{-10}$ A.

## 4.3 Co-Adsorption of Cobalt and DMC

**DMC** molecules, (as introduced in figure 2.1) have been co-adsorbed with Co atoms on a Au(111) single crystal at room temperature. The STM topography shown in figure 4.4 (a) shows two types of characteristic structures, which are clearly different from the purely adsorbed molecule as seen in figures 2.3 (c), 2.6 (a) or 3.4 (a). The brighter almost circular clusters appear with various heights of up to 6.5 Å (close up in figure 4.4 (b)). Mostly, they are surrounded by eight protrusions, which clearly correspond to four 3,5'-*trans*-**DMC** molecules. Since the centers of these structures strongly vary in height, size and shape and because they do not show an unambiguous spectroscopic fingerprint, it is highly probable that they are three-dimensional clusters of Co atoms.

The second type of adsorbate structure is significantly different. Here the molecules are assembled to chains, spreading over the Au(111) surface. They are not affected

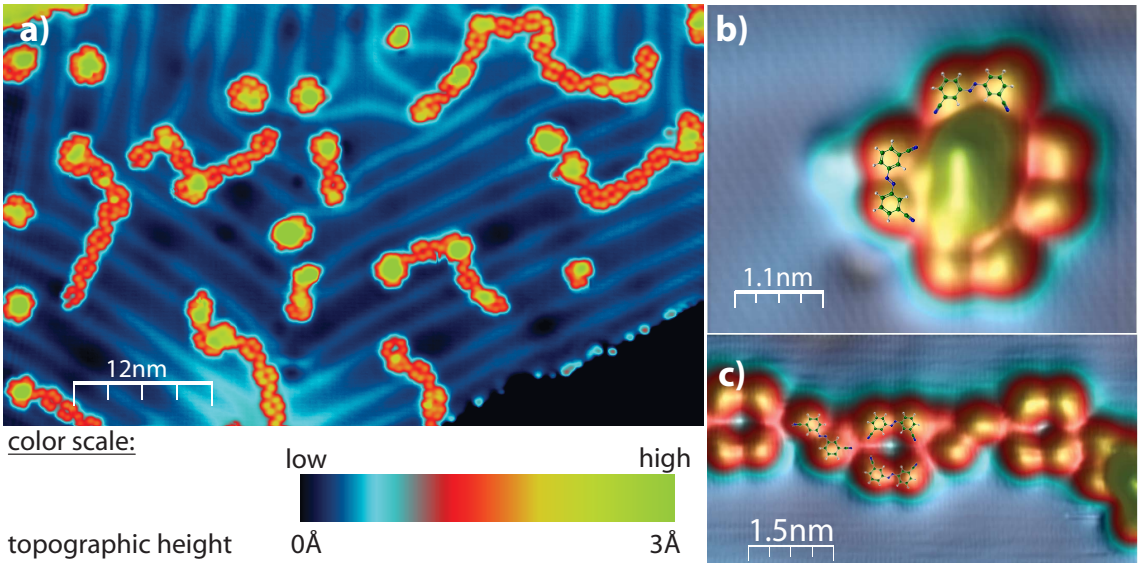


**Figure 4.4:** Topography of co-adsorbed **DMC** molecules and cobalt atoms. Clusters of usually four 3,5'-*trans*-**DMC** molecules surrounding higher protrusions and chain structures are seen. $^{2}/_{3}$ of the chains consist of 3,5'-*trans* **DMC** and $^{1}/_{3}$ of 3,3'-*trans* **DMC**. Scanning conditions: (a) $V_B$= 356 mV, $I = 2.5 \times 10^{-11}$ A; (b, b) $V_B = 331$ mV, $I = 1.0 \times 10^{-10}$ A, (c) $V_B = 277$ mV, $I = 8.7 \times 10^{-11}$ A.

by the surface's herringbone reconstruction and do not follow any particular direction in a longer range. This evidences that the overall surface interaction is rather weak, while the inter-adsorbate coupling dominates the adsorbate recognition. Focussing on one chain structure in the high resolution image of figure 4.4 (c), we can identify the conformations of the *trans*-**DMC** molecules as indicated by superimposed molecular structures. The chains consist of two pairwise 3,5'-*trans*-**DMC** molecules, facing each other with their functional cyano units and of one 3,3'-*trans*-**DMC** in an alternating pattern. The characteristic sites where the three cyano end groups face each other, are attributed to Co atoms, as further analysis will show. However the Co ad-atom cannot be resolved in the STM topographies, but without such ad-atom, the electron rich cyano moieties would repel each other due to electro static repulsion. Instead, we assume that coordination bonds are formed here between the three lone-pair electron orbitals of functional cyano groups and one Co atom, very similar as seen in references [Schl 08, Schl 07, Step 07, Step 08] and in figures 4.1 (b), and 4.2 (a).

Adsorption of only **DMC** revealed that the probability of observing 3,3'- and 3,5'-*trans*-**DMC** molecules is equal. Here we recognize a much larger number of 3,5'-*trans*-conformers ($\gtrsim$ 70 %). This highlights the interaction strength of Co atoms and **DMC** molecules. Most likely **DMC** changes in great amounts its conformation upon the interplay with Co.

## 4.4 Spatially Resolved Tunnelling Spectroscopy

The interaction of Co and **DMC** molecules also stabilizes the adsorbates. Contrary to the behavior observed for isolated **DMC** molecules on Au(111), now the overall stability of **DMC** clusters is much higher, such that no dragging or diffusion of adsorbates on the surface was observed while scanning. In the former case the stability was enforced by intermolecular hydrogen bonds, when assembled in clusters, here we attribute that to the formation of a network of coordination bonds mediated by Co atoms. The resulting higher stability allows us to perform tunneling spectroscopy to higher energies.

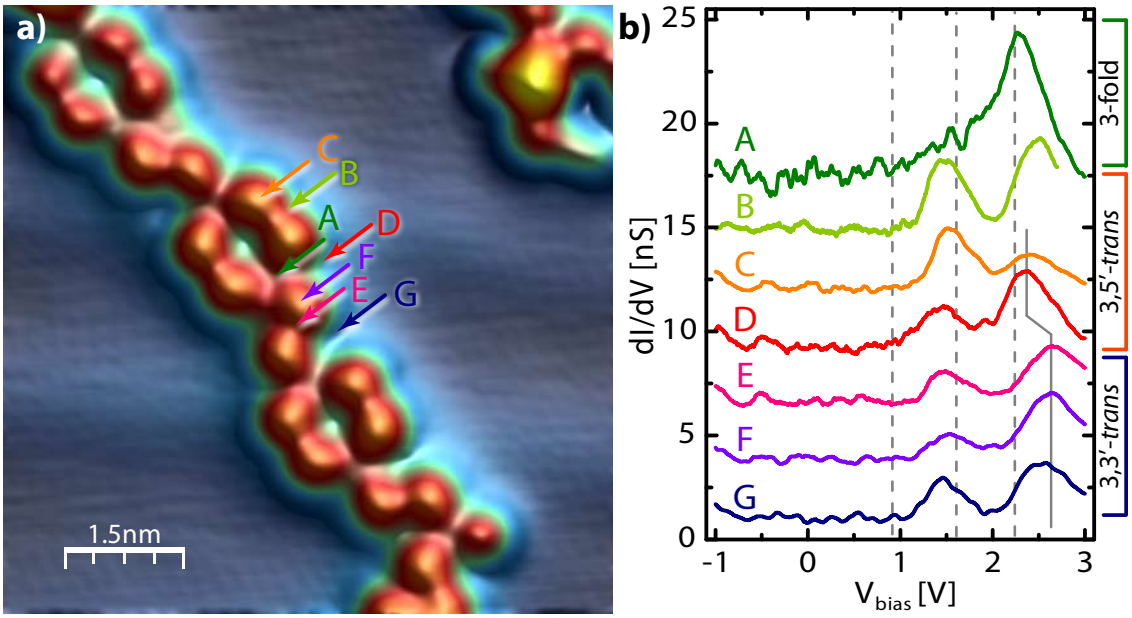


**Figure 4.5:** (a) STM topography of **DMC** joint with Co on a Au(111) and ordered in a chain structure, scanned at $V_B = 0.9$ V and $I = 7.8 \times 10^{-11}$ A. (b) STS spectra recorded at different sites in the chain, as indicated by arrows in (a). Exceptional is the site **A** between three functional cyano groups showing one resonance at 2.2 V, which is associated to a Co atom in three-fold coordination to functional cyano groups. The molecular spectra (**B**-**G**) show significant differences between the pairwise adsorbed 3,5'-*trans*- and the 3,3'-*trans*-rotamers. Surprisingly, aside of the molecules resonance intensities are present, contrary to the observation of pure **DMC** on Au(111). The gray solid line indicates the spectroscopic difference between the pairwise adsorbed molecules and the molecule in between; dashed gray lines refer to the energy of conductance maps presented in figure 4.6.

In figure 4.5 (b) tunneling spectra are shown related to seven different sites within a molecular chain, as indicated in panel (a) of the figure. A three-fold Co adsorption site, indicated by arrow **A**, shows a spectroscopic line shape with a resonance at 2.3 V. The spectra taken at 3,5'-*trans*- and the 3,3'-*trans*-rotamers, are shown in the plots **B**-**D** and **E**-**G** respectively. They show two resonances, one at ∼1.5 V and a second one at somewhat above 2.4 V. The low energy feature is energetically close to the LUMO of pure **DMC** on Au(111). However, the intensities vary a lot. In contrast to the pure species the signal is slightly stronger in the diazo bridge

(**B**) than in the phenyl ring (**C**). Surprisingly, there is intensity clearly seen aside of the topographic protrusions (**D**), too. The higher energy feature is pronounced in the diazo site (**B**) and aside of the molecule (**D**) but much weaker on top of the phenyl ring (**C**). We hence attribute this to be not related to molecular states, but originating from Co states, signing somehow its positions in the proximity of the molecules.

The 3,3'-*trans*-**DMC** shows very similar spectroscopic line shapes at the diazo site (**E**) and on top of the phenyl ring (**F**). The low energy peak is comparable weak (like in **D**) and the high energy features are visible at slightly larger bias voltage of $\sim$2.6 V than in the pair-wise 3,5'-case above. Again it is remarkable, that aside of the molecule (**G**) features of the $dI/dV$ spectra are seen, too. This spectrum also shows both resonances, which might be related to states originating from the Co atom, probable coupled to the molecule.

When Co interacts with the molecules strong enough to form these structures, it is also evident that the molecule's electron distribution, and hence its energy levels change with respect to the pure molecular case. In particular, the expected charge redistribution between Co and **DMC** is substantiated by the spectroscopic feature at the Co atoms. The clearly different geometry of 3,5'-*trans*-molecules and the less-frequent 3,3'-*trans*-ones being pairwise inter-connected in the former case and completing the chain structure in the latter case, reasons the faint differences in the spectroscopic line shapes.

## 4.5 Spatial Mapping of Cobalt States

$dI/dV$-mapping, as introduced in section 1.1.2, is a powerful technique to resolve spectroscopic features in space. Here we use it to visualize the spectroscopic features of Co adsorption sites. We have obtained $dI/dV$-maps for various energies, shown in figure 4.6. Panel (a) shows the well resolved topography of one chain structure at a bias energy of 0.9 eV. The molecular models are superimposed as a guide to the eye. In panel (b) the simultaneously recorded $dI/dV$ signal from a lock-in amplifier is shown in color scale. This mapping shows overall little intensity, as expected since no spectroscopic feature has been observed in that energy range. On the one hand this is the reason why the corrugation in panel (a) is pure LUMO topography (tunneling through the onset of this molecular resonance). On the other hand we can justify to exclude that by the feedback-controlled $Z$-motion artefact features are induced in the $dI/dV$ signal.

At a bias voltage of 1.6 V, as shown in panel (c) and (d), the topographic structures change slightly. The corresponding $dI/dV$ map reveals many features. By the superposition of molecular models it is easy to see, that all the features have maximum intensities aside of the molecules. In fact, the molecules lay in the valleys between areas of maximal spectroscopic signal. All features, which are indicated by yellow arrows, have at least one nitrogen moiety from the molecules' diazo bridges very close. We assume they correspond to orbitals of Co atoms after their coupling

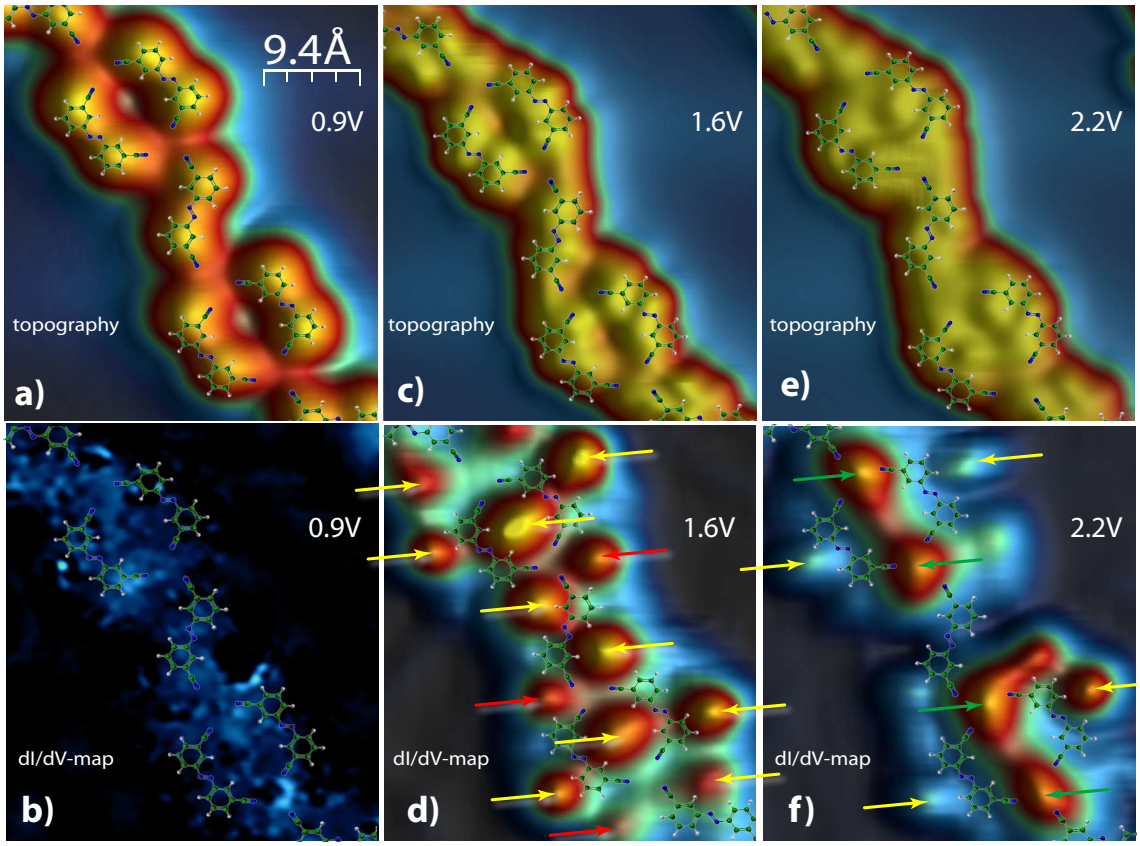


**Figure 4.6:** (a) Topography and (b) simultaneous $dI/dV$-mapping of a row of **DMC** molecules, joint with Co, scanned at 0.9 V. In the electronic gap no particular intensity is seen, discarding the influence of vertical tip motion on the $dI/dV$ signal, causing artefact signals. (c) The topography and (d) $dI/dV$ map at 1.6 V, and correspondingly at 2.2 V shown in panel (e) and (f). All data were recorded at a tunneling current of $I = 7.8 \times 10^{-11}$ A.

with one lone-pair electron orbital of the diazo's N. The position of these features fits to the expected Co sites, when interaction of the diazo unit and Co atoms occurs (sketched in figure 4.1 (b)). The features between two 3,5'-*trans*-molecules are particular large. Probably this is caused by the resonances of two molecules trapping a cluster of two Co atoms and their resonances overlap laterally.

The protrusions indicated by red arrows in the 1.6 V $dI/dV$-map (figure 4.6 (d)) cannot be related to any diazo unit nearby. An artifact increase due to a vertical motion of the tip towards the sample can be excluded, when comparing with the topography (c), because the topographic corrugation is rather weak at these positions. However, there are two electron rich cyano groups in the surrounding, which might induce local resonances at the Co sites similar as in the case of the diazo sites. The different intensity (compared to the yellow arrow sites) can hence result from a slight deviation in energy due to the chemical surrounding.

At a higher bias energy of 2.2 eV the $dI/dV$-features change their aspect, as it is seen in panel (f) of figure 4.6. The according topography is shown in panel (e). While the enhanced signals in proximity of the diazo bridge show weak intensity, a very strong

signal is seen in between three molecules, where their cyano functionalities face each other. The geometry suggests that also this site is related to a metal-ligand complex formed by the three lone-pair electron orbitals of the cyano groups and a Co center [Schl 08, Schl 07, Step 07, Step 08]. This Co site is assumed to govern the assembly structure with its characteristic three-fold geometry. By comparing with the spectra **A** in in figure 4.5 (b) it is evident that this site differs strongly from all other sites, presenting one unoccupied electronic resonance in the STS data.

## 4.6 Coordination Geometry Mediated by Electron Donation

The electron configuration of Cobalt is $[[\mathrm{Ar}]3d^7 4s^2]$. The filling of the $d$-shell by three more electrons and the $4p$ shell with six electrons in order to reach the noble gas configuration of Krypton $[[\mathrm{Ar}]3d^{10}4s^2 4p^6]$ describes the electrophilic character of Co. Thus, the Co atoms attracts free orbitals of ligands, for instance the lone-pair electron orbitals of **DMC** as sketched in figure 4.7 (b). In the previously observed molecular structure we have identified cobalt complexes of two different types. The geometrical surrounding reveals that the difference of the

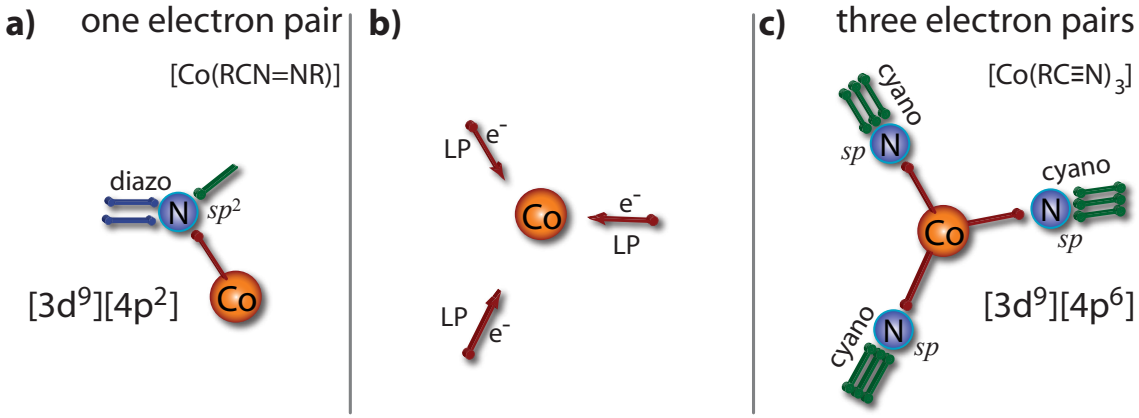


**Figure 4.7:** Schemes of cobalt-ligand complexes by means of the formation of coordination bonds between Co and lone-pair electron orbitals. Depending on whether one or three lone-pair electron orbitals are donating the complex, its valence electron configuration changes, resulting in different line-shapes in the $dI/dV$ spectra. The fact, that the involved N orbitals are $sp^2$-hybridized in the case of the diazo unit but $sp$-hybridized in the case of the cyano groups, results in a three-fold geometry for the former and a linear bond geometry for the latter case.

two types lays in the number of surrounding nitrogen units, donating electrons from their non-bonding orbitals to the cobalt. We will interpret this in the picture of covalent-like bonds. In the case of the diazo bridge (panel (a) of figure 4.7), one electron pair forms a metal-ligand complex [Jean 05]. The resulting electron configuration of non bonding Co electrons in the complex is $[[\mathrm{Ar}]3d^9]$, which results from the redistributed Co valence electrons. The donated electrons are distributed in directional orbitals, most probable they fill orbitals with $[4p^2]$-like configuration, oriented in the direction of the diazo group, forming the coordination bond. The

spectroscopic data revealed similar behavior as for a weakly coupled Co atom in the proximity of two cyano groups (red arrow sites in figure 4.6 (d)).

In the case of the three-fold Co sites, three lone-pair electrons contribute to another metal-ligand-complex, depicted in panel (c) of figure 4.7. The Co's non bonding electron configuration results to be the same as before. The redistributed valence electron system is now resembling energetically degenerated orbitals of a $[4p^6]$ electron configuration, three-fold oriented as the **DMC**'s cyano units show.

The two different electron configurations of the two metal organic complexes in the investigated structure reveal considerable different fingerprints in their LDOS. Hence, they show different line shapes in the $dI/dV$ spectra, because the Co atom accumulates a different amount of charge.

It should be mentioned, that in the two types of complexes (N$\cdots$Co) the nitrogen atoms respectively have a different character due to its varying embedding in the molecule. In the diazo unit the three-fold bond configuration highlights a $sp^2$-hybridized orbital distribution, while in the cyano group the linear triple bonds evidences a *sp*-hybridized orbital structure. It is possible that these different orbital distributions affect also the energetic alignment of the respectively involved lone-pair electron orbitals, bonding to the two- or three fold Co sites. A different energy value of bonding orbitals in the coordination complex may easily affect its electronic structure. Hence, the chemical embedding of nitrogen atoms in the molecule can give rise to differently observed fingerprints in the Co atoms.

## 4.7 Conclusion

We have shown Co atoms control the growth of **DMC** molecules on Au(111). By means of STS and $dI/dV$-mapping different spectroscopic features could be related to adsorption sites of Co atoms. They are anchoring points for both **DMC** rotamers, such that metal-organic complexes are formed in a two- and three-fold geometry. On the one hand the metal-organic complex between three cyano functionalities and one Co atom could be specified by the donation of three electron pairs from the molecule to the Co atom. On the other hand at the diazo unit, the Co atom is coupled by the donation of only one electron pair. This is the predicted situation (figure 4.1 (b)), stabilizing the azobenzene molecule on the surface. Still, with **DMC** there is no isomerization observed, since the cyano end-groups also interact with Co adatoms and couple to the surface. In fact they dominate the ordering in rows and clusters. Consequently, an upwards bending of phenyl rings that would support the *cis*-configuration, is suppressed.

# Conclusion

## Summary

In this work we have investigated various mechanism of inducing configurational and conformational changes in azobenzene derivatives on noble metal surfaces by means of low temperature STM. The introduction into the used technique and into general adsorption phenomena laid the foundation for interpreting the presented results.

Upon adsorption, the molecular geometrical and electronic structures are affected. This arises not only from interactions to the surface but also from interactions between adsorbates. In diverse example systems the effects of molecular ordering and recognition were identified as due to the formation of hydrogen or coordination bonds. In the adsorption process, these interactions compete with molecule-surface interactions, by means of $\pi$-surface coupling or local covalent bond formation between the center of the molecules and surface atoms.

On weakly adsorbed systems, the $\pi$-surface interaction dominates the adsorption of azobenzene and favors the molecular geometry of a planar *trans*-conformation. The azobenzene's phenyl rings, which are free to rotate in gas phase, adsorb planar on metallic surfaces due to $\pi$-surface coupling. This frozen degree of freedom can be switched by STM induced manipulation but also can be activated thermally or upon the high molecular density. Tip induced conformational changes were shown in the case of **DMC** when adsorbed on a gold surface. The related switching dynamics could be explained by the excitation of the anionic state and subsequent de-excitation within an electrical field.

When stronger surface interactions are present the molecules favor a three-dimensional structure. For instance on the copper surface **DMC** was proved to switch irreversible into a *cis*-like conformation. This is due to the formation of covalent bonds established via the lone-pair electron orbitals at the diazo unit and metal atoms. Since the reactivity of the surfaces acts differently on the diazo switching functionality, the switching of **DMC** could be tuned, exchanging the substrate materials. On the Ag(100) surface, which interacts stronger to organic adsorbates than gold but weaker than copper, reversible switching was possible.

The role of lone-pair electron orbitals of the **DMC** molecule, which do not contribute to internal molecular bonds, were utilized upon co-adsorption with cobalt

atoms on a Au(111) surface where they form metal-organic complexes. Different electron donation of lone-pair electron orbitals to metal centers could be identified by tunneling spectroscopy.

## Outlook

The knowledge about anchoring a molecule in such a way on a surface that switching is supported, exhibits the importance of a substrate material. It allows to tune individually the stability of conformational states. Not only the exchange of substrate materials but also metallic ad-atoms have proven to establish bond conformations to the diazo units and to strongly influence the electronic structure of the molecules. However, the functional end groups of the studied molecules, determine the molecular ordering and couple to the metal atoms, prohibiting isomeric switching. A modification in the molecules' structures, for instance by the exchange end groups will help to weaken the molecular *trans*-conformation and recover a switchable system.

The central diazo unit plays the key role in the switching of azobenzene. Small variation of this unit but also in its proximity has shown promising changes in the coupling to the surface or to ad-atoms, but also influences the energy barrier for isomerization.

Further variations in order to gain a switching system can be achieved by the surface. The change of anchoring sites promises to modify the stability of the two conformational states. For instance, surface alloys will have special atomic sites, which tune the metal-organic bond configuration locally, favoring a switching.

The molecular decoupling from the surface is expected to extend the lifetimes of anionic or excited molecular states. When conformational changes are mediated via these excitations, their longer lifetimes will assist the probability for switching directly. Besides the usage of bulky end groups, which lift the molecules from the surface, a decoupling can be achieved by oxide layers or salt layers between molecule and metallic sample [Alem 06]. This will also weaken the $\pi$-surface coupling, and hence support the switching into the three-dimensional *cis*-like adsorption structure.

Instead of varying the switching system by either changes in the surface or in the molecular system, the initiation of the isomerizing process can be changed. Thus, instead of tunneling electrons, light can be irradiated switch molecules and used to induce molecular switching [Coms 07, Levy 09]. Besides technical challenges for such goals, photons of selected energy may be well suited to efficiently switch molecular configurations.

# Bibliography


[Ai 08] M. Ai, S. Groeper, W. Zhuang, X. Dou, X. Feng, K. Müllen, and J. P. Rabe. "Optical switching studies of an azobenzene rigidly linked to a-hexaperihexabenzocoronene derivative in solution and at a solid liquid interface". *Appl. Phys. A*, Vol. 93, p. 533, 2008.

[Alem 06] M. Alemani, M. Peters, S. Hecht, K.-H. Rieder, F. Moresco, and L. Grill. "Electric Field-Induced Isomerization of Azobenzene by STM". *J. Am. Chem. Soc.*, Vol. 128, p. 14446, 2006.

[Amim 05] K. Amimoto and T. Kawato. "Photochromism of organic compounds in the crystal state". *Journal of Photochemistry and Photobiology C: Photochemistry Reviews*, Vol. 6, p. 207, 2005.

[Ashc 01] N. W. Ashcroft and N. D. Mermin. *Festkörperphysik*. Oldenburg, München, 2001.

[Bard 61] J. Bardeen. "Tunneling from a many particle point of view". *Phys. Rev. Lett.*, Vol. 6, p. 57, 1961.

[Bart 07] J. V. Barth. "Molecular Architectonic on Metal Surfaces". *Annu. Rev. Phys. Chem.*, Vol. 58, p. 375, 2007.

[Bart 90] J. V. Barth, H. Brune, G. Ertl, and R. J. Behm. "Scanning tunneling microscopy observations on the reconstructed Au(111) surface: Atomic structure, long-range superstructure, rotational domains, and surface defects". *Phys. Rev. B*, Vol. 42, p. 9307, 1990.

[Beve 66] D. Beveridg and H. Jaffe. "Electronic Structure and Spectra of Cis- and Trans-Azobenzene". *J. Am. Chem. Soc.*, Vol. 88, p. 1948, 1966.

[Binn 82a] G. Binnig, H. Rohrer, C. Gerber, and E. Weibel. "Tunneling through a Controllable Vacuum Gap". *Appl. Phys. Lett.*, Vol. 40, p. 178, 1982.

[Binn 82b] G. Binning, H. Rohrer, C. Gerber, and E. Weibel. "Surface Studies by Scanning Tunneling Microscopy". *Phys. Rev. Let*, Vol. 49, p. 57, 1982.

[Binn 83] G. Binnig, H. Rohrer, C. Gerber, and E. Weibel. "7X7 Reconstruction on Si(111) Resolved in Real Space". *Phys. Rev. Lett.*, Vol. 50, p. 120, 1983.

[Binn 87] G. Binnig and H. Rohrer. "Scanning Tunneling Microscopy - from Birth to Adolescence". *Angew. Chem. Int. Ed.*, Vol. 26, p. 606, 1987.

[Bode 98] M. Bode, M. Getzlaff, and R. Wiesendanger. "Spin-Polarized Vacuum Tunneling into the Exchange-Split Surface State of Gd(0001)". *Phys. Rev. Lett.*, Vol. 81, p. 4256, 1998.

[Bran 80] B. H. Bransden and C. J. Joachain. *Physics of Atoms and Molecules*. Longman, London, New York, 1980.

[Choi 06] B.-Y. Choi, S.-J. Kahng, S. Kim, H. Kim, H. W. Kim, Y. J. Song, J. Ihm, and Y. Kuk. "Conformational Molecular Switch of the Azobenzene Molecule: A Scanning Tunneling Microscopy Study". *Phys. Rev. Lett.*, Vol. 96, p. 156106, 2006.

[Coms 05] M. J. Comstock, J. W. Cho, A. Kirakosian, and M. F. Crommie. "Manipulation of azobenzene molecules on Au(111) using scanning tunneling microscopy". *Phys. Rev. B*, Vol. 72, p. 153414, 2005.

[Coms 07] M. J. Comstock, N. Levy, A. Kirakosian, J. W. Cho, F. Lauterwasser, J. H. Harvey, D. A. Strubbe, J. M. J. Frechet, D. Trauner, S. G. Louie, and M. F. Crommie. "Reversible photomechanical switching of individual engineered molecules at a metallic surface". *Phys. Rev. Lett.*, Vol. 99, p. 038301, 2007.

[Cond 26] E. Condon. "A Theory of Intensity Distribution in Band Systems". *Phys. Rev.*, Vol. 28, p. 1182, 1926.

[Cond 28] E. Condon. "Nuclear Motions Associated with Electron Transitions in Diatomic Molecules". *Phys. Rev.*, Vol. 32, p. 858, 1928.

[Cool 36] A. Coolidge, H. M. James, and R. D. Present. "A Study of the Franck-Condon Principle". *The Journal of Chemical Physics*, Vol. 4, p. 193, 1936.

[Dela 96] E. Delamarche and B. Michel. "Structure and stability of self-assembled monolayers". *Thin Solid Films*, Vol. 273, p. 54, 1996.

[Dri 08] C. Dri, M. V. Peters, J. Schwarz, S. Hecht, and L. Grill. "Spatial periodicity in molecular switching". *Nat. Nanotechnol.*, Vol. 3, p. 649, 2008.

[Drr 90] H. Dürr and H. Bouas-Laurent. *Photochromism: Molecules and Systems*. Elsevier Science, Amsterdam, USA, 1990.

[Duli 03] D. Dulic, S. J. van der Molen, T. Kudernac, H. T. Jonkman, J. J. D. de Jong, T. N. Bowden, J. van Esch, B. L. Feringa, and B. J. van Wees. "One-way optoelectronic switching of photochromic molecules on gold". *Phys. Rev. Lett.*, Vol. 91, p. 207402, 2003.

[Elsa 98] T. Elsässer, J. Fujimoto, D. Wiersma, and W. Zinth, Eds. *Ultrafast Phenomena XI*. Springer, Berlin, Heidelberg, 1998.

[Elst 08] F. Elste, G. Weick, C. Timm, and F. von Oppen. "Current-induced conformational switching in single-molecule junctions". *Appl. Phys. A*, Vol. 93, p. 345, 2008.

[Ertl 08] G. Ertl. "Reactions at Surfaces: From Atoms to Complexity (Nobel Lecture)13". *Angew. Chem. Int. Ed.*, Vol. 47, p. 3524, 2008.

[Ertl 90] G. Ertl. "Elementary Steps in Heterogeneous Catalysis". *Angew. Chem. Int. Ed.*, Vol. 29, p. 1219, 1990.

[Feri 01] B. L. Feringa, Ed. *Molecular switches*. Willey-VCH, Weinheim, Germany, 2001.

[Fern 06] I. Fernandez-Torrente, K. Franke, N. Henningsen, G. Schulze, M. Alemani, C. Roth, R. Rurali, N. Lorente, and J. Pascual. "Spontaneous Formation of Triptycene Supramolecules on Surfaces". *J. Phys. Chem. B*, Vol. 110, p. 20089, 2006.

[Fran 08] K. J. Franke, I. Fernández-Torrente, J. I. Pascual, and N. Lorente. "Adsorption of N 2 O on Cu (100): a combined scanning tunneling microscopy and density functional theory study". *Phys. Chem. Chem. Phys.*, Vol. 10, p. 1640, 2008.

[Fran 09] K. Franke and J. I. Pascual. "Vibrational spectroscopy study of $C_{60}$ molecules in a superconductor tunneling junction". *submitted*, 2009.

[Fuch 06] G. Füchsel, T. Klamroth, J. Dokić, and P. Saalfrank. "On the Electronic Structure of Neutral and Ionic Azobenzenes and Their Possible Role as Surface Mounted Molecular Switches". *J. Phys. Chem. B*, Vol. 110, p. 16337, 2006.

[Gaud 00] J. Gaudioso, L. J. Lauhon, and W. Ho. "Vibrationally mediated negative differential resistance in a single molecule". *Phys. Rev. Lett.*, Vol. 85, p. 1918, 2000.

[Gril 05] L. Grill, K.-H. Rieder, F. Moresco, S. Stojkovic, A. Gourdon, and C. Joachim. "Controlling the Electronic Interaction between a Molecular Wire and Its Atomic Scale Contacting Pad". *Nano Lett.*, Vol. 5, p. 859, 2005.

[Gril 07] L. Grill, K. H. Rieder, F. Moresco, G. Rapenne, S. Stojkovic, X. Bouju, and C. Joachim. "Rolling a single molecular wheel at the atomic scale". *Nat. Nanotechnol.*, Vol. 2, p. 95, 2007.

[Gron 00] H. Grönbeck, A. Curioni, and W. Andreoni. "Thiols and Disulfides on the Au(111) Surface: The Headgroup-Gold Interaction". *J. Am. Chem. Soc.*, Vol. 122, p. 3839, 2000.

[Gros 03] L. Gross, F. Moresco, M. Alemani, H. Tang, A. Gourdon, C. Joachim, and K.-H. Rieder. "Lander on Cu(2 1 1) - selective adsorption and surface restructuring by a molecular wire". *Chem. Phys. Lett.*, Vol. 371, p. 750, 2003.

[Grtn 01] W. Gärtner. "Das Licht weise den Weg - oder: die Konformationsänderungen des Retinalchromophors im Sehpigment Rhodopsin nach Lichtanregung". *Angw. Chem.*, Vol. 113, p. 3065, 2001.

[Hage 07] S. Hagen, F. Leyssner, D. Nandi, M. Wolf, and P. Tegeder. "Reversible switching of tetra-tert-butyl-azobenzene on a Au(111) surface induced by light and thermal activation". *Chem. Phys. Lett.*, Vol. 444, p. 85, 2007.

[Hart 36] G. S. Hartley. "The Critical Concentration for Micelles in Solutions of Cetane Sulfonic Acid". *J. Am. Chem. Soc.*, Vol. 58, pp. 2347–, 1936.

[Hein 00] S. Heinze, M. Bode, A. Kubetzka, O. Pietzsch, X. Nie, S. Blugel, and R. Wiesendanger. "Real-Space Imaging of Two-Dimensional Antiferromagnetism on the Atomic Scale". *Science*, Vol. 288, p. 1805, 2000.

[Henn 07] N. Henningsen, K. Franke, I. Torrente, G. Schulze, B. Priewisch, K. Ruck-Braun, J. Dokić, T. Klamroth, P. Saalfrank, and J. Pascual. "Inducing the Rotation of a Single Phenyl Ring with Tunneling Electrons". *J. of Phys. Chem. C*, Vol. 111, p. 14843, 2007.

[Henn 08a] N. Henningsen, K. Franke, G. Schulze, I. Fernandez-Torrente, B. Priewisch, K. Ruck-Braun, and J. Pascual. "Active intramolecular conformational dynamics controlling the assembly of azobenzene derivatives at surfaces.". *ChemPhysChem*, Vol. 9, p. 71, 2008.

[Henn 08b] N. Henningsen, R. Rurali, K. J. Franke, I. Fernandez-Torrente, and J. I. Pascual. "Trans to cis isomerization of an azobenzene derivative on a Cu(100) surface". *Appl. Phys. A*, Vol. 93, p. 241, 2008.

[Henz 06] J. Henzl, M. Mehlhorn, H. Gawronski, K.-H. Rieder, and K. Morgenstern. "Reversible cis-trans Isomerization of a Single Azobenzene Molecule". *Angew. Chem. Int. Ed.*, Vol. 45, p. 603, 2006.

[Henz 07] J. Henzl, T. Bredow, and K. Morgenstern. "Irreversible isomerization of the azobenzene derivate Methyl Orange on Au(111)". *Chem. Phys. Lett.*, Vol. 435, p. 278, 2007.

[Hla 03] S.-W. Hla, K.-F. Braun, and K.-H. Rieder. "Single-atom manipulation mechanisms during a quantum corral construction". *Phys. Rev. B*, Vol. 67, p. 201402, 2003.

[Hla 04] S.-W. Hla, K.-F. Braun, B. Wassermann, and K.-H. Rieder. "Controlled Low-Temperature Molecular Manipulation of Sexiphenyl Molecules on Ag(111) Using Scanning Tunneling Microscopy". *Phys. Rev. Lett.*, Vol. 93, p. 208302, 2004.

[Ho 02] W. Ho. "Single-molecule chemistry". *J. Chem. Phys.*, Vol. 117, p. 11033, 2002.

[Horc 07] I. Horcas, R. Fernández, J. Gómez-Rodríguez, J. Colchero, J. Gómez-Herrero, and A. Baró. "WSXM: A software for scanning probe microscopy and a tool for nanotechnology". *Rev. Sci. Inst.*, Vol. 78, p. 013705, 2007.

[Huge 02] T. Hugel, N. B. Holland, A. Cattani, L. Moroder, M. Seitz, and H. E. Gaub. "Single-Molecule Optomechanical Cycle". *Science*, Vol. 296, p. 1103, 2002.

[Ianc 06] V. Iancu and S.-W. Hla. "Realization of a four-step molecular switch in scanning tunneling microscope manipulation of single chlorophyll-a molecules". *PNAS*, Vol. 103, p. 13718, 2006.

[Ingo 96] O. Ingolfsson, F. Weik, and E. Illenberger. "The Reactivity of Slow Electrons with Molecules at Different Stages of Aggregation: Gas Phase, Clusters and Condensed Phase". *Int. J. Mass spectrom.*, Vol. 155, p. 1, 1996.

[Irie 88] M. Irie and M. Mohri. "Thermally irreversible photochromic systems. Reversible photocyclization of diarylethene derivatives". *The Journal of Organic Chemistry*, Vol. 53, p. 803, 1988.

[Jakl 66] R. C. Jaklevic and J. Lambe. "Molecular Vibration Spectra by Electron Tunneling". *Phys. Rev. Lett.*, Vol. 17, p. 1139, 1966.

[Jean 05] Y. Jean, Ed. *Molecular Orbitals of Transition Metal Complexes*. Oxford University Press, Oxford, Great Britain, 2005.

[Kitt 02] C. Kittel. *Einführung in die Festkörperphysik*. Oldenburg, München, 2002.

[Klam 08] T. Klamroth. "private communication". 2008.

[Klei 73] J. Klein, A. Léger, M. Belin, D. Défourneau, and M. J. L. Sangster. "Inelastic-Electron-Tunneling Spectroscopy of Metal-Insulator-Metal Junctions". *Phys. Rev. B*, Vol. 7, p. 2336, 1973.

[Kock 09] D. Kockmann, B. Poelsema, and H. J. W. Zandvliet. "Transport through a Single Octanethiol Molecule". *Nano Lett.*, Vol. 9, p. 1147, 2009.

[Kome 02] T. Komeda, Y. Kim, M. Kawai, B. N. J. Persson, and H. Ueba. "Lateral Hopping of Molecules Induced by Excitation of Internal Vibration Mode". *Science*, Vol. 295, p. 2055, 2002.

[Kons 08] M. Konschake. "Ultradünne metallorganische Filme - Der Ladungstransferkomplex TTF-TCNQ auf Pb(111)". 2008.

[Laff 09] L. Lafferentz, F. Ample, H. Yu, S. Hecht, C. Joachim, and L. Grill. "Conductance of a Single Conjugated Polymer as a Continuous Function of Its Length". *Science*, Vol. 323, p. 1193, 2009.

[Lang 86] N. D. Lang. "Spectroscopy of single atoms in the scanning tunneling microscope". *Phys. Rev. B*, Vol. 34, p. 5947, 1986.

[Last 05] M. Lastapis, M. Martin, D. Riedel, L. Hellner, G. Comtet, and G. Dujardin. "Picometer-scale electronic control of molecular dynamics inside a single molecule". *Science*, Vol. 308, p. 1000, 2005.

[Lauh 00] L. J. Lauhon and W. Ho. "Single-molecule chemistry and vibrational spectroscopy: Pyridine and benzene on Cu(001)". *J. Phys. Chem. A*, Vol. 104, p. 2463, 2000.

[Lehn 02] J. M. Lehn. "Toward self-organization and complex matter". *Science*, Vol. 295, p. 2400, 2002.

[Levy 09] N. Levy, M. J. Comstock, J. Cho, L. Berbil-Bautista, A. Kirakosian, F. Lauterwasser, D. A. Poulsen, J. M. J. Fre´chet, and M. F. Crommie. "Self-Patterned Molecular Photoswitching in Nanoscale Surface Assemblies". *Nano Letters*, Vol. 9, p. 935, 2009.

[Lilj 07] P. Liljeroth, J. Repp, and G. Meyer. "Current-Induced Hydrogen Tautomerization and Conductance Switching of Naphthalocyanine Molecules". *Science*, Vol. 317, p. 1203, 2007.

[Ling 07] M. Lingenfelder, G. Tomba, G. Costantini, L. C. Ciacchi, A. De Vita, and K. Kern. "Tracking the chiral recognition of adsorbed dipeptides at the single-molecule level". *Angew. Chem. Int. Ed.*, Vol. 46, p. 4492, 2007.

[Lotz 09] C. Lotze. "An imine based molecular switch on a gold surface: structural, electronic and isomerization properties". 2009.

[Maks 08] P. Maksymovych, D. C. Sorescu, K. D. Jordan, and J. T. J. Yates. "Collective Reactivity of Molecular Chains Self-Assembled on a Surface". *Science*, Vol. 322, p. 1664, 2008.

[Mats 04] K. Matsuda and M. Irie. "Diarylethene as a photoswitching unit". *J. Photochem. Photobiol., C*, Vol. 5, p. 169, 2004.

[Mena 08] H. Mena. *Synthesis and characterization of metal-organic and supramolecular compounds based on the 1,2-bis(1,2,4-triazol-4-yl)ethane ligand*. PhD thesis, Albert-Ludwigs-Universität Freiburg, 2008.

[Meye 00] G. Meyer, J. Repp, S. Zöphel, S.-W. Braun, K.-F. Hla, S. Fölsch, L. Bartels, F. Moresco, and K.-H. Rieder. "Controlled Manipulation of Atoms and Small Molecules with a Low Temperature Scanning Tunneling Microscope". *Single Molecules*, Vol. 1, p. 79, 2000.

[Meye 96] G. Meyer, S. Zöphel, and K.-H. Rieder. "Controlled manipulation of ethen molecules and lead atoms on Cu(211) with a low temperature scanning tunneling microscope". *Appl. Phys. Lett.*, Vol. 69, p. 3185, 1996.

[Meye 98] G. Meyer, L. Bartels, S. Zöphel, and K.-H. Rieder. "Possibilities for atom by atom restructuring of surfaces employing native substrate atoms as well as foreign species". *Appl. Surf. Sci.*, Vol. 130-132, p. 527, 1998.

[Miwa 06] J. A. Miwa, S. Weigelt, H. Gersen, F. Besenbacher, F. Rosei, and T. R. Linderoth. "Azobenzene on Cu(110): Adsorption site-dependent diffusion". *J. Am. Chem. Soc.*, Vol. 128, p. 3164, 2006.

[Moor 65] G. E. Moore. "Cramming more components onto integrated circuits". *Electronics Magazine*, Vol. 38, 1965.

[Morg 09] K. Morgenstern. "Isomerization Reactions on Single Adsorbed Molecules". *Accounts of Chemical Research*, Vol. 42, p. 213, 2009.

[Mull 98] B. Müller, L. Nedelmann, B. Fischer, H. Brune, J. V. Barth, and K. Kern. "Island shape transition in heteroepitaxial metal growth on square lattices". *Phys. Rev. Lett.*, Vol. 80, p. 2642, 1998.

[Nage 97] T. Nägele, R. Hoche, W. Zinth, and J. Wachtveitl. "Femtosecond photoisomerization of cis-azobenzene". *Chem. Phys. Lett.*, Vol. 272, p. 489, 1997.

[Nara 92] S. Narasimhan and D. Vanderbilt. "Elastic stress domains and the herringbone reconstruction on Au(111)". *Phys. Rev. Lett.*, Vol. 69, p. 1564, 1992.

[Neel 07] N. Néel, J. Kröger, L. Limot, T. Frederiksen, M. Brandbyge, and R. Berndt. "Controlled Contact to a C[sub 60] Molecule". *Phys. Rev. Lett.*, Vol. 98, p. 065502, 2007.

[New 98] "New drugs from the forest - Biotech's Secret Garden". *The Economist*, p. 75, 1998.

[Nobl 56] A. Noble. "Zur Geschichte des Azobenzols und des Benzidins". *Annalen der Chemie und Pharmacie*, Vol. 98, p. 253, 1856.

[Ohar 06] M. Ohara, Y. Kim, and M. Kawai. "Controlling the reaction and motion of a single molecule by vibrational excitation". *Chem. Phys. Lett.*, Vol. 426, p. 357, 2006.

[Orde 96] P. Ordejón, E. Artacho, and J. M. Soler. "Self-consistent order-N density-functional calculations for very large systems". *Phys. Rev. B*, Vol. 53, p. R10441, 1996.

[Ovar 07] L. Ovari, M. Wolf, and P. Tegeder. "Reversible changes in the vibrational structure of tetra-tert-butylazobenzene on a Au(111) surface induced by light and thermal activation". *J. Phys. Chem. C*, Vol. 111, p. 15370, 2007.

[Pasc 00] J. I. Pascual, J. Gómez-Herrero, C. Rogero, A. M. Baró, D. Sánchez-Portal, E. Artacho, P. Ordejón, and J. M. Soler. "Seeing molecular orbitals". *Chem. Phys. Lett.*, Vol. 321, p. 78, 2000.

[Pasc 03] J. I. Pascual, N. Lorente, Z. Song, H. Conrad, and H.-P. Rust. "Selectivity in vibrationally mediated single-molecule chemistry". *Nature*, Vol. 423, p. 525, 2003.

[Pasc 06] J. I. Pascual and N. Lorente. "Single-Molecule Vibrational Spectroscopy and Chemistry". *Singapore: World Scientific*, 2006.

[Perd 92] J. P. Perdew, J. A. Chevary, S. H. Vosko, K. A. Jackson, M. R. Pederson, D. J. Singh, and C. Fiolhais. "Atoms, Molecules, Solids, and Surfaces - Applications of the Generalized Gradient Approximation for Exchange and Correlation". *Phys. Rev. B*, Vol. 46, p. 6671, 1992.

[Pian] M. Piantek, A. Krüger, K. Navio, M. Bernien, J. Miguel, K. Herrmann, and W. Kuch. "*In Preparation:* Surface- and coverage-induced conformational changes of azobenzene derivatives on Cu(001)".

[Pian 09] M. Piantek, G. Schulze, M. Koch, K. Franke, F. Leyssner, A. Krüger, C. Navío, J. Miguel, M. Bernien, M. Wolf, W. Kuch, P. Tegeder, and J. Pascual. "Reversing the thermal stability of a molecular switch on a gold surface: ring-opening reaction of nitro-spiropyran". *submitted*, 2009.

[Piet 00] O. Pietzsch, A. Kubetzka, M. Bode, and R. Wiesendanger. "Real-Space Observation of Dipolar Antiferromagnetism in Magnetic Nanowires by Spin-Polarized Scanning Tunneling Spectroscopy". *Phys. Rev. Lett.*, Vol. 84, p. 5212, 2000.

[Prie 05] B. Priewisch and Rück-Braun, K. *J. Org. Chem.*, Vol. 70, p. 2350, 2005.

[Prie 06] B. Priewisch. *Photoschaltbare Aminosäuren.* PhD thesis, Technische Universität Berlin, 2006.

[Qiu 03] X. H. Qiu, G. V. Nazin, and W. Ho. "Vibrationally Resolved Fluorescence Excited with Submolecular Precision". *Science*, Vol. 299, p. 542, 2003.

[Qiu 04a] X. H. Qiu, G. V. Nazin, and W. Ho. "Mechanisms of reversible conformational transitions in a single molecule". *Phys. Rev. Lett.*, Vol. 93, p. 196806, 2004.

[Qiu 04b] X. H. Qiu, G. V. Nazin, and W. Ho. "Vibronic States in Single Molecule Electron Transport". *Phys. Rev. Lett.*, Vol. 92, p. 206102, 2004.

[Rapp 00] A. Rappe and E. Bernstein. “Ab Initio Calculation of Nonbonded Interactions: Are We There Yet?”. *J. Phys. Chem. A*, Vol. 104, pp. 6117–6128, 2000.

[Repp 05] J. Repp, G. Meyer, S. M. Stojković, A. Gourdon, and C. Joachim. “Molecules on Insulating Films: Scanning-Tunneling Microscopy Imaging of Individual Molecular Orbitals”. *Phys. Rev. Lett.*, Vol. 94, p. 026803, 2005.

[Reut 07] C. Reuter. “private communication”. 2007.

[Sanc 97] D. Sánchez-Portal, P. Ordejón, E. Artacho, and J. M. Soler. “Density-functional method for very large systems with LCAO basis sets”. *International Journal of Quantum Chemistry*, Vol. 65, p. 453, 1997.

[Schl 07] U. Schlickum, R. Decker, F. Klappenberger, G. Zoppellaro, S. Klyatskaya, M. Ruben, I. Silanes, A. Arnau, K. Kern, H. Brune, and J. V. Barth. “Metal-Organic Honeycomb Nanomeshes with Tunable Cavity Size”. *Nano Lett.*, Vol. 7, pp. 3813–3817, 2007.

[Schl 08] U. Schlickum, R. Decker, F. Klappenberger, G. Zoppellaro, S. Klyatskaya, W. Auwarter, S. Neppl, K. Kern, H. Brune, M. Ruben, and J. V. Barth. “Chiral kagome lattice from simple ditopic molecular bricks”. *J. Am. Chem. Soc.*, Vol. 130, p. 11778, 2008.

[Schm 07] P. M. Schmidt, K. Horn, J. H. Dil, and T. U. Kampen. “Conformational isomers of stilbene on Si(100)”. *Surf. Sci.*, Vol. 601, p. 1775, 2007.

[Schm 08a] R. Schmidt, E. McNellis, W. Freyer, D. Brete, T. Gießel, C. Gahl, K. Reuter, and M. Weinelt. “Azobenzene-functionalized alkanethiols in self-assembled monolayers on gold”. *Appl. Phys. A.*, Vol. 93, p. 267, 2008.

[Schm 08b] P. Schmidt-Weber. *Functionalisation of Surfaces: Isomerisation and Chirality of Adsorbed Molecules*. PhD thesis, Freie Universität Berlin, 2008.

[Schu 08] G. Schulze, K. J. Franke, A. Gagliardi, G. Romano, C. S. Lin, A. L. Rosa, T. A. Niehaus, T. Frauenheim, A. D. Carlo, A. Pecchia, and J. Pascual. “Resonant Electron Heating and Molecular Phonon Cooling in Single C[sub 60] Junctions”. *Phys. Rev. Lett.*, Vol. 100, p. 136801, 2008.

[Schw 02] F. Schwabl. *Quantenmechanik*. Springer, Berlin, Heidelberg, 2002.

[Sekk 02] Z. Sekkat and W. Knoll. *Photoreactive organic thin films*. Elsevier Science, San Diego, USA, 2002.

[Sell 85] A. Selloni, P. Carnevali, E. Tosatti, and C. D. Chen. “Voltage-dependent scanning-tunneling microscopy of a crystal surface: Graphite”. *Phys. Rev. B*, Vol. 31, p. 2602, 1985.

[Shan 75] R. D. Shannon, J. Chenavas, and J. C. Joubert. "Bond strength considerations applied to cation coordination in normal and high-pressure oxides". *J. Solid State Chem.*, Vol. 12, p. 16, 1975.

[Sloa 05] P. A. Sloan and R. E. Palmer. "Two-electron dissociation of single molecules by atomic manipulation at room temperature". *Nat.*, Vol. 434, p. 367, 2005.

[Spag 71] P. Spagnolo, L. Testafer, and M. Tiecco. "Photochemical Production of Electrophilic Cyano-Radical - Homolytic Aromatic Cyanation". *J. Chem. Soc. B*, Vol. 1971, p. 2006, 1971.

[Step 07] S. Stepanow, N. Lin, D. Payer, U. Schlickum, F. Klappenberger, G. Zoppellaro, M. Ruben, H. Brune, J. V. Barth, and K. Kern. "Surface-assisted assembly of 2D metal-organic networks that exhibit unusual threefold coordination symmetry". *Angew. Chem. Int. Ed.*, Vol. 46, p. 710, 2007.

[Step 08] S. Stepanow, N. Lin, and J. v. Barth. "Modular assembly of low-dimensional coordination architectures on metal surfaces". *Journal of Physics: Condensed Matter*, Vol. 20, p. 184002, 2008.

[Stip 98] B. C. Stipe, M. A. Rezaei, and W. Ho. "Single-Molecule Vibrational Spectroscopy and Microscopy". *Science*, Vol. 280, p. 1732, 1998.

[Stok 98] K. Stokbro, C. Thirstrup, M. Sakurai, U. Quaade, B. Y. K. Hu, F. Perez-Murano, and F. Grey. "STM-induced hydrogen desorption via a hole resonance". *Phys. Rev. Lett.*, Vol. 80, p. 2618, 1998.

[Sze 85] S. M. Sze. *Semiconductor Devices*. John Wiley & Sons, 1985.

[Tana 02] S. Tanaka, S. Itoh, and N. Kurita. "Possibility of nonequilibrium isomerization of azobenzene triggered by vibrational excitations". *Chem. Phys. Lett.*, Vol. 362, p. 467, 2002.

[Tege 07] P. Tegeder, S. Hagen, F. Leyssner, M. V. Peters, S. Hecht, T. Klamroth, P. Saalfrank, and M. Wolf. "Electronic structure of the molecular switch tetra-tert-butyl-azobenzene adsorbed on Ag(111)". *Appl. Phys. A*, Vol. 88, p. 465, 2007.

[Temi 08a] R. Temirov, A. Lassise, F. B. Anders, and F. S. Tautz. "Kondo effect by controlled cleavage of a single-molecule contact". *Nanotechnology*, Vol. 19, p. 065401, 2008.

[Temi 08b] R. Temirov, S. Soubatch, A. Lassise, and F. S. Tautz. "Bonding and vibrational dynamics of a large $\pi$-conjugated molecule on a metal surface". *Journal of Physics: Condensed Matter*, Vol. 20, 2008.

[Ters 83] J. Tersoff and D. R. Hamann. "Theory and application for the Scanning Tunneling Microscope". *Phys. Rev. Lett.*, Vol. 59, p. 1998, 1983.

[Ters 85] J. Tersoff and D. R. Hamann. “Theory of the Scanning Tunneling Microscope”. *Phys. Rev. B*, Vol. 31, p. 805, 1985.

[Tsuj 00] T. Tsuji, H. Takashima, H. Takeuchi, T. Egawa, and S. Konaka. “Molecular structure of trans-azoxybenzene determined by gas electron diffraction combined with ab initio calculations”. *J. Mol. Struct.*, Vol. 554, p. 203, 2000.

[Tsuj 01a] T. Tsuji, H. Takashima, H. Takeuchi, T. Egawa, and S. Konaka. “Molecular structure and torsional potential of trans-azobenzene. A gas electron diffraction study”. *J. Phys. Chem. A*, Vol. 105, p. 9347, 2001.

[Tsuj 01b] T. Tsuji, H. Takashima, H. Takeuchi, T. Egawa, and S. Konaka. “Molecular Structure and Torsional Potential of trans-Azobenzene. A Gas Electron Diffraction Study”. *J. Phys. Chem. A*, Vol. 105, p. 9347, 2001.

[Tsuk 09] N. Tsukahara, K.-i. Noto, M. Ohara, S. Shiraki, N. Takagi, Y. Takata, J. Miyawaki, M. Taguchi, A. Chainani, S. Shin, and M. Kawai. “Adsorption-Induced Switching of Magnetic Anisotropy in a Single Iron(II) Phthalocyanine Molecule on an Oxidized Cu(110) Surface”. *Phys. Rev. Lett.*, Vol. 102, p. 167203, 2009.

[Wach 04] J. Wachtveitl, S. Sporlein, H. Satzger, B. Fonrobert, C. Renner, R. Behrendt, D. Oesterhelt, L. Moroder, and W. Zinth. “Ultrafast conformational dynamics in cyclic azobenzene peptides of increased flexibility”. *Biophys. J.*, Vol. 86, p. 2350, 2004.

[Wang 08] Y. Wang, X. Ge, G. Schull, R. Berndt, C. Bornholdt, F. Koehler, and R. Herges. “Azo Supramolecules on Au(111) with Controlled Size and Shape”. *J. Am. Chem. Soc.*, Vol. 130, p. 4218, 2008.

[Webe 03] R. Weber, B. Winter, I. Hertel, B. Stiller, S. Schrader, L. Brehmer, and N. Koch. “Photoemission from Azobenzene Alkanethiol Self-Assembled Monolayers”. *J. Phys. Chem. B*, Vol. 107, p. 7768, 2003.

[Weig 06] S. Weigelt, C. Busse, L. Petersen, E. Rauls, B. Hammer, K. V. Gothelf, F. Besenbacher, and T. R. Linderoth. “Chiral switching by spontaneous conformational change in adsorbed organicmolecules”. *Nat. Mater.*, Vol. 5, p. 112, 2006.

[Wu 04] S. W. Wu, G. V. Nazin, X. Chen, X. H. Qiu, and W. Ho. “Control of Relative Tunneling Rates in Single Molecule Bipolar Electron Transport”. *Phys. Rev. Lett.*, Vol. 93, p. 236802, 2004.

[Zang 88] A. Zangwill. *Physics at Surfaces*. Cambridge University Press, Cambridge, GB, 1988.

[Zhan 04] C. Zhang, M.-H. Du, H.-P. Cheng, X.-G. Zhang, A. E. Roitberg, and J. L. Krause. “Coherent Electron Transport through an Azobenzene Molecule: A Light-Driven Molecular Switch”. *Phys. Rev. Lett.*, Vol. 92, p. 158301, 2004.

## Design of Sample Fixing

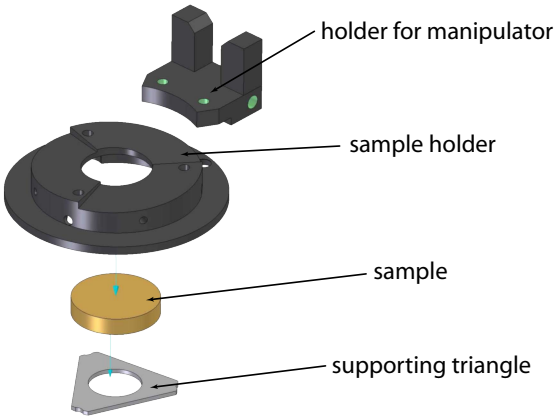


**Figure 5.1:** The triangular plate, fixing the sample in the sample holder is the newest part in the STM's design. The screwing mechanism allows a comfortable exchange of samples and is safe against sample drop off due to its stability. Also the thermal coupling to the cryostats (on the manipulator and in the measuring stage) is improved.

## Single Crystal Preparation Temperatures

| | Au(111) | Ag(100) | Cu(100) |
|---|---|---|---|
| Annealing Temperature | 800 K | 820 K | 800 K |

**Table 5.1:** For the sample preparation the polished single crystals of according orientations have been repetitively heated to the listed temperatures and sputtered by $Ne^+$ ions of 1.5 keV. The Temperatures are related to approximately 70% of the metals' melting temperature.

## Sublimation Parameters of the Molecules

| | **DMC** | **DPC** | **CMA** | **CPA** | **DSA** |
|---|---|---|---|---|---|
| Sublimation Temperatures | $\sim$ 370 K | $\sim$ 380 K | $\sim$ 380 K | $\sim$ 400 K | $\sim$ 445 K |
| Time for one Monolayer | $\sim$ 6 min | $\sim$ 5 min | $\sim$ 2.5 min | $\sim$ 3 min | $\sim$ 3 min |

**Table 5.2:** The sublimation of molecules in UHV conditions is very critical in its temperature, since the density of molecules grows exponentially to this parameter. On the one hand low dosing rates allow a precisely predictable coverage on the samples, on the other hand at low sample temperatures and long dosing times the contamination of the sample by undefined species rises. This may for instance become problematic, when *i.e.* solvents cannot be de-gased properly from the substance, because the temperature window for sublimation is so small. Note that the dosing rate strongly depends on the geometry and distance of sample and Knudsen Cell.

# Acknowledgements

Many people supported my work during the last years that it would be not possible to name them all. I am very grateful for all their help and participation in this work and want to at least announce some of their contributions.

First of all I want to thank Nacho Pascual, who offered me the possibility to work on the topic of switchable molecules and who gave me the chance to improve my experimental and analytic skills in physics as well as to join his young and ambitious work group.

Furthermore I want to acknowledge Prof. Dr. Karsten Horn from the Fritz-Haber-Institute becoming second referee of this thesis. The exchange of experimental knowhow and equipment with his group was supporting a lot the work in our laboratory.

I owe special thanks to my former office mate Katharina Franke, who was a great support discussing the results of measurements, working in the lab, and finding precise wording. Also, I want to thank my still office mate Isabel Fernández-Torrente, who always created a grat atmosphere and always offered her helping hands in the lab. In the year of my diploma, Christian Roth was the one who taught me so many things about cryo- and UHV-techniques, during the construction of the STM, thank you for that. Angelika Scheffler, Ania Strozecka, Ingeborg Staß, Dagmar Kreikemeyer, Gunnar Schulze, Wolfgang Theis, Sergio Valencia, Mario Konschake, Chris Lotze, Christoph Limbach, Dennis Engberding, and Cornelius Krull: You all took a special part in supporting this work and it was a great experience to get in touch with you and having you as colleagues. I also would like to thank the people of the laboratory next door, the collaborators of Leonard Grill's group.

Beate Priewisch and Christin Gebhard from the work group of Karola Rück-Braun, thank you for the work of synthesising all the investigated molecules. A special thank goes to Jadranka Dokić, Tillman Klamroth and Peter Saalfrank for the fruitful discussions and for performing the calculations, which helped to understand the molecular switching dynamics. Also Riccardo Rurali has contributed to great amounts with his calculations for the adsorption structures. Furthermore I want to acknowledge the intensive conversations about all the azobenzene molecules with the People of Wolfgang Kuch's work group in general and Marten Piantek in particular, as well as the switching molecules community of the SFB 658.

Very special thanks, respect and a big hug goes to my beloved wife Christine for suffering and understanding the stress I had in the last weeks and for the endless moral support she gave to me in the last three years. Also my parents and my sister accompanied me on the way with their good wishes and help as well as my good friends Ina, Philipp, Sebastian and Max. Thanks to all of you.

This work could only be realized because of the financial support of the German Research Foundation (DFG) by the collaborative research center (SFB 658) about molecular switches on surfaces.

# Curriculum Vitae

Due to privacy protection the CV has been removed from the online version.

## List of Publications

### Articles

*Spontaneous formation of triptycene supramolecules on surfaces.* **I. Fernandez-Torrente**, K. J. Franke, N. Henningsen, G. Schulze, M. Alemani, Ch. Roth, R. Rurali, N. Lorente, and J. I. Pascual; J. of Phys. Chem. B **110**, 20089 (2006)

*Inducing the rotation of a single phenyl ring with tunneling electrons.* **N. Henningsen**, K. J. Franke, I. F. Torrente, G. Schulze, B. Priewisch, K. Rück-Braun, J. Dokic, T. Klamroth, P. Saalfrank, and J. I. Pascual; J. Phys. Chem. C **111**, 14843 (2007)

*Reducing the molecule-substrate coupling in C60-based nanostructures by molecular interactions.* **K. J. Franke**, G. Schulze, N. Henningsen, I. Fernandez-Torrente, J. I. Pascual, S. Zarwell, K. Rück-Braun, M. Cobian, and N. Lorente; Phys. Rev. Lett. **100**, 036807 (2008)

*Active intramolecular conformational dynamics controlling the assembly of azobenzene derivatives at surfaces.* **N. Henningsen**, K. J. Franke, G. Schulze, I. Fernandez-Torrente, B. Priewisch, K. Rück-Braun, and J. I. Pascual; Chem. Phys. Chem. **9**, 71 (2008)

*Trans to cis Isomerization of an azobenzene derivative on a Cu(100) surface.* **N. Henningsen**, R. Rurali, K. J. Franke, I. Fernandez-Torrente, and J. I. Pascual; Chem. Phys. Chem. **9**, 71 (2008)

*Fingerprint of coordination complexes: DMC co-adsorbed with Co atoms on a Au(100) surface.* **N. Henningsen**, R. Rurali, C. Limbach, J. I. Pascual, and K. J. Franke; *in preparation* (2009)

## Conference Contributions

*Construction of a Low Temperature Scanning Tunneling Microscope* N. Henningsen, C. Roth, I. Fernandez-Torrente, and J. I. Pascual; Frühjahrstagung der Deutschen Physikalischen Gesellschaft (2005) Berlin [Poster]

*Self-Organisation and Spectroscopic Analysis of Azobenzene Derivatives* N. Henningsen, K. J. Franke, G. Schulze, I. Fernandez-Torrente, P. Balani, and J. I. Pascual; Scanning Probe Spectroscopy (2006) Hamburg [Poster]

*Conformational switches - inducing rotation of a phenyl ring by attaching tunnelling electrons to molecular orbital* N. Henningsen, I. Fernandez-Torrente, K. J. Franke, G. Schulze, B. Priewisch, K. Rück-Braun, and J. I. Pascual; Desorption induced by electron transitions (2007) Berlin [Talk]

*Conformational switching in the self assembling process of azobenzene on Au(111)* N. Henningsen, K. J. Franke, I. Fernandez-Torrente, B. Priewisch, K. Rück-Braun, and J. I. Pascual; Frühjahrstagung der Deutschen Physikalischen Gesellschaft (2007) Regensburg [Talk]

*The role of surface-molecule interaction in the isomerisation of Azobenzene molecules* N. Henningsen, R. Rurali, K.J. Franke, I. F. Torrente, G. Schulze, B. Priewisch, K. Rück-Braun, and J. I. Pascual; Frühjahrstagung der Deutschen Physikalischen Gesellschaft (2008) Berlin [Talk]